AD

ADDENDUM TO TECHNICAL REPORT ECOM-00394-14

HIGH VOLTAGE BREAKDOWN STUDY

Prepared by:

ION PHYSICS CORPORATION

BURLINGTON, MASSACHUSETTS

ECOM

UNITED STATES ARMY ELECTRONICS COMMAND · FORT MONMOUTH, N.J. 07703

SPONSORED BY: Advanced Research Projects Agency, ARPA Order No. 517
CONTRACT DA-28-043-AMC-00394(E)

ION PHYSICS CORPORATION
Burlington, Massachusetts 01803

802-TR-310

SOME FACTORS AND ASSOCIATED MECHANISMS INFLUENCING HIGH VOLTAGE INSULATION FAILURE IN VACUUM

Alan Watson

SOME FACTORS AND ASSOCIATED MECHANISMS INFLUENCING HIGH VOLTAGE INSULATION FAILURE IN VACUUM

Submitted to the Faculty of
Mathematics and Physics of
the Technische Hochschule Darmstadt

In Partial Fulfillment of Requirements for
the Degree of
Doktor der Naturwissenshaften (Dr. rer. nat.)

Dissertation
by

Alan Watson
(M. Sc. Tech.; Dipl. Electronics, B. Sc.)
Burlington, Massachusetts, U. S. A.

ABSTRACT

An experimental program has been initiated to study dc breakdown in vacuum up to 300 kV without reliance upon preconceived convictions of what are the mechanisms or participating factors. A range of possible factors previously reported to be influential in determining vacuum breakdown voltage was chosen with a view to studying their effects and interactions using the techniques of factorial experimental design. These methods are particularly useful in complex problems of applied physics in which many well understood fundamental physical processes operate simultaneously but with varying degrees of significance. The nature of the vacuum breakdown mechanism presents just such a problem and the relative significance or total absence of several processes may be inferred from the results. A wide selection of physical monitoring techniques has also been employed to collect supplementary data from which some basic theoretical ideas of the possible breakdown mechanism were developed. These ideas have been analyzed in detail, leading to a mathematical theory of the breakdown mechanism. The theory not only explains the experimental data satisfactorily but also extends naturally into other operating regimes. Previously reported laws relating breakdown voltage and gap separation appropriate to cathode or anode dominated conditions have been confirmed and explained by the theory. New data on the influences of a weak magnetic field and of gas dissolved in the electrodes is presented and compares very satisfactorily with analytical predictions. A novel experimental technique was also developed for monitoring gas evolution instantaneously using the X-rays emitted as prebreakdown current accelerates through it.

The successful results of factorial experimental methods has led to the development of a unifying theory which it is hoped will form the foundation for the understanding of vacuum breakdown.

BLANK PAGE

TABLE OF CONTENTS

TABLE OF CONTENTS (Continued)

TABLE OF CONTENTS (Continued)

TABLE OF CONTENTS (Continued)

Section | Page

APPENDIX D

THE INFLUENCE OF CURVATURE

LIST OF ILLUSTRATIONS

LIST OF ILLUSTRATIONS (Continued)

LIST OF ILLUSTRATIONS (Continued)

LIST OF ILLUSTRATIONS (Continued)

LIST OF TABLES

BLANK PAGE

SECTION 1
INTRODUCTION

1.1 Historical Review

When an electron or a positive ion moves through a gas which does not form negative ions, it is likely to excite or ionize atoms or molecules by collisions provided its energy exceeds the corresponding critical values. If such an inelastic collision takes place in a field-free space, new electrons and ions or excited atoms are produced which remain for a short while in the path of the primary particle, but they are not distributed throughout the gas. In the presence of an electric field, excited atoms as well as electrons and ions are produced throughout the region bounded by the electrodes and the walls confining the space. The more important aspect of this process is, however, that electrons and ions formed by impact are being driven by the electric field to the respective electrodes, and collide on their way with gas molecules and thereby produce new ions and electrons; the excited atoms on the other hand move unaffected by the field. Thus, one primary electron, starting at a negative electrode, can be multiplied in an electric field a great many times; for instance, simple theory indicates that the current multiplication i/i_o across a plane-parallel interelectrode gap of width d is:

$$\frac{i}{i_o} = \exp(\alpha d) \tag{1-1}$$

where α is Townsend's first ionization coefficient.[1, 2] Experiments show, however, that secondary effects occurring at the cathode cause deviations from this relationship. These effects were originally associated with positive ions impinging on the cathode to produce secondary electrons; more recently it has been realized that secondary electrons can be produced by the incidence of photons, neutral and metastable particles as well. Such considerations lead to more sophisticated, but not fully comprehensive, formulas, such as:

$$\frac{i}{i_o} = \exp(\alpha d)\left\{1 - \gamma(e^{\alpha d} - 1)\right\}^{-1} \tag{1-2}$$

where in this case γ is the number of secondary electrons produced for each positive ion arriving at the cathode. Also, the nature of the ambient gas is important, since current multiplication is reduced when certain gases form negative ions (e.g., H^-, O^-, O_2^-, etc) by electron attachment.[3]

An alternative (or complementary) theory shows that photoionization of the interelectrode gas can be a competing process in gaseous breakdown and is the dominating process on occasion.[4] It can thus be concluded from the literature that the mechanisms of current multiplication and breakdown in a gaseous medium are reasonably well understood. However, it is not possible to extrapolate from data even at low pressures ($\approx$ 1 torr) to vacuum conditions. This is because in the pressure region

below 10^{-3} torr, the mean free path of residual gas molecules is between 1 and 10 cm, which is normally greater than the electrode separation. Under these conditions, discharge initiation resulting from interelectrode multiplication processes seems improbable, and others become important; however, processes of multiplication in the interelectrode volume can still be relevant to the later stages of the discharge.

The phenomena of vacuum breakdown have been studied with various degrees of skill by a large number of experimenters, who have been responsible for an almost equally large number of theories. While it is generally accepted that the vacuum arc occurs in vapor or gas generated at the electrodes, the cause of the transition from the field emission to the arcing state, that is the breakdown mechanism, is still uncertain. The requirement is probably a local temperature sufficiently high to produce the necessary vaporization for the arc. This may in turn be produced by particle bombardment, by an increase in field emission due, perhaps, to change in local geometry, or by both of these acting together. Several of the theories which have been proposed to account for breakdown are given below.

(1) Breakdown occurs in the vapor produced at the anode by bombardment with field-emission electrons from the cathode.[5] Boyle et al[6] developed this theory to account for breakdown at very small gaps. They proposed that there is a high yield of electrons at the cathode per positive ion produced in the gap, owing to enhancement of the field at the cathode by positive-ion space charge rather than by ion bombardment. This gives breakdown of the anode vapor in the gap when the multiplication by electron avalanche is below that in the more usual forms of Townsend breakdown.

(2) Field-emission electrons from the cathode strike the anode and produce, by secondary emission, positive ions which are accelerated toward and bombard the cathode.[7] When the potential and number of ions are large enough, a rupture of the cathode occurs which leads to breakdown.

(3) Prior to breakdown, field currents flow from surface projections (where the local field and mechanical force are greatest). There is local resistive heating, which depends on the size and geometry of these projections and their thermal contact with the body of the cathode. As the field is increased, a rupture occurs at the projection where conditions of mechanical force, resistive heating and tensile strength are most favorable. Breakdown follows.[8]

(4) The production of charged particles becomes cumulative and breakdown results when $AB + CD > 1$, where the coefficients are as specified below:[9]

1 electron striking the anode produces A positive ions,
1 positive ion striking the cathode produces B electrons,
1 electron striking the anode produces C photons, and
1 photon striking the cathode produces D electrons.

(5) A breakdown occurs when $AB + EF > 1$, where A and B are specified as in (4) and:

1 positive ion striking the cathode produces E negative ions, and
1 negative ion striking the anode produces F positive ions.[10]

(6) Looseiy adhering materiai (termed a 'clump' by Cranberg) can be detached from an electrode by electrostatic repulsion. Breakdown is initiated when this 'clump' crosses the gap and strikes the opposite electrode, where, it has been shown, iocal temperatures are produced which are greater than any known boiling points.[11] It can be assumed that production of such a condition would lead to breakdown. Cranberg suggested that breakdown would take place when the energy per unit area delivered to the target electrode exceeded a vaiue C' - a constant for any given pair of electrodes. He showed that the breakdown criterion became simpiy:

$$VE > C \tag{1-3}$$

where V is the gap voitage, E is the field strength at the electrode where the 'clump' originated, and C is the product of C', some numerical factors, and possibiy a fieid-intensifying factor due to microscopic distortion of the field in the neighborhood of the clump during detachment from its parent electrode. For a uniform field gap the breakdown criterion becomes:

$$V > (Cd)^{1/2} \tag{1-4}$$

where d is the gap spacing. Cranberg suggested that the ciump could come from either electrode, but the cathode seemed the more likely source in most cases.

(7) The foliowing mechanism is suggested as the cause of breakdown at comparatively small gaps (< 1 mm) and high surface gradients, if the positive-ion transit time is short compared with the time of duration of the gap voltage.[12] With a gap voltage close to the breakdown value, there are, at microscopic projections on the cathode, high electrical and thus mechanical stresses. Due to fieid emission, a high current density exists which produces resistive heating of the projections, the temperature being increased also by the bombardment of the point by positive ions produced at the anode by the electron stream. These conditions of tensile stress and high temperature lead to a fracture of the weakest projection, which initiates breakdown. The extent to which the sparking potential depends on the current density is determined by the gap voltage (icn energy); and the number of positive ions produced by the electron stream, which is infiuenced by the material and condition of the anode surface.

(8) Slivkov[13] has proposed a mechanism which is simiiar in some respects to Cranberg's.[11] Again 'clumps' of charged material cross the gap and strike the opposing electrode. Cranberg based his process on the increase of temperature at the point of incidence on the electrode, but Slivkov noted that most of the kinetic energy of the particle wiil go into heating the particie, which is vaporized. Townsend ionization phenomena then develop in the gas bubble so formed (which rapidly decreases in pressure as it expands) and the minimum discharge voltage is determined by Paschen's Law. The criterion for breakdown then becomes:

$$V E_k E_a^{2/3} = K \tag{1-5}$$

where:

V is the voltage across the gap,

E_k is the field at the cathode,

E_a is the field at the anode, and

K is a constant.

(9) Borovik and Batrakov[14] have proposed that the mechanism proposed by Van Atta et al,[9] which subsequently appeared inadequate because of the low coefficient of emission of positive ions by electrons, might still hold because of a strong focusing of the electron beam at the anode surface. The focusing, it was suggested, was due to a positive ion space charge, and the coefficient of emission of positive ions might be quite high for a dense electron beam.

Recent work has provided data on vacuum breakdown to a total voltage of 1.7×10^6 volts,[15] superceding the previous highest single gap potential differences which were obtained by Trump et al,[16] while other authors are presently investigating breakdown in a lower voltage regime.[17-19] Thus, there is no shortage of suggestions for a vacuum breakdown process, only the experimental proof that any of the processes are valid.[20-23]

It is for this reason that new work had to be undertaken with an open mind. Theories of breakdown, while they have value in the final analysis, must not influence the design of experiments and in this sense 'theories' include both academic and industrial preconceptions.

New work has, therefore, been carried out utilizing the factorial design technique of experimentation. Two major experiments of this kind were carried out to investigate ss many as eleven independent factors and their interactions. A preliminary experiment provided experience in new instrumentation techniques and in testing procedures. Valuable physical measurements were made during the approach to voltage breakdown and the physical analysis of these together with the results of factorial analysis were used to construct a theory of the breakdown process.

The principal aims of the foregoing thesis are twofold. Firstly, the vacuum breakdown problem is investigated by the factorial experimentation technique which has not been hitherto employed. A major advantage over conventional experimental techniques lies in its capability to uncover not only the significant physical factors influencing the breakdown voltage, but also their combined influences when they interact with one another. This is very important when making comparisons between experimental data and the predictions of various theories.

The second major aim of the thesis has been to use the results to confirm the validity of one theory. This was only partially successful because the author found it necessary to add yet one more theory to the above list. It constitutes, however, only a modification to an existing theory of breakdown initiation by field emission current and it does succeed in explaining the experimental results as well as those of other workers. The theoretical notions, moreover, have been subjected to fairly rigorous mathematical analysis.

1.2 Experimental Parameters

In any designed experimental program, it is important to be aware of all the parameters which may be significant. If one strongly significant parameter is omitted (i.e., not controlled), the correct treatment of the experimental data will indicate this by a random presentation. It will not, of course, indicate the factor which has been omitted, and the effort involved in running the experiments is largely lost. For example, the first factorial (Pilot) experiment about to be described resulted in a large statistical error which detracted from the reliability of the significant results because a factor was overlooked. In the second factorial experiment, however, this factor, the pretreatment of electrodes by baking in hydrogen or vacuum, was included and an enormous improvement in accuracy and reliability characterized the results.

Recognition of all the important factors is essential for the proper design of the experiments in a proposed program. In the early stages of all these factors will be determined, but it is relevant to review here those which were initially considered important. The many parameters postulated for vacuum gap performance are discussed in detail below.

1.3 Environmental Effects

1.3.1 Residual Gas

The residual gas can influence the breakdown voltage of a gap through adsorption on the electrode surfaces and through interelectrode collisions and ionization. If an electrode surface is initially completely desorbed of all gas, a monolayer of nitrogen would be adsorbed in eight hours at 7.5×10^{-10} torr and a monolayer of water vapor at 4×10^{-10} torr. The present limitations at very high voltage (e.g., 300 kV) are believed related to surface "contamination" effects, but as far as is known no tests at very high voltage have been conducted in the truly "clean surface" pressure regime to determine what improvements could be obtained. However, to maintain a completely desorbed surface would require pressures of many orders of magnitude below that mentioned above, which does not seem practical for present engineering purposes.

At the other end of the pressure range ($\sim 10^{-4}$ torr) collision processes in the gap can be important, and it has been demonstrated[24] that in the range above 200 kV, operation at 10^{-4} torr can give a 100% improvement in attainable voltage compared with operations at 10^{-6} torr.

Between these extremes, say at 10^{-6} to 10^{-8} torr, it is generally believed that there is no pressure effect, but the rigor of the experiments from which this conclusion is drawn is suspect and further investigation is desirable. It is only in the last few years that experiments at the University of Illinois,[25] and independently at Ion Physics Corporation,[26] showed that with small vacuum gaps ($\sim$ 1 mm) performance at 10^{-4} torr is better than at 10^{-6} torr, which is contrary to earlier opinion.

On the basis of the above remarks, it seems reasonable to include the pressures 10^{-6} and 10^{-8} torr as experimental parameter levels. It is important, however, that the nature of the residuals should be known through the use of mass spectrometer techniques, and, where needed, controlled, pure gases should be used. This is also a partial check that satisfactory electrode cleaning processes are

being followed. There is a considerable body of evidence[27, 28] which shows that a significant partial pressure of organic vapor is undesirable in very high voltage vacuum equipment.

1.3.2 Temperature

The effect of electrode temperature on vacuum breakdown has not been studied extensively, but it appears from experiments by Slivkov[29] that there is no deterioration in vacuum insulation properties up to about 800°C (for nickel). Recent studies at the Naval Research Laboratories by Little and Whitney[30] appear to confirm this, although Maitland's[31] information does not. It seems that temperature as a parameter should not be investigated until later in the program, if then, and that initially the experiments should be at room temperature.

1.3.3 Envelope

The discussion of the envelope effect is included in the environment group because there has been some evidence[32] that the presence of glass can influence gap performance. Certainly the presence of a closely confining envelope could influence the field in a gap, particularly if a geometry such as a sphere to plane was being used - and it could also be a source of contamination or ions. The diameter of the envelope is a parameter which could be important to gap performance.

The dielectric envelope has to withstand the total voltage and this poses a breakdown problem which may be separate from that of the gap. A recent investigation by Watson[33] attributes flashover along the dielectric surface to secondary electron multiplication, but the initiating process is thermionic emission of hot electrons from within. The factors which are important to the insulating properties of the dielectric envelope are: the end conditions, the length, the material and, possibly, the diameter - probably in that order of importance. Conditions at the negative end are particularly important, because intense fields can produce a copious supply of electrons from the metal termination.

So-called "corona shields" can also be utilized to reduce the electric field at the ends of the envelope, but these will be most effective, and perhaps unnecessary, or even undesirable, when proper attention is paid to end conditions.

The materials which should be examined are ceramic (alumina) and glass. These could be either glazed or unglazed. A typical tube glass and alumina should be chosen for the initial experiments. If it is found that the presence of the envelope material has a weakening effect on the vacuum gap, or if the envelope itself is electrically weak, decisions can be made later to examine either other materials or a graded structure.

It is thought important to the lucid conduct of the program to be able to test gaps without the presence of the envelope and vice versa. Further, when both gap and envelope are together they should be arranged to permit the separate monitoring of the prebreakdown current associated with each, and the equipment should be provided with an indicator to show which has broken down when the test is taken to the limit.

1.3.4 Circuitry and Energy

At the present time, very high voltage vacuum equipment requires a conditioning process involving low energy discharges to reach the desired operating range, and during operation is likely to break down occasionally. During operation, high power electron devices are supplied from energetic sources, and the discharge energy through them at breakdown is limited by crowbarring devices.[34] These facts make it desirable to determine the effect on subsequent performance of discharging different energies through a vacuum insulated system; but there is more than energy involved. A fast discharge (high current) will probably produce a different result from a slow discharge, and if the circuitry is suitable voltage reversal can take place, which some evidence[17] suggests may lead to deterioration of gap performance. Voltage reversals are known to occur in klystrons at breakdown. As can be judged from the following miscellany, not enough is known about circuitry and energy effects.

If the supply across a vacuum gap at breakdown is simply a charged capacitor with some series resistance, and the first fraction of a microsecond is disregarded, the discharge current follows the usual exponential law and chops at a few tenths of an ampere.[12] This is so for small gaps (~ 1 mm) and probably also holds for large gaps when complete breakdown takes place. If the series resistance (R_s) is so large that V/R_s is less than the chopping current, a series of suppressed breakdowns occurs.[12]

It is obviously desirable to examine energy effects during the program. At the lower end of the energy range, it is difficult to get much less than 10 joules at discharge because of the intrinsic capacitance of the electrode system, and 7000 joules has been suggested as a suitable value for the high energy range. Thought should also be given to the significance of series inductance and resistance which will determine the spark, or arc current, and whether or not polarity reversal will occur.

1.4 Fields and Geometry

1.4.1 Electrostatic Field, Macroscopic

The significance of electric field to breakdown in high vacuum is well known, if not well defined. At small gaps, less than a few millimeters, breakdown takes place approximately at a constant gradient (→ 100 kV/mm) after suitable conditioning. At larger gaps, a large body of evidence supports for uniform field electrodes a relationship:[11, 24]

$$V_s = C d^{1/2} \tag{1-6}$$

where V_s is the breakdown voltage, d is the gap spacing and C a constant. This relationship holds for the range of greatest interest here, but the support data is from tests subject to contaminating influences which should not exist in ultra-high vacuum. Cranberg[11] derived expression (1-6) from:

$$V_s E_s = \text{Constant} \tag{1-7}$$

where E_s is the field at an electrode surface on which a "clump" originates. However, experiments at voltages up to 1.7 MV[15] using sphere to plane geometry did not confirm this expression, nor did they confirm a criterion $V_s E_c E_a^{2/3}$ = Constant, developed by Slivkov.[13] The relationship E_s = Constant was found to be more representative of experimental data.

The macroscopic field at the electrode surface is obviously determined by the electrode geometry and, to a lesser extent, by the proximity of shields. Further information is required on macroscopic field effects for the design of high voltage equipment, particularly in the relatively clean environment of high power electron devices, and this is a good area for investigation during the program.

1.4.2 Electrostatic Field, Microscopic

The field as determined by gross geometry is intensified by the presence of asperities or roughness on the electrode surface. The microscopic field is difficult to control, but a first step is through surface finish. It has been variously stated that surface finish has been determined to be not an important parameter, which is surprising considering the mechanisms postulated for vacuum breakdown. However, recent experiments[35] with perhaps other parameters under better control than previous investigators have shown that it can be important. In other experiments[18] to examine the effect of residual gas pressures on breakdown, much greater field enhancement factors have been measured. This effect has been attributed to the growth of sharp whiskers on the electrode surface. These intensifications can be calculated from the Fowler-Nordheim equation when the current, voltage and gap are known.

Electrolytic, mechanical and chemical techniques are available for application to electrode surfaces and the first two seem most attractive. Electropolishing has not compared well with other methods, probably because it influences another important parameter (surface hardness - later). Hadden[36] failed to improve the breakdown strength of copper electrodes by electropolishing. However, both mechanical and electropolished surfaces should be compared at the large gaps and low gradients used in tubes.

1.4.3 Magnetic Field

It is known that the presence of a magnetic field can change the maximum electric field which can be supported by a vacuum gap. For example, Pivovar et al[37] have used a magnetic field parallel to the electrode surfaces in studies up to 170 kV to remove the electron component of pre-breakdown conduction and hence to raise the breakdown voltage. Also, the interaction of the magnetic and electric fields in crossed field particle separators is known to be a problem. The difficulties are believed to exist in the fringing fields rather than within the gap. Separators at Brookhaven National Laboratory are now operating at 500 kV across a 4-inch gap at a pressure of about 10^{-6} torr with one spark every 5 to 6 hours.[38] The magnetic field is 200 to 300 gauss and must be applied after the electric field. In the event of a spark, the magnetic field has to be interrupted to re-establish the electric field, and it is expected that operation at higher fields than 300 gauss will cause difficulties.

The magnetic field used for focusing high current beams in some tubes can also influence voltage performance.

It is believed that the magnetic field experiments will be most valuable to the elucidation of high vacuum discharge mechanisms.

1.5 Electrode Materials and Surface Properties

In "low voltage" experiments, correlation has been found between vacuum breakdown and the metallurgical state of the electrodes as regards surface finish, particle content, surface hardness and grain size. Surface finish has been treated in the earlier discussion of microscopic field. The importance of selecting the best alloy and metallurgical condition is illustrated by reference to Table 1-1, which shows results from tests with various alloys of the stainless steel family.

Table 1-1. Insulation Strength at 1 mm Gap for Several Metals

Metal	Strength (kV/mm)
304 Stainless Steel	60
Udimet A	55
Nickel, Inconel-718	50
303 Stainless Steel	44
Inconel	44
Inconel-X, Molybdenum	40
Haynes-25	30
Udimet-41	28
Hastelloy B	15
Multimet	10

The following properties are included to indicate what may be important parameters, and the existing evidence requires substantiation.

1.5.1 Particle Content

Tests and microscopic examination of electrodes have shown that many breakdowns occur at sites of non-metallic inclusions. These inclusions are oxides, silicides, carbides, etc, introduced during processing of the metal, or precipitates which are compounds of alloying constituents introduced to improve strength properties. When alloys were tested which depend upon phase transformation of the crystal structure for their strength properties and which were relatively free of impurities and precipitates, high fields could be insulated (up to 115 kV/mm with Ti-7Al-4Mo alloy).

1.5.2 Grain Size

Using 304 stainless steel electrodes it has been found that 80 kV could be insulated across a 1 mm gap when the average grain size was ~ 500 grains/mm^2, which compares with 40 kV with 62 grains/mm^2.

1.5.3 Hardness

When the surface of electrodes of 304 stainless steel are hardened by cold working, tests have shown that the same fields (80 kV/mm) can be insulated without breakdown as when the electrodes are annealed. However, in the former case, the gap currents are normally 1 to 2 orders of magnitude lower at maximum voltage. Germain[19] has suggested that hardness is an important parameter at the high voltages of interest here, and has attributed poor experience with electropolishing to the relatively soft surface this polishing technique produces.

1.5.4 Physical Properties

Several attempts have been made to match vacuum breakdown performance with one or more of the physical properties of the material. Rosanova and Granovskii,[39] for example, suggest that electric "strength" of the gap increases with the tensile strength of the anode material. Other properties which could be important include work function, secondary emission coefficients, electrical conductivity, sputtering coefficient, density, thermal conductivity, specific heat, and boiling point. One could add others such as susceptibility to whisker growth, which would require a program on its own to determine.

It seems likely that experiments in the past did not demonstrate a convincing correlation between performance and some physical properties because the parameters were not adequately controlled. The extensive effort and the precise control of parameters which are expended under the present program should permit such a correlation.

1.5.5 Contamination

The sensitivity of spark gaps to dust particles is well known, and the vacuum gap is particularly so. In early experiments, breakdown voltage was raised by 50% just by improved methods of installing dust-free electrodes.

Organic contamination is known to be deleterious to vacuum insulation.[28] Such contamination can be from processing of electrodes before installation, oil vapor in the atmosphere, or from sources inside the vacuum system. The vacuum system should be designed to be free of organic contamination, and to confirm this a continuous check should be made of the residuals using a mass spectrometer. The elimination of dust particles and organic contamination introduced to the system on the electrode surfaces is best accomplished using a clean bench processing system coupled to the vacuum chamber.

It is possible using the above methods to eliminate contamination which is not necessarily present in the average high power electron device. There is also the possible contaminant BaO which

originates at thermionic cathodes, and it is important to determine if the presence of BaO adversely affects vacuum insulation.

1.5.6 Oxide Films

A film of oxide forms almost instantly on most, if not all, freshly prepared metal surfaces. The film continues to grow with time after preparation, and it is reasonable to assume that the thickness of this film should be important to vacuum insulation; but no experiments seem to have been made to examine electrodes with controlled film growth. It is necessary to examine recent experiments on breakdown in liquid dielectrics and high pressure gas to assess what might be the effect.

Lewis[40] has studied breakdown in liquid dielectrics and high pressure gas, and noted that gap performance is influenced by the time for which freshly surfaced electrodes were exposed to air before immersion in the dielectric. Apparently, oxide growth significant to breakdown voltage occurred for the first several hours after preparation. Growth on the cathode improved the subsequent insulation strength and on the anode reduced the strength; and with growth permitted on both electrodes there was an optimum exposure time of about 10 minutes. The theory of oxide layer growth has been reviewed by Cabrera and Mott.[41]

The oxide growth effect is a possible parameter which has not been appreciated, and it may account for some of the conflicting data obtained from past experiments. It is important to the proposed program to determine if oxide growth between preparation and installation of electrodes is important, and to design the subsequent experiments according to the results obtained.

1.5.7 Area Effect

It has been known for some time by those acquainted with vacuum insulation problems that increasing the area of a stressed surface reduced the stress which could be supported. However, it was not until recently that quantitative information on this effect was obtained to assist in the design of vacuum insulated electrostatic generators, which are large area devices. Figure 1-1 shows a plot of early data indicating the severity of the problem at a 1 mm gap.

Area effects have been studied in other dielectrics such as oil and capacitor insulation. It can be expected that breakdown mechanisms depending on randomly distributed weak spots will have values for their occurrence which decrease with area. Statistically this is covered by the theory of extreme values[42] which has been applied successfully to the reduced breakdown voltage with area in liquid and solid dielectrics.[43] Statistical influences alone do not seem to account for the severity of the effect in vacuum, and other factors such as the difficulty in surface preparation of large surfaces and the limited gap pumping speed (at 1 mm) may also be important.

At the higher voltages of particular relevance to the proposed program, there is no specific data on area effect as that for the 1 mm gap, although experience indicates that increasing surface area makes conditioning to high voltage more difficult. Where possible during the program electrode

surface area should be kept constant, and in the studies of various electrode geometries the possible significance of differences in area should be borne in mind.

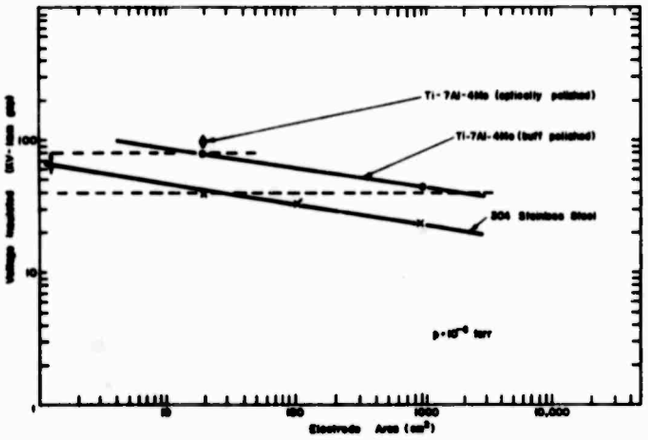

Figure 1-1. Electrode Area Effect

1.6 References

(1) von Engel, A., Ionized Gases, Clarendon Press, Oxford, England (1955).

(2) Townsend, J. S., Handbuch der Radiologie, Bd. 1, Akad. Verlag, Leipzig (1920).

(3) Massey, H. S. W., Negative Ions, Cambridge University Press (1950).

(4) Kritzinger, J. J., "Impulse Corona and the Pre-Breakdown Mechanisms of Long Sparks", Nature 197, 1165 (1963).

(5) Myers, O. E. and Raatz, W. A., "Vacuum Sparking", U. S. Atomic Energy Commission, Lawrence Radiation Laboratory, 158 (1955).

(6) Boyle, W. S., Kisliuk, P. and Germer, L. H., J. Appl. Phys. 26, 720 (1955).

(7) Chambers, C. C., "Emission of Electrons from Cold Metal Surfaces", J. Franklin Inst. 218, 463 (1934).

(8) Ahearn, A. J., "The Effect of Temperature, Degree of Thoriation and Breakdown on Field Current from Tungsten and Thoriated Tungsten", Phys. Rev. 50, 238 (1936).

(9) Van Atta, L. C., Van de Graaff, R. J. and Barton, H. A., "A New Design for a High Voltage Discharge Tube", Phys. Rev. 43, 158 (1933).

(10) McKibben, J. L. and Beauchamp, R. K., "Insulation Flashover Tests in Vacuum and Pressure", U. S. Atomic Energy Commission, AECD 2039 (1948).

(11) Cranberg, L. C., "The Initiation of Electrical Breakdown in Vacuum", J. Appl. Phys. 23, 518 (1952).

(12) Denholm, A. S., "The Electrical Breakdown of Small Gaps in Vacuum", Can. J. Phys. 36, 476 (1958).

(13) Slivkov, I. N., "Mechanism for Electrical Discharge in Vacuum", Sov. Phys.-Tech. Phys. 2, 1928 (1957).

(14) Borovik, E. S. and Batrakov, B. P., "Investigation of Breakdown in Vacuum", Sov. Phys. -Tech. Phys. 3, 1811 (1958).

(15) Arnold, K. W., et al, "Electrical Breakdown Between a Sphere and a Plane in Vacuum", Proceedings of Sixth International Conference on Ionization Phenomena in Gases, Paris (1963).

(16) Trump, J. G. and Van de Graaff, R. J., "The Insulation of High Voltages in Vacuum", J. Appl. Phys. 18, 327 (1947).

(17) Britton, R. B., "Transition in the Electrical Conduction Mechanism in Vacuum", Proceedings of Twenty-Fourth Annual Conference on Physical Electronics, Massachusetts Institute of Technology (1964).

(18) Coenraads, C. N., "Field Emission and Its Influence on Electrical Breakdown in Vacuum", Proceedings of Twenty-Fourth Annual Conference on Physical Electronics, Massachusetts Institute of Technology (1964).

(19) Germain, C. and Rohrbach, F., "Mechanisme des Decharge dans le Vide", Proceedings of Sixth International Conference on Ionization Phenomena in Gases, Paris (1963).

(20) Mazeau, J. and Goldman, M., C. R. Acad. Sc. Paris 258, 2774 (1964).

(21) Jones, F. L. and Owen, W. D., "Initial Current Build-Up in Vacuum Breakdown", Proceedings of Sixth Conference on Ionization Phenomena in Gases, Paris (1963).

(22) Maitland, A., "Spark Conditioning of Electrodes at Pressures in the Range 10^{-5} to 10^{-6} Torr", Proceedings of Sixth Conference on Ionization Phenomena in Gases, Paris (1963).

(23) Goldman, M. and Goldman, A., "Sur la Formation de L'arc Electrique dans le Vide Pousse", Proceedings of Sixth Conference on Ionization Phenomena in Gases, Paris (1963).

(24) "Power Sources for Directed Energy Weapons (U)", (S) Final Report Under Contract AF08(635)-2166, Ion Physics Corporation, Burlington, Massachusetts (1964).

(25) Tomaschke, H. E., "A Study of the Projection on Electrodes and Their Effect on Electrical Breakdown in Vacuum", University of Illinois, Coordinated Science Laboratory, Report R-192 (1964).

(26) "Electrostatic Power Generator", Quarterly Report No. 1 Under Contract AF33(615)-1168, Ion Physics Corporation, Burlington, Massachusetts (1964).

(27) Chodorow, M., et al, "Design and Performance of a High-Power Pulsed Klystron", Proc. IRE 41, 1584 (1953).

(28) Mansfield, W. K., "Prebreakdown Conduction Between Electrodes in Continuously Pumped Vacuum Systems", Brit. J. Appl. Phys. 8, 73 (1957).

(29) Slivkov, I. N., "The Influence of the Electrode Temperature on the Electrical Breakdown Strength of a Vacuum Gap", Sov. Phys. -Tech. Phys. 3, No. 4, 708 (1958).

(30) Little, R. P. and Whitney, W. T., "Studies of the Initiation of Electrical Breakdown in Vacuum", Naval Research Laboratories Report 5944 (1963).

(31) Maitland, A., "Influence of the Anode Temperature on the Breakdown Voltage and Conditioning Characteristics of a Vacuum Gap", Brit. J. Appl. Phys. 13, 122 (1962).

(32) Donaldson, E. E. and Rabinowitz, M., "Effects of Glass Contamination and Electrode Curvature on Electrical Breakdown in Vacuum", J. Appl. Phys. 34, No. 2, 319 (1963).

(33) Watson, Alan, "Pulsed Flashover in Vacuum", J. Appl. Phys. 38, 2019 (1967).

(34) Schneider, S., et al, "A Versatile Electronic Crowbar System", Proceedings of Seventh Symposium on Hydrogen Thyratrons and Modulators, 436 (1962).

(35) Bennette, C. J., Swanson, L. W. and Charbonnier, F. M., Proceedings of Second International Symposium on Insulation of High Voltages in Vacuum (1966).

(36) Hadden, R. J. B., "The Effect of Surface Treatment on the Electrical Breakdown Between Copper Electrodes at 50 Cycles at Very Low Pressure", Atomic Energy Research Establishment, England, G/M92 (1951).

(37) Pivovar, L. I., et al, "The Effect of the Electron Current Component on Development of Electrical Breakdown in High Vacuum", Sov. Phys. -Tech. Phys. 2, No. 5, 909 (1957).

(38) Sanford, J., Brookhaven National Laboratory, Private Communication (June 1964).

(39) Rosanova, N. B. and Granovskii, V. L., "On the Initiation of Electrical Breakdown of a High Vacuum Gap", Sov. Phys. -Tech. Phys. 1, No. 3, 471 (1957).

(40) Lewis, T. J., Queen Mary College, London, England, Private Communication (November 1963).

(41) Cabrera, N. and Mott, N. F., Reports on Progress in Physics, 163 (1949).

(42) Gumbel, E. J., "Statistical Theory of Extreme Values and Some Practical Applications", National Bureau of Standards Applied Mathematics Series, No. 33, U. S. Government Printing Office, Washington, D. C. (1954).

(43) Hill, L. R. and Schmidt, P. L., "Insulation Breakdown as a Function of Area", AIEE Trans. 67, 442 (1948).

PART A

EXPERIMENTAL

BLANK PAGE

SECTION 2

PREBREAKDOWN PHENOMENA IN VACUUM GAPS

2.1 Abstract

A method for conditioning vacuum gaps by progressive gas evolution has been developed with minimal electrode spark damage. Surface roughening, however, ultimately appears and the field emission current grows. Gas evolution takes place at some voltage threshold and is shown to be dominantly hydrogen, although nitrogen is also significant. X-radiation from the interelectrode space suggests that less metal atoms enter the gap as the voltage is raised, confirming the proposition that cathode sputtering plays a significant role in the process. Just prior to breakdown gas evolution, X-radiation, light output and current can increase slowly beyond control at constant voltage to gap failure.

2.2 Introduction

A characteristic of electrode gaps in vacuum is that there exists no unique breakdown voltage but only a band of possible values attainable after many prior sparks have passed during an initial "conditioning" procedure. The literature to date is confused about the significance of this procedure and of the electrode materials, shapes and finish in determining breakdown voltage. It is pertinent to question whether shape and finish, which are disturbed after sparking, can be preserved by a different choice of procedure for voltage application, leaving them available for the experimenter to vary at will.

It should be theoretically possible to monitor enough physical variables during voltage application to describe adequately the processes leading up to gap failure. Recognition of an incipient breakdown without damaging the electrodes would permit repetitive testing under similar conditions, being particularly useful with low impedance power supplies.

The present investigation was directed towards developing a conditioning procedure involving minimal sparking and to search for a criterion for incipient breakdown.

One shape only of large area, unbaked, metallurgically polished stainless steel electrodes was used throughout. During stepwise voltage application the variables monitored were gap current, light output, partial pressure of hydrogen or nitrogen, and X-radiation. The processes accompanying the approach to gap failure were thus monitored, to see if they were slow enough to permit recognition of a breakdown criterion.

2.3 Apparatus

Hollow domes of 304 stainless steel serving as approximately uniform field electrodes, 8 inches in diameter, were centrally positioned at fixed gaps of up to 1 cm within the 3 foot wide stainless steel vacuum chamber at the ends of two 250 kV bushings, as previously described by Britton.[1] Organic contamination was eliminated by using gold gaskets throughout, and pumping down to 6×10^{-7} torr with a mercury diffusion pump and liquid nitrogen cold trap. The mass spectrometer ion source, protruding inside from the wall was screened from the large applied field within the chamber which

otherwise perturbed it. Outside of the 3/4 inch thick glass monitoring port were two thallium activated NaI scintillators viewing, respectively, either the whole electrode region or only the interelectrode space through a collimator made from two narrowly separated parallel aluminum slabs. Visible radiation from this port was reflected sideways by a plane mirror to a photomultiplier to separate it from accompanying X-radiation, thus avoiding damage to the photocathode.

Gap current fluctuations were observed using a 160 kV, 1.5 ma rectifier source and external resistors of 400 kilohm and 15 megohm to vary the effective output impedance.

The electrodes were hand ground initially with wet silicon carbide paper of successively finer grade, followed by finer grinding on a variable speed wheel. This was continued with silk using a succession of fine grades of alumina powder and was completed with a wash and wipedown with gamal cloth.

2.4 Electrode Conditioning

Starting with fresh unconditioned electrodes, the voltage was increased in steps of 2, 5 or 10 kV, depending on the gap setting and the voltage, while at the same time monitoring the N_2 or H_2 partial pressure peak on the mass spectrometer. It was found, by observing the current pulse shapes and the associated partial pressure rises, that a threshold voltage existed for the appearance of microdischarges. A plot of initial threshold voltage versus gap separation is shown in Figure 2-1. This is in good agreement with a similar plot of Arnal.[2] Microdischarges appeared as groups of apparently damped oscillatory waveforms similar to those described by Mansfield et al[3] and associated with X-radiation pulses modulated in frequency according to the pressure rise (Figure 2-2).

During the course of the microdischarge investigation, no pressure increases were observed until the microdischarge threshold voltage was reached, and above this the magnitude increased with the height of the voltage steps. Frequent breakdowns occurred when the pressure increases were large and it was found that these could be reduced in number, if not eliminated, by using smaller voltage steps. Occasionally, large pressure increases did occur, in which case the voltage was reduced or switched off before breakdown could take place.

From these observations, a conditioning procedure was evolved for unbaked but clean polished electrode surfaces. Initially, the voltage was increased incrementally every two minutes until a pressure rise was observed, and then allowed to decay to zero. The height of the voltage steps was limited to a level at which breakdowns were unlikely to occur during the gas surge and the stepwise voltage increase was continued until surface roughening took place (to be described later).

The conditioning apparently involves the controlled removal of gas from the electrodes.

Comparison in Figure 2-3 of the breakdown voltages measured with the new technique and with spark conditioning clearly shows improvement in the breakdown voltage and its deterioration as a function of number of sparks.

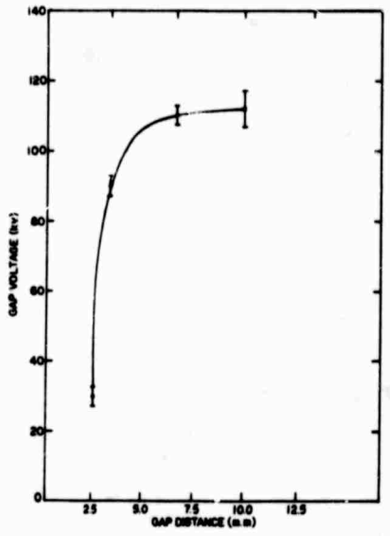

Figure 2-1. Variation of Microdischarge Threshold Voltage as a Function of Gap Distance

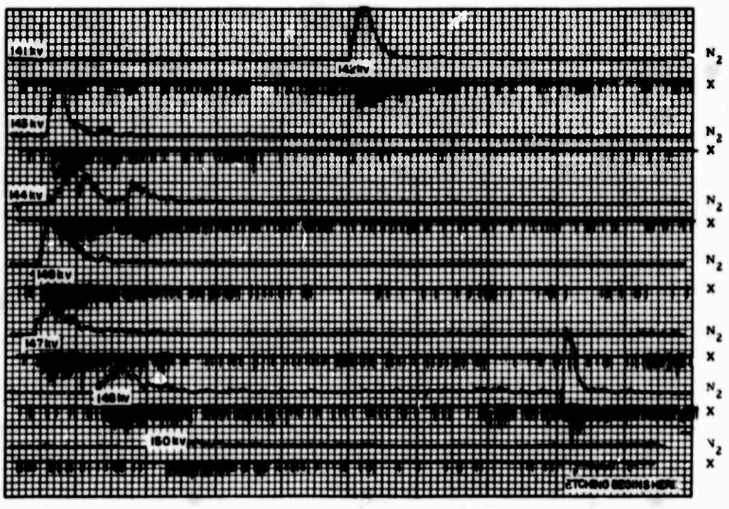

Figure 2-2. Simultaneous Recording of N_2 Partial Pressure and X-Ray Output

2.5 Monitoring Techniques

Pulse height histograms drawn from scintillator signal oscillograms of microdischarge activity showed that during the pressure surge there were two peaks in the photon energy spectrum (Figure 2-4) but after its decay the lower energy peak disappeared. Microdischarge current, although initiated by an ion exchange mechanism, was shown by Mansfield[3] and Pivovar and Gordienko[4] to be mostly electrons. The anode presents a thick absorbing X-ray target to these, most of which assume the whole applied potential but during the pressure surge, interelectrode gas intervenes as an additional thin target, intercepting some electrons to generate the lower photon energy peak.

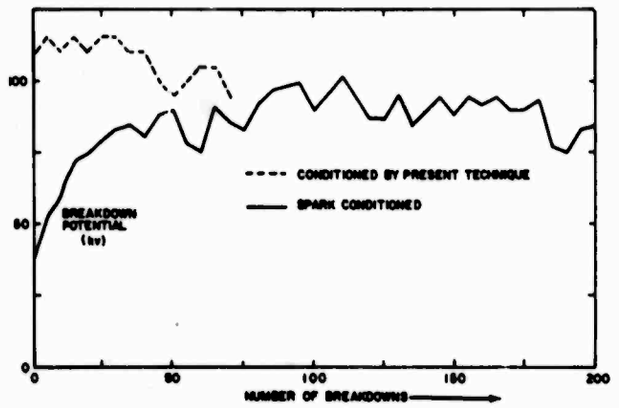

Figure 2-3. Comparison of Breakdown Sequence Diagrams for Electrodes Conditioned by Sparking and by Present Technique (Gap = 2.5 mm, Pressure = 5×10^{-7} Torr)

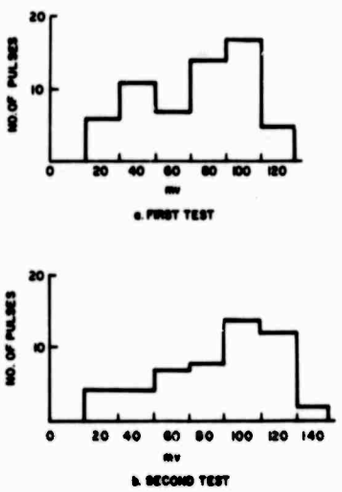

Figure 2-4. Experimentally Determined Pulse Height Spectra of X-Rays During Conditioning

When high voltages were reached with the new conditioning procedure, a steady X-radiation level grew due to cold cathode Fowler-Nordheim emission from sites of enhanced field strength just as Pivovar and Gordienko[4] have observed and attributed to surface etching. At still higher voltages the level rose while microdischarges abated, permitting an accurate measurement of the steady X-ray level as a function of voltage. Typical recordings are shown in Figure 2-5.

In thick targets, electrons generate X-radiation intensity U_x proportionally to the square of the applied voltage, V.[5] Hence relative changes in electron current can be derived from corresponding X-radiation densities and this technique has been used throughout the present investigation. Electrons emitted according to the Fowler-Nordheim law thus produce X-radiation according to:

$$U_x = AK \frac{\beta^2 V^4}{d^2} \exp\left(-\frac{Bd}{\beta V}\right) \qquad (2\text{-}1)$$

where:

B, K = constants

A = emitting area

d = gap separation

β = field enhancement factor

A plot of log (U_x/V^4) as a function of V^{-1} should thus be linear.

Without measured work functions, these plots yield only relative values of field enhancement factor and emitting area but their present value is in signifying changes in these parameters taking place as breakdown is approached. While linear plots occurred in this investigation, the commoner non-linear variety (Figure 2-6) evidenced cathode surface changes as the voltage increased. Repetitively raising and lowering the voltage in increments without sparking failed to yield reproducible results (Figure 2-7). When extended to the breakdown limit, this procedure failed to show any correlation between the penultimate field enhancement factor and breakdown voltage (Figure 2-8).

Emission parameters, being derived from the slope of the Fowler-Nordheim plot, require readings at several voltage levels for their measurement. When they are time dependent, the parameter changes should be small during the interval between voltage increments to permit approximate measurement. As breakdown approached, the changes grew faster and rendered their measurement impossible. Changes in field enhancement factor and emitting area were occurring at constant voltage.

Gas or vapor evolution rate just prior to breakdown then suggested itself as a potentially significant parameter with which to describe the approaching breakdown since the accompanying X-ray

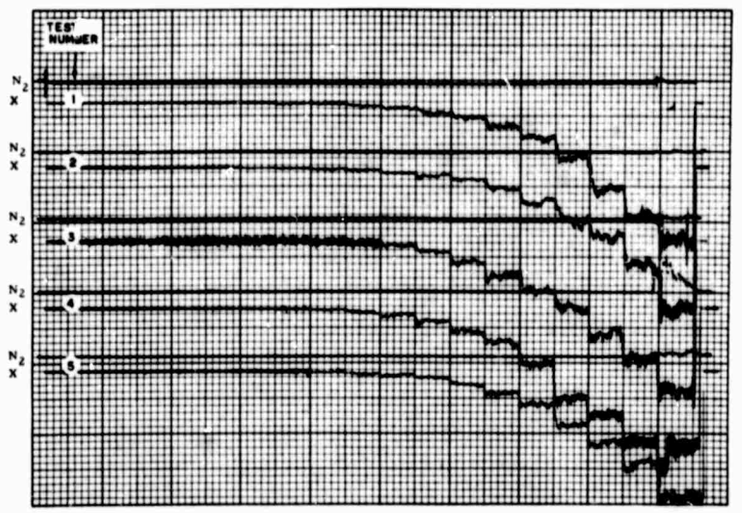

Figure 2-5. Typical Recording of X-Radiation from Etched Surface as the Voltage is Increased in Steps

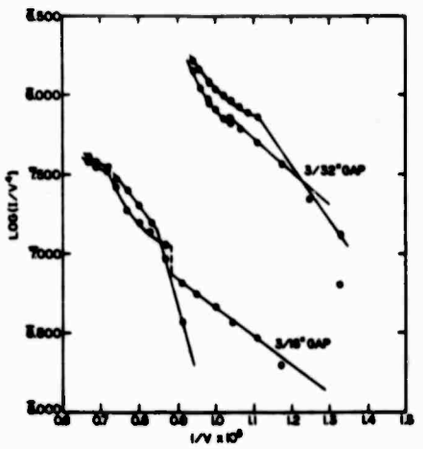

Figure 2-6. Equivalent Fowler-Nordheim Plots of X-Ray Output Showing Result of Variations in Field Enhancement Factor and Effective Emitting Surface Area

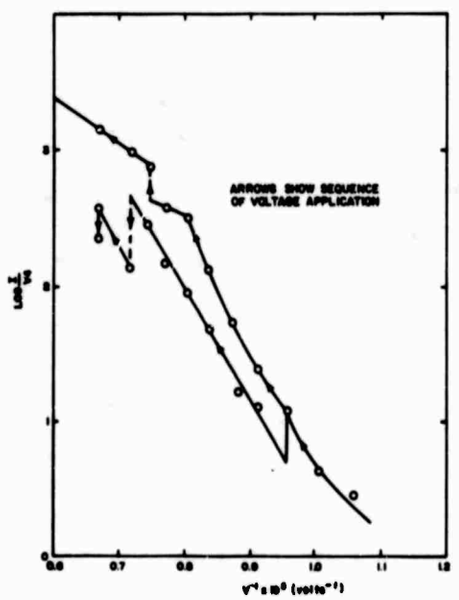

Figure 2-7. Fowler-Nordheim Plots for Two Consecutive Voltage Applications Without Breakdown

emission is readily detectable in the case of microdischarges. Radiation density U_{xc} from the interelectrode space is proportional to the product of gas density, n_g, electron current I_e and the Bremsstrahlung cross section σ_B.[5]

U_{xc} was accordingly monitored by directing at the interelectrode space a collimator made from two narrowly separated aluminum slabs between which photons passed to a scintillator. The current was simultaneously monitored and the relative gas density was derived from:

$$n_g = \frac{U_{xc}}{I_e \sigma_B} \tag{2-2}$$

$$\sigma_B = \frac{8}{3\pi} \cdot \frac{1}{137} \cdot Z^2 \cdot \frac{c^2}{v^2} \doteq K Z^2 V^{-1} \tag{2-3}$$

where K = constant. Hence:

$$n_g = \frac{U_{xc} V}{K I_e Z^2} \tag{2-4}$$

A typical recording appears in Figure 2-9.

The right-hand side of Equation (2-4) was evaluated experimentally and is plotted in Figure 2-10 as a function of voltage up to breakdown. Surprisingly, the gas density appears to decrease but it must be noted that the average value of σ_B can decrease if the interelectrode gas is progressively diluted with hydrogen. Evidence of this was gathered from hydrogen partial pressure records from the mass spectrometer which show surges as breakdown is approached. It thus appears that hydrogen gas accumulated in the gap.

Thus the quantity measured by this technique is:

$$n_g \overline{Z^2} = n_m Z^2 + n_H \tag{2-5}$$

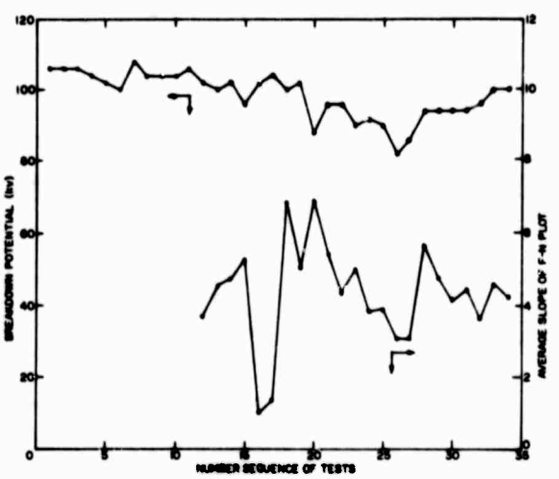

Figure 2-8. Sequence of Diagrams of Breakdown Voltages with the Corresponding Average Enhancement Factors

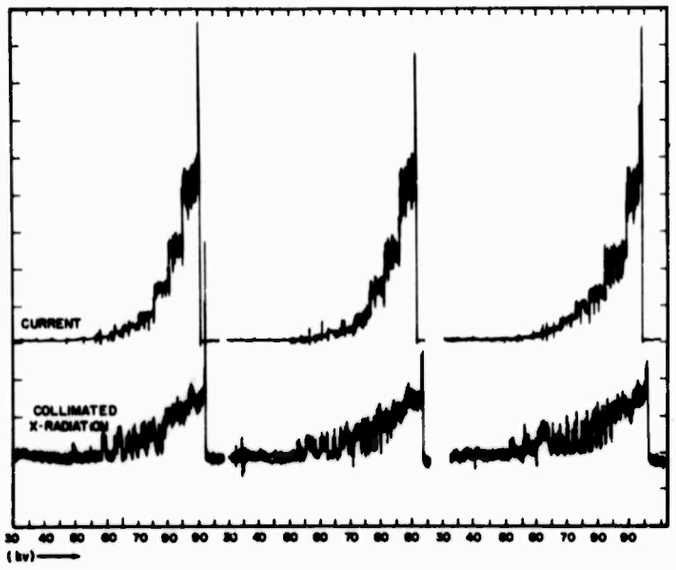

Figure 2-9. Current and Collimated X-Radiation as a Function of Voltage for Three Consecutive Step Tests

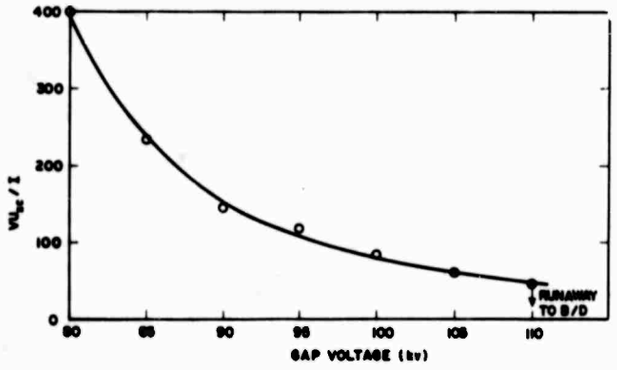

Figure 2-10. Variation of Effective Interelectrode Gas Density Calculated from Experimental Results

where n_m and n_H are the atomic densities of the metal and hydrogen, respectively. As the voltage increases, these increase also by evaporation from the anode and an increase in n_g must be observed. In Section 8.3.3, however, it is shown how n_g will multiply itself by sputtering and its capability to do this decreases as the sputtering yield and the factor g fall notably when the relative hydrogen concentration is greater. Thus this experimental result must be taken as evidence of the significance of sputtering.

Light intensity was monitored under these conditions as it increased stepwise with voltage together with X-ray intensity (Figure 2-11). At higher voltages, both X-radiation and light output rose at constant voltage as well as the light output per unit current. Since the light growth occurs during the gas evolution phase, it seems most likely due to gas luminescence. Transition radiation would

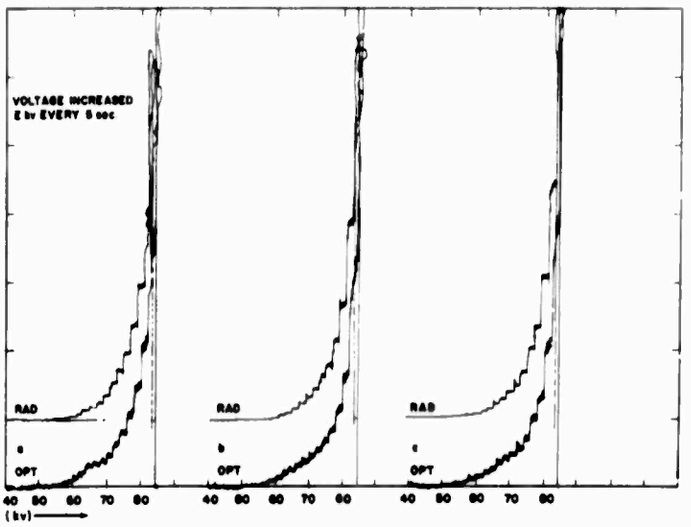

Figure 2-11. Typical Recordings of Visible and X-Radiation (2.5 mm Gap)

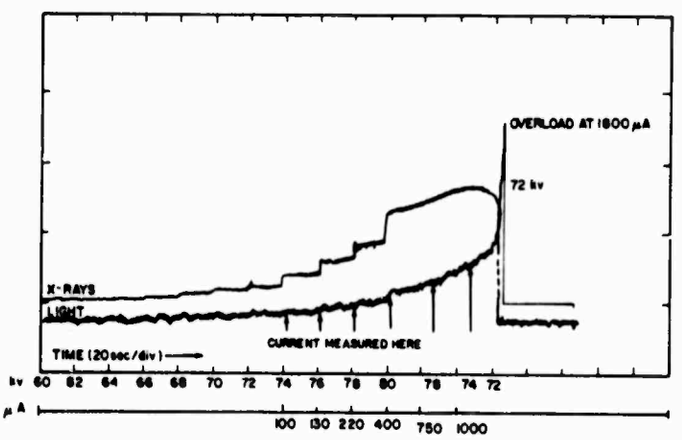

Figure 2-12. Visible and X-Ray Recording Demonstrating Runaway

also appear, but it cannot explain the increase in light output per unit current which would have to remain fixed at constant voltage.

This gradual increase at constant voltage of all of the measured parameters, total and collimated X-radiation, hydrogen partial pressure and light output, was found to increase steadily during the last few voltage increments of 1 kV or less prior to breakdown. The phenomenon has been termed "runaway".

Reduction of the voltage by up to 10% was found to be insufficient to arrest this regenerative process which may take many seconds to complete (see Figure 2-12, the apparent fall in X-ray level is due to scintillator saturation). Breakdown voltages were very reproducible when voltage was applied in 5, 10 or 25 second intervals, but a conditioning effect took place. Experiments with 2.5 mm

and 5 mm gaps established that the breakdown voltage varies approximately as the square root of the gap separation.

2.6 Conclusions

From this work, it appears that only under restricted conditions is there a nondestructive criterion for incipient breakdown of vacuum gaps. Nonetheless, the techniques developed and enumerated below are of value in permitting the vacuum gap to be completely described prior to and during breakdown. Thus, current or total X-radiation monitoring each give information on the state of the cathode surface and on microdischarge activity. Collimated X-radiation gives the total residual gas or vapor pressure in the gap with a rapid response time and is complemented by mass spectrometry which yields only chamber pressure but can resolve gas constituents. A steady uncontrolled runaway is indicated by the total and collimated X-radiation measurements under restricted conditions. This is further supported by visible radiation monitoring which is extremely sensitive to the effect.

In conclusion, the preliminary program has been successful in yielding data from which the steps leading up to breakdown have been identified. Prebreakdown phenomena associated only with unbaked electrodes have been studied and the principal conclusions derived from this program can be summarized as follows:

(1) A conditioning technique has been developed which does not involve sparking and consequent electrode damage. The technique has been compared with the more conventional spark conditioning method and the decrease in gap strength by sparking has been measured.

(2) Microdischarge phenomena have been studied and the results largely verify the work of previous investigators. In addition, an associated rise in the partial pressures of residual gases has been studied.

(3) Microdischarge activity has been shown to be followed by a field enhancement at the cathode and the consequent Fowler-Nordheim field emission probably occurs from a variety of sites. Discontinuities in current changes as a function of voltage are believed to be due to the disappearance or reshaping of some sites.

(4) X-rays are produced by microdischarges and by field emitted electrons. Photons can be generated in the gas or vapor released into the interelectrode space as well as from the anode as a target. The X-rays produced by field emission yield equivalent Fowler-Nordheim plots.

(5) At high potentials, the enhancement factor grows at constant voltage and can run away to breakdown. Small reductions of voltage will only delay the breakdown after growth has proceeded.

(6) The visible radiation from the gap is consistent with a model in which transition radiation may appear at low currents but gas luminescence seems significant at runaway.

(7) Monitoring by collimated X-radiation and mass spectrometry shows that there are both pulsed and continuous changes in interelectrode gas density prior to breakdown. The gas appears

to be hydrogen which probably diffuses out from the anode when it is heated sufficiently by electron bombardment.

(8) Gap failure can occur under two apparently separate circumstances: (a) when gas pressure rises if microdischarges become too great, (b) after surface etching and the runaway of the field enhancement factor. In case (b), the buildup of hydrogen density in the gap may also be the cause of breakdown since it seems to be always associated with it.

(9) The breakdown voltages at runaway are consistent and the conditioned breakdown voltages appear to be approximately proportional to the square root of the gap separation.

2.7 References

(1) Britton, R. B., "Transition in the Electrical Conduction Mechanism in Vacuum", Proceedings of Twenty-Fourth Annual Conference on Physical Electronics, Massachusetts Institute of Technology (1964).

(2) Arnal, R., "On the Initiation of Electric Discharges in Vacuum", C. R. Acad. Sci. (Paris), 238, 2061 (1954); "Electric Microdischarges in Dynamic Vacuum", Ann. Phys. (Paris), 10, 830 (1955); Available as Translation USAEC-TR-2837.

(3) Mansfield, W. K., "Prebreakdown Conduction in Continuously Pumped Vacuum Systems", Brit. J. Appl. Phys. 11, 454 (1960).

(4) Pivovar, L. I. and Gordienko, V. I., "Microdischarges and Predischarges Between Metal Electrodes in High Vacuum", Sov. Phys.-Tech. Phys. 28, 2101 (1958); "Prebreakdown Conduction Between Electrodes in Ultrahigh and High Vacuum", Sov. Phys.-Tech. Phys. 7, 908 (1963).

(5) Evans, R. D., "The Atomic Nucleus", Chapt. 20, 21, McGraw-Hill (1955).

BLANK PAGE

SECTION 3
DESIGN AND INTERPRETATION OF FACTORIAL EXPERIMENTS

3.1 The Principles of Factorial Experimental Design

The principles of factorial experimentation[1] are most simply described with a three factor example such as the kind used in the small block experiments (Section 5).

Three independent factors A, B, C representing respectively anode treatment, cathode treatment and electrode size are defined, each in two states known as "levels" for which a corresponding variable, the breakdown voltage, is measured.

Familiar techniques of physical experimentation arrive at the effect of A upon breakdown voltage by subtracting the measured values of breakdown voltage with A in each state, and similarly for B and C. This method, however, takes no account of possible interactions between factors. By this, it is meant that the difference in breakdown voltage for A in each of its states may vary when either of B or C are in each of their states. If the effect of A is measured as was just described, then the result must be accepted without concern for any coupling influence from B or C and is said to be "confounded" with these interactions. To avoid such a compromise, the effect of A alone can be derived from eight measurements corresponding to eight combinations of factors for which they are once only in each of their states.

It is convenient to label each of these eight combinations, or "treatments", by a sequence of letters. The presence of a letter signifies that the factor labeled similarly is in one of its two states, arbitrarily known as the "high level". When the factor is in the remaining "low level" its symbol is omitted from the treatment code.

Not only can the main factorial influences A, B, C be derived from eight readings, but also the interactions AB, AC, BC, ABC and, of course, the overall average breakdown voltage I. An interaction, say AB, as opposed to a factor A signifies the influence of B upon the factorial effect of A. In all cases, the factors and interactions are derived by combining four of the eight measurements with positive signs and four negatively in the manner given by Table 3-1 and dividing by four. This excludes the mean effect I for which an overall average of eight results is taken. The particular code sequence and array of signs constitute a method of calculation known as the "Yates Algorithm".

The origin of these signs will be derived as follows. Each letter occurs four times in the treatment sequence, thus there are four readings with the A factor in its high level state and four in its low level state. The A effect is, therefore, simply obtained by subtracting the average breakdown voltage with A at its low level from that with A at its high level. Similar procedures apply for B and C.

Of the four treatments with A in its high level state, two include B at its high level together with two at its low level and similarly for factor C. By subtracting the average results for these two pairs, the B effect is extracted but only for A in its high level state. Another B effect for A in its low level state may be similarly derived from the remaining four treatments. The AB interaction is then defined as the difference between the B effect for A at the high and low levels. It may be calculated by subtracting the two average B effects just mentioned.

Table 3-1. Sign Sequences for Derivation of Effects and Interactions (Capital Letters) from Treatments (Small Letters)

Treatments	Factors							
	A	B	AB	C	AC	BC	ABC	I
(1)	-	-	+	-	+	+	-	+
a	+	-	-	-	-	+	+	+
b	-	+	-	-	+	-	+	+
ab	+	+	+	-	-	-	-	+
c	-	-	+	+	-	-	+	+
ac	+	-	-	+	+	-	-	+
bc	-	+	-	+	-	+	-	+
abc	+	+	+	+	+	+	+	+

An inspection of the signs in the table will readily verify the statements made above. There is, however, an interesting and useful property of the table. If the signs in the A and B columns are multiplied together they are each the same as the corresponding sign in the AB column. The inverse process of multiplying the AB column by the B column will also yield the A column. Thus the multiplicative properties of the columns are:

$$A \times B \equiv AB \tag{3-1}$$

$$AB \times B \equiv A \tag{3-2}$$

The latter property requires:

$$B \times B \equiv 1 \tag{3-3}$$

In a similar manner, all of the interactions may be obtained from the A, B and C columns. Neither of these three, however, can be obtained by multiplication of the other two and they are, therefore, independent.

The properties just described are those of a finite cyclic group and A, B and C are an irreducible set. They are not unique, however, and other sets can be derived by multiplication. Thus, any pair of A, B, C with ABC gives three other sets and any two second order interactions with I gives three more, making seven in all.

Sometimes it is neither desirable nor economical to perform all eight of the treatments and a technique exists for cutting these in half but at the same time confounding some factors and interactions. The choice of which factors will be confounded is of course up to the experimenter's discretion. This deliberate confounding of effects produces a "partial factorial design" as follows.

Replace the ABC column by the I column so there are now two columns alike. Multiplication of each of the other columns according to the rules just given reveals that three others also turn out alike. Thus:

$$\left.\begin{aligned} I &= ABC \\ A &= BC \\ B &= AC \\ C &= AB \end{aligned}\right\} \qquad (3\text{-}4)$$

A, B and C are no longer independent factors, but are confounded with the second order interactions. If all eight treatments were carried out and processed in this way, the maximum information would not be extracted. This is, of course, because the full factorial method uses each reading only once to calculate a factor or interaction, hence the concept that any column is independent of the others. When two columns are equal, the same readings are used twice for calculating different factors.

This calculation method would be clearly wasteful but, since certain factors are clearly confounded, it is of no use to perform treatments with confounded codes. Thus, in the case above, identical treatments would be:

$$\left.\begin{aligned} (1) &\equiv abc \\ a &\equiv bc \\ b &\equiv ac \\ c &\equiv ab \end{aligned}\right\} \qquad (3\text{-}5)$$

Hence, the number of treatments can be halved. The ground rule for this case was:

$$I = ABC \qquad (3\text{-}6)$$

and is known as the "defining relation". Other defining relations and their consequences are given in Table 3-2.

There are, in this case, four possible ways to confound the treatments and to cut the experiment in half, creating what is called a "half replicate" factorial experiment.

A second order of confounding is possible by making two columns alike and one defining relation is:

$$I = AB = ABC \tag{3-7}$$

This will cut down the eight treatments to the minimum possible which is two. Such a design is known as a "quarter replicate" factorial experiment.

Table 3-2. Defining Relations and Consequently Confounded Factors

$I \equiv AB$	$I \equiv BC$	$I \equiv AC$
$A \equiv B$	$A \equiv ABC$	$A \equiv C$
$C \equiv ABC$	$B \equiv C$	$B \equiv ABC$
$BC \equiv AC$	$AB \equiv AC$	$AB \equiv BC$

A geometrical way to visualize the process is shown in Figure 3-1. An abstract vector space is constructed in three-dimensions representing the three irreducible factors A, B, C which are vector quantities. The eight corners of a cube can be labeled with the appropriate treatment code since they are displacements along the abstract vector directions. Each displacement along a vector is noted by a letter, thus abc means that it is reached from treatment (1) in three steps along mutually orthogonal vectors, there being six ways of doing this. Movement along a vector implies subtraction of two treatment results and that the corresponding factor is being accounted for in the measurement. Parallel vectors can be used to remove confounding. Thus, averaging with bc - c removes the confounding of the b - (1) result by c with which it is orthogonal. Likewise, abc - ac removes the confounding represented by either of the two orthogonal vectors ac - (1) and abc - b which represent the AC interaction. Thus, any four measurements on a surface represent two results which are mutually confounding. The surface is characterized by the normal which is the vector product of the sides, in this case it is B x AC.

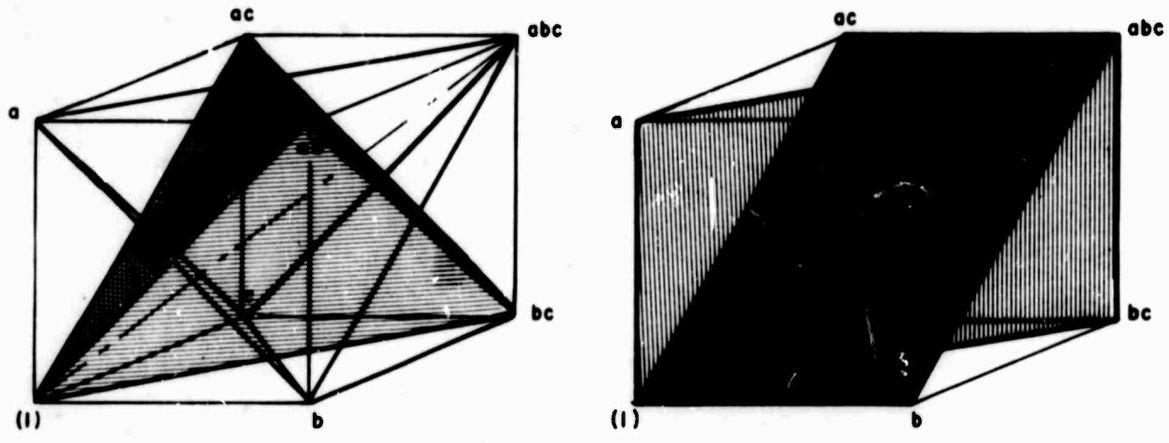

Figure 3-1. Geometrical View of Factorial Design

Two other similar diagonal hypersurfaces through the cube have one of their corners at treatment (1) and are specified by the vectors A x BC and C x AB. Thus, three surfaces exist which are specified by mutually orthogonal vectors and correspond with each other in the manner prescribed by the defining relation I = ABC. All of these surfaces have the vector abc - (1) in common, so they are derived from each other by orthogonal rotation about this axis. The defining relation thus specifies the vector axis about which three mutually orthogonal hypersurfaces are rotated and upon which measurements are made. If any of these three sets of four treatments are chosen, the factors represented by the components of the vector product representing the surface are confounded. Since only half of the results are needed, then only those on either one of the tetrahedra shown need to be used. The edges of these tetrahedra are orthogonal diagonals of each side of the original cube but their faces are parallel, signifying confounding of all vector factors on those sides.

It is worthy of note that the three hypersurfaces A x BC, B x AC and C x AB are also orthogonal by rotation about any of the three diagonals abc - (1), ac - b and bc - a, each of which is orthogonal to a face of both tetrahedra, so the system is completely symmetrical.

All that has been said can be carried out for any number of independent vectors and the principles are the same, but of course the level of abstraction is greater.

The breakdown voltage, V_B, can be considered as a function of several factors defining an abstract vector space. By measuring the changes in V_B due to small changes in each factor, the appropriate partial derivatives of V_B with regard to these factors are derived. Hence the higher order interactions correspond to higher order partial derivatives. If the perturbations of the main factors are not small then the changes induced in V_B are not good indications of the first derivatives. Better estimates would, of course, be obtained from three level experiments.

The defining relation chosen for the seven factor exploratory experiment to be described in Section 4 is:

$$I = - ABDFG = - CDEFG = ABCE \qquad (3\text{-}8)$$

The seven main factors and the interactions with which they are confounded appear in Table 3-3. It is assumed as a design philosophy that the third order interactions will be much smaller in magnitude than the main effects and so can be neglected as can those interactions of still higher order.

The justification for this assumption can most easily be argued from the geometrical standpoint. It is instructive to compare the Yates Algorithm with the numerical analogue of calculating partial differential coefficients from a set of data. There is really no fundamental difference because each method calculates derivatives of a function in abstract space. Since each succeeding order derivative is obtained from the difference between estimates from the order before it, then the errors involved are cumulative (Table 3-4). It is, therefore, to be expected that statistical variations will ultimately mask any small effect which may occur.

It can be argued that if widely spaced levels could be chosen for the main effects, then this would be less severe. Such a situation is, of course, possible because nothing is known initially about the effects. In this case, reliable estimates would be obtained for some derivatives but the main order

Table 3-3. Main Effects and Their Confounding Interactions

I	= - ABDFG	= - CDEFG	= ABCE
A	= - BDFG	= - ACDEFG	= BCE
B	= - ADFG	= - BCDEFG	= ACE
C	= - ABCDFG	= - DEFG	= ABE
D	= - ABFG	= - CEFG	= ABCDE
E	= - ABDEFG	= - CDFG	= ABC
F	= - ABDG	= - CDEG	= ABCEF
G	= - ABDF	= - CDEF	= ABCEG

Table 3-4. Analogy Between Yates Algorithm and Numerical Differentiation Method

(i)			
	[a - (i)]		
a			
		[ab - b - a + (i)]	
b			
	[ab - b]		
ab			
			[abc - bc - ac + c - ab + b + a - (1)]
c			
	[ac - c]		
ac			
		[abc - bc - ac + c]	
bc			
	[abc - bc]		
abc			
	↑ Average These for First Derivative (A Effect)	↑ Average These for Second Derivative (AB Effect)	↑ Third Derivative (ABC Effect)

effects (first derivatives) would be unreliable as is readily observed from the appropriate Taylor-McLauren expansion.

Thus the neglect of high order interactions implies that the initially chosen difference in factor levels is small.

With this in mind, the yields from this experiment will be those in Table 3-5. Six second order interactions (AB, CE, AC, BE, AE, BC) appear confounded with each other in this design and so cannot be defined specifically.

Table 3-5. I = - ABDFG = - CDEFG = ABCE Yields of Yates Algorithm

1	Mean	12	ABE + C	23	BDG - AF
2	A	13	DE	24	ABDG - F
3	B	14	ADE	25	EG
4	AB + CE	15	BDE	26	AEG
5	D	16	ABDE + CD	27	BEG
6	AD	17	G	28	ABEG + CG
7	BD	18	AG	29	DEG - CF
8	ABD - FG	19	BG	30	ADEG
9	E	20	AGB - DF	31	BDEG
10	AE + BC	21	DG	32	ABDEG - EF
11	BE + AC	22	ADG - BF		

3.2 Statistical Techniques

In an exploratory investigation such as will be described, there is no guarantee that all of the relevant factors are under control, so some statistical scatter must be anticipated. To deal with this, statistical techniques must be employed to separate the influences of controlled factors from the background fluctuations. A valuable graphical method is that known as the "half-normal plot" pioneered by Daniel.[2]

Consider the 31 effects and the overall average derived from a seven factor quarter replicate experiment. If none of the controlled factors are significant, the corresponding estimates will be scattered about the average in a Gaussian distribution according to the lack of control of unexpected influences. The estimates of the effects can be ordered as a set in order of rank independent of their signs.

The signs of estimates are arbitrary; they merely depend on what is labeled positive and what is labeled negative in the two levels of each factor. So the absolute values of the estimates are all that are needed, so far as significance is concerned. If the normal distribution of estimates is "folded" in the middle (at 0) and all probabilities to the left of the fold are added to those to the right of the fold, the distribution of the now-positive estimates is obtained; that is, the probability distribution of the absolute values of the estimates. Let us consider this distribution.

Let a random variable, x, be normally distributed with mean λ and variance σ^2. The density function of x is:

$$f(x) = \frac{1}{\sigma\sqrt{2\pi}} \exp\left\{-\frac{1}{2}\left|\frac{x-\lambda}{\sigma}\right|^2\right\} \qquad -\infty < x < \infty \qquad (3\text{-}9)$$

Consider $u = |x|$; the normal distribution is "folded" at $x = 0$. The density function of $|x|$ is well known. It is:

$$g(u) = \frac{1}{\sigma\sqrt{2\pi}} \left[\exp\left\{ -\frac{(u-\lambda)^2}{2\sigma^2} \right\} + \exp\left\{ -\frac{(u+\lambda)^2}{2\sigma^2} \right\} \right] \qquad (3\text{-}10)$$

$$u \leq 0$$

The mean E (u) and the variance σ^2 (u) are given by:

$$E(U) = \int_0^\infty u\, g(u)\, du = \sqrt{\frac{2}{\pi}}\,\sigma \exp\left(-\frac{\lambda^2}{2\sigma^2} \right) + \lambda \left[1 - 2F\left(-\frac{\lambda}{\sigma} \right) \right] \qquad (3\text{-}11)$$

$$\sigma^2(u) = \int_0^\infty \left[u - E(u) \right]^2 g(u)\, du$$

$$= \lambda^2 + \sigma^2 - \left\{ \sqrt{\frac{2}{\pi}}\,\sigma \exp\left(-\frac{\lambda^2}{2\sigma^2} \right) + \lambda \left[1 - 2F\left(-\frac{\lambda}{\sigma} \right) \right] \right\}^2 \qquad (3\text{-}12)$$

where:

$$F(t) = \frac{1}{2\pi} \int_{-\infty}^{t} \exp\left(-\frac{x^2}{2} \right) dx$$

sometimes written:

$$\int_{-\infty}^{t} N(0, 1)$$

In the case being considered, the normal distribution is folded at the mean; that is, $\lambda = 0$ is the point of the fold. This simplifies results greatly. We have:

$$g(u) = \frac{2}{\sigma\sqrt{2\pi}} \exp\left(-\frac{u^2}{2\sigma^2} \right) \qquad u \geq 0 \qquad (3\text{-}13)$$

$$E(u) = \sqrt{\frac{2}{\pi}}\,\sigma \qquad (3\text{-}14)$$

$$\sigma^2(u) = \sigma^2 - \left\{ \sqrt{\frac{2}{\pi}}\,\sigma \right\}^2 = \sigma^2 \left(1 - \frac{2}{\pi} \right) = \sigma^2 \left(\frac{\pi - 2}{\pi} \right) \qquad (3\text{-}15)$$

Leone, Nelson and Nottingham[3] (LNN) give a table of:

$$G(t) = \int_0^t g(u)\,du \tag{3-16}$$

classified by values of $E(u)/G(u)$. In our situation:

$$\frac{E(u)}{\sigma(u)} = \frac{\sqrt{\frac{2}{\pi}}\,\sigma}{\sqrt{\frac{\pi - 2}{\pi}}\,\sigma} = \sqrt{\frac{2}{\pi - 2}} = \sqrt{1.75194} = 1.3236 \tag{3-17}$$

It is important to note that the values of t in their tables are in standard u units.

When the normal distribution is folded at the mean $\lambda = 0$, as it is here, these values of $G(t)$ can be obtained directly from normal tables themselves. This fact leads to half-normal plots. We have:

$$G(t) = \int_0^t \frac{2}{\sigma\sqrt{2\pi}} \exp\left(-\frac{u^2}{2\sigma^2}\right) du \tag{3-18}$$

Let $u/\sigma = z$, $du = \sigma\,dz$:

$$G(t) = 2\int_0^{t/\sigma} \frac{1}{\sqrt{2\pi}} \exp\left(-\frac{z^2}{2}\right) dz = 2\int_0^{t/\sigma} N(0,1) \tag{3-19}$$

Values of t given by LNN are in standard u units:

$$t = K\sigma(u)$$

$$\frac{t}{\sigma} = K\frac{\sigma(u)}{\sigma} = K\sqrt{\frac{\pi - 2}{\pi}}$$

$$G(t) = 2\int_0^{\sqrt{\frac{\pi-2}{\pi}}\,t} N(0,1) \tag{3-20}$$

Graph paper can be suitably scaled using Table 3-6 so that normally distributed estimates fall on a straight line.

If, however, any factors are significant, they will influence the breakdown voltage in a systematic, rather than random, way. There will be two consequences. Firstly, the distribution

curve becomes non-symmetrical about the average because a real effect has a fixed sign. Secondly, repeated measurements will place the influences in an approximately well ordered sequence according to rank of significance. The rank of a significant factor will not vary much among the 31 possible levels, unless its magnitude is comparable with the fluctuations of uncontrolled factors. Thus, even if the half-normal plot is close to a straight line, the constancy of the rank of each factor is a guide to its significance if the experiment can be repeated. This is a useful guide if the estimates are small and masked by uncontrolled fluctuations.

Table 3-6. Half-Normal Function

t (in σ (u) Units)	$\frac{\pi - 2}{\pi}$	$\frac{\pi - 2}{\pi} t$	$2 \int_0^{\frac{\pi-2}{\pi} t} N(0,1)$	
0.5	0.60285	0.30143	2 x 0.118	= 0.236
1.0	0.60285	0.60285	2 x 0.227	= 0.454
1.5	0.60285	0.90428	2 x 0.317	= 0.634
2.0	0.60285	1.20570	2 x 0.386	= 0.772
2.5	0.60285	1.50713	2 x 0.434	= 0.868
3.0	0.60285	1.80855	2 x 0.4646	= 0.929

3.3 References

(1) Kempthorne, O., "The Design and Analysis of Experiments", Wiley (1967).

(2) Daniel, C., "Use of Half-Normal Plots in Interpreting Factorial Two-Level Experiments", Technometrics 1, 311 (1959).

(3) Leone, F. C., Nelson, L. S. and Nottingham, R. B., Technometrics 3, 543 (1961).

SECTION 4
A PARTIAL FACTORIAL EXPLORATORY EXPERIMENT

4.1 Abstract

A partial factorial experiment has been designed in which the main factors were confounded with at least third order interactions to explore the most likely influences on vacuum breakdown. It was assumed that higher order interactions become progressively less important so that the confounding of the main effects was insignificant. Anode shape, cathode shape and system bakeout were most consistently important while electrode materials and their combination with bakeout appeared less so. Some important second order interactions between electrode materials and shape were confounded with one another.

The logarithm of the prebreakdown current was found to decrease with the square root of gap separation after conditioning but only for gap separations above about 0.5 cm. Prebreakdown pressure surges preceded breakdown at a threshold voltage increasing approximately as the square root of gap separation in a similar way to the breakdown voltage.

The results are consistent with a breakdown mechanism in which gas and vapor is evolved from the anode by electron beam heating and then ionized sufficiently to lead to voltage collapse.

4.2 Factors Affecting Breakdown

The 16 factors shown in Table 4-1 were considered the most likely contributors to the breakdown process. They are separated into two groups, flexible and inflexible. The flexible factors can all be varied continuously without disturbing the test setup. The inflexible factors, on the other hand, are constructional and with the exception of bakeout they cannot be varied without opening the vacuum test chamber. It was also recognized that the last four of the inflexible factors were concerned with a particular application and they were dropped from the initial investigation to reduce the complexity and accelerate the investigation. They will be introduced into another phase of the experiment.

Meanwhile the remaining factors will be investigated at two levels. It is of interest to note here that the magnetic field may be regarded as two independent factors; namely, horizontal and vertical, and will be described in Section 5.

No factorial experiments have been completed yet to study the influence of the dielectric envelope, residual gas pressure, energy storage in the power supply, or contaminant.

4.3 Apparatus

The apparatus has to satisfy the following requirements. The vacuum test chamber should evacuate to 10^{-9} torr and be free of organic contamination. Further, it is required to bake to 400°C either the chamber and contents, or the electrodes alone. Within the chamber a voltage up to 300 kV is specified for application across the electrode gap, and in some experiments a magnetic field of

Table 4-1. Inflexible and Flexible Factors

Inflexible Factors	Flexible Factors
1. Cathode Material	12. Residual Gas Pressure
2. Anode Material	13. Energy of Supply
3. Cathode Finish	14. Contaminant
4. Anode Finish	15. Magnetic Field
5. Cathode Geometry	16. Electrode Spacing
6. Anode Geometry	
7. Vehicle Bakeout	
8. Envelope Material	
9. Envelope Diameter	
10. Electrode Shield Size	
11. Electrode Shield Placement	

500 gauss is required either perpendicular or parallel to the electric field vector. Finally, two levels of energy storage, 100 J and 7000 J, are desired together with the facility for diverting it in the latter case at variable times after initiation of a vacuum breakdown. The monitoring instrumentation developed during a preliminary experiment[1] is fitted to provide a continuous recording of the total and collimated X-radiation, the visible radiation, the gap current magnitude and wave shape, and the partial pressure of hydrogen as described in Section 2.

The test vehicle is shown in Figure 4-1. The vacuum chamber is made by welding together two spun hemispherical sections of 304 stainless steel, 36 inches in diameter by 1-1/8 inches thick. This thickness eliminates the need for welded flanges at the ports. The chamber is equipped with three 16-inch diameter ports. One is at the top for the electrode support and adjusting mechanism, another at the bottom for the bakeable feedthrough bushing, and the third at the side for access and electrode changes. There is also a 10-inch port for the ion pump, and 6-inch ports are available for optical and X-ray detectors, a mass spectrometer and controlled leak valve. Gold or copper O-ring seals are used throughout.

The power supply is a Van de Graaff generator located in its pressure vessel beneath the vacuum chamber (Figure 4-1). It has a stabilizing circuit which reduces the ripple and long term fluctuations to less than 1% and it provides precise voltage control up to 300 kV with a maximum current of 200 μa. It is connected to the electrodes via a 100 ohm resistor and the bakeable feedthrough bushing and has in parallel a 12-foot length of high voltage cable which both aids in the stabilization and stores up to 20 joules of energy, or serves as connection with the larger energy store. The design of the feedthrough bushing is shown in Figure 4-2. It consists of a bakeable ceramic-copper column which extends into the vacuum chamber and non-bakeable glass-aluminum column located in the Van de Graaff pressure tank. The ceramic column is brazed via a Monel alloy 404 flexure ring to a stainless steel flange and the latter makes a gold O-ring seal at the bottom port. The two columns are held

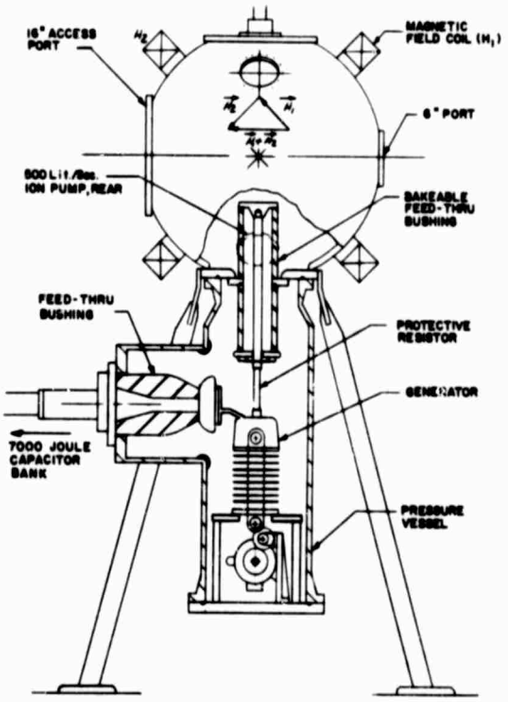

Figure 4-1. 300 kV Test Vehicle

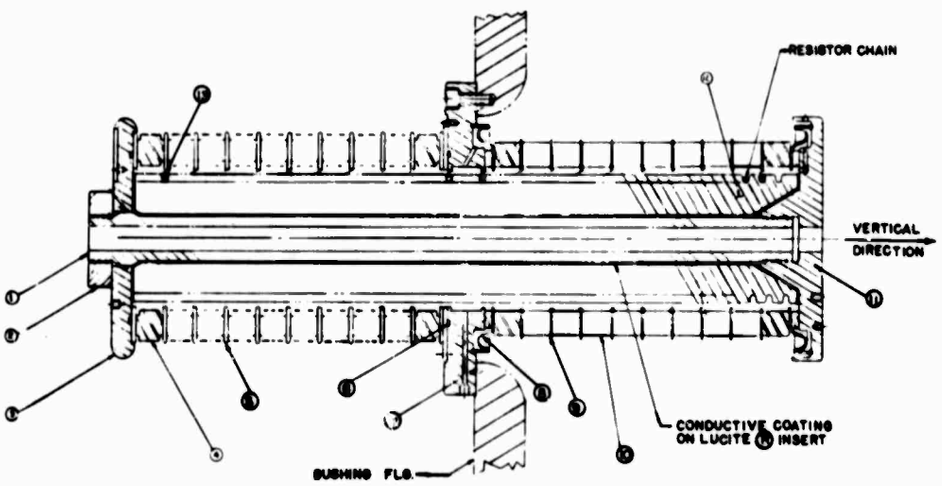

1. Tension Shaft
2. Tension Nut
3. End Cap
4. Glass Insulator
5. Aluminum Plane
6. Rubber O-Ring
7. Gold O-Ring
8. Monel 404 Flexure
9. Copper Plane
10. Ceramic Insulator
11. Pass For Electrode Structure
12. Lucite (R) Insert
13. Contact Spring

Figure 4-2. Bakeable Feedthrough Bushing

together using a stainless steel tension rod which also carried the heater and thermocouple leads for the high voltage electrode. The bushing is pressurized to 45 psia SF_6 and voltage grading is effected using a solid dielectric insert with a spiral groove along which are would two strings of 100 megohm resistors, one for each column. This insert also provides axial insulation at the ground plane.

Two electrode materials, OFHC copper and forged Ti-7Al-4Mo alloy have been used. The electrodes are 3 inches in diameter and have either spherical or Bruce profile.[2] The anode is fixed in position on top of the bakeable feedthrough bushing while the insulating support and adjusting mechanism for the cathode consists of a welded bellows construction which enables gaps up to 3 cm to be obtained. The cathode support system was designed with a minimum of stray capacitance to permit fast current monitoring. Heaters and thermocouples are located in each electrode so that they could be baked independently of the system.

The requirement of producing a magnetic field of 500 gauss in any selected direction relative to the electrode geometry was achieved using water-cooled cross coils (Figure 4-3) which could be placed over the chamber for test and removed for system bakeout. The dimensions are as follows:

Coil	Mean Radius	Copper Weight	Approximate Power
Inner	56.00 cm	430 lb	12.5 kw
Outer	67.44 cm	610 lb	17.0 kw

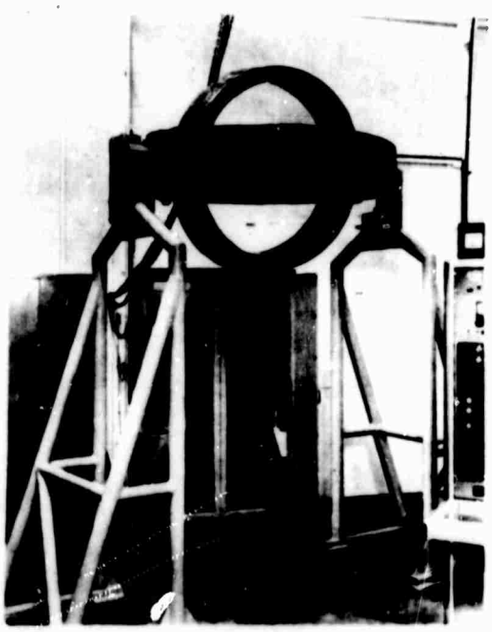

Figure 4-3. 500 Gauss Magnetic Field Coils and Power Supply

The 7000 joule energy storage unit consists of four 80 kV, 0.6 μF cylindrical Tobe Deutschmann capacitors, 20 inches high and 13 inches in diameter. They are stacked vertically as shown in

Figure 4-4 with grading resistors housed axially inside each unit in a vessel pressurized to 2 atmospheres of SF_6. Figure 4-4 also shows the location of the grounding mechanism and the energy diverter (crowbar). The control circuitry is so designed that it will cause the crowbar to fire and divert the stored energy at predetermined times after initiation of the main gap breakdown.

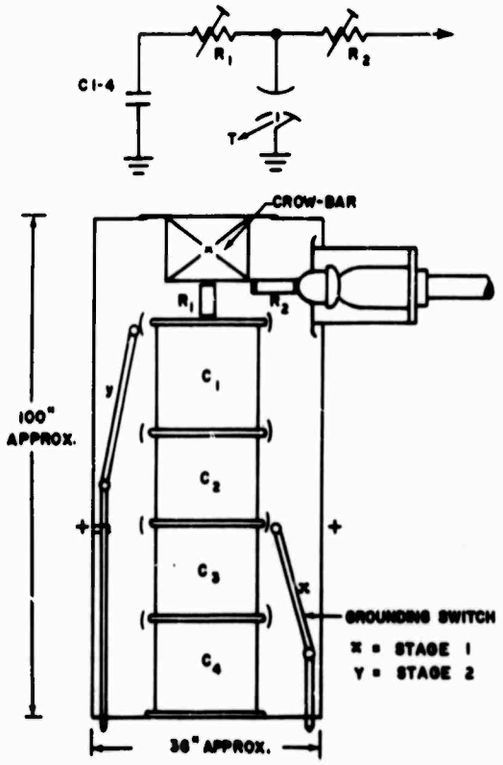

Figure 4-4. Outline of 300 kV Energy Storage System with Crowbar

4.4 Seven Factor Pilot Experiment

In applying factorial design to experiments on vacuum breakdown it was decided to conduct initially a two level, seven factor pilot experiment. This experiment should show that all factors are under adequate control and provide information on the effect of varying the most likely factors. A one-fourth replicate factorial design involving 32 treatments was chosen.[3] From this, the importance of all factors can be determined, but not all the interactions.

The factors for this pilot experiment were chosen on a basis of potential importance and the simplicity with which they could be varied. In fact, they consisted of the first seven inflexible factors listed in Table 4-1.

The selection of a particular experimental design and the assigning of letters to the factors determined which two-factor interactions are confounded. First, therefore, the several processes which have been proposed for breakdown were considered including field emission dependent processes,

the clump mechanism and ion exchange effects (microdischarges). The resultant assignment of letters to factors is shown in Table 4-2. The factors are represented by the letters A-G and the levels, high and low, by the letters a-g or the numeral 1, spectively. From this the main factor reactions and all but the following two factor interactions are measurable, AB, CE, AC, BE, AE, and BC, and also the effect of any two factor interaction involving the bakeout factor D is independent of any other main effect or two-factor interaction of interest.

The order of the 32 experiments was determined in a random manner and then arranged in a circle as shown in Figure 4-5. It is statistically acceptable to initiate the pilot experiment at any point of the circle and then to proceed either clockwise or counterclockwise. Treatment "bdefg" was chosen as the starting point and it was decided to proceed in the clockwise direction. The factor level for all treatments is shown in Table 4-3. Thus, for this first experiment, the electrodes only were baked and they were both highly polished titanium and of Bruce profile. Just prior to this treatment, the complete system was baked out, ensuring a clean test vehicle at the outset of the experiment.

4.5 Procedures

Controlled procedures are, of course, essential to reproducible results and good control is mandatory for the designed experiment. Methods for electrode preparation, installation, bakeout and voltage application were determined, and used to standardize the levels of the factors to be examined and to keep constant those factors to be held invariant.

4.5.1 Electrode Preparation and Installation

For coarse finish the electrode surfaces were wet ground with silicon carbide paper using successively finer grits in the sequence 180, 320, 400 and 600. For fine finish, the surfaces after grinding were polished with 15 micron alumina abrasive, and then with microcloth and alumina abrasives of 5, 1, 0.3 and 0.05 micron size both using a powered felt covered wheel or a spindle and by hand. At the termination of the grinding or polishing operations, the electrodes were rinsed in water and methyl alcohol and dried in hot air. Just prior to assembly in the test chamber, they were rinsed in acetone and trichloroethylene and wiped with acetone and methanol using cheese cloths. Finally, they were wiped with Foamwipes in the chamber. During electrode installation the chamber was continuously flushed with dry nitrogen which exhausted through the access port.

4.5.2 Bakeout

The baking cycle for both system and electrode bakeout was fixed at 16 hours. For 12 hours, the electrodes were between 400°C and 450°C, and for 8 hours the chamber was between 350°C and 400°C. In each case, the electrodes were allowed to cool to less than 75°C before test initiation. The pressure then was in the low 10^{-7} torr to mid 10^{-8} torr region if electrodes only were baked out, and in the low 10^{-8} torr region for system bakeout.

Table 4-2. Factors and Levels for Pilot Experiment

Factors	Letters	Levels
Cathode Material	C	1 - Ti-7Al-4Mo c - OFHC Cu
Cathode Finish	G	g - Fine 1 - Coarse
Cathode Geometry	B	b - Bruce Profile 1 - Sphere
Bakeout	D	1 - Complete System Bakeout d - Electrode Bakeout Only
Anode Material	A	1 - Ti-7Al-4Mo a - OFHC Cu
Anode Finish	F	f - Fine 1 - Coarse
Anode Geometry	E	e - Bruce Profile 1 - Sphere

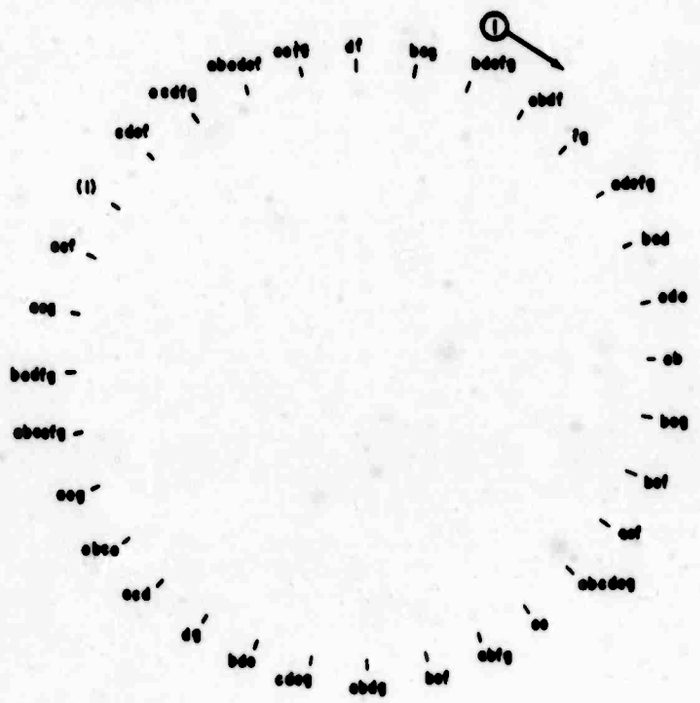

Figure 4-5. Random Selection Wheel for Pilot Experiment

Table 4-3. Order and Factor Level for Pilot Experiment

Experiment	Material	Cathode Finish	Geometry	Bakeout	Material	Anode Finish	Geometry
bdefg	Ti	Fine	Bruce	Electrode	Ti	Fine	Bruce
abdf	Ti	Coarse	Bruce	Electrode	Cu	Fine	Sphere
fg	Ti	Fine	Sphere	System	Ti	Fine	Sphere
adefg	Ti	Fine	Sphere	Electrode	Cu	Fine	Bruce
bcd	Cu	Coarse	Bruce	Electrode	Ti	Coarse	Sphere
ade	Ti	Coarse	Sphere	Electrode	Cu	Coarse	Bruce
ab	Ti	Coarse	Bruce	System	Cu	Coarse	Sphere
beg	Ti	Fine	Bruce	System	Ti	Coarse	Bruce
bef	Ti	Coarse	Bruce	System	Ti	Fine	Bruce
acf	Cu	Coarse	Sphere	System	Cu	Fine	Sphere
abcdeg	Cu	Fine	Bruce	Electrode	Cu	Coarse	Bruce
ce	Cu	Coarse	Sphere	System	Ti	Coarse	Bruce
abfg	Ti	Fine	Bruce	System	Cu	Fine	Sphere
bcf	Cu	Coarse	Bruce	System	Ti	Fine	Sphere
abdg	Ti	Fine	Bruce	Electrode	Cu	Coarse	Sphere
cdeg	Cu	Fine	Sphere	Electrode	Ti	Coarse	Bruce
bde	Ti	Coarse	Bruce	Electrode	Ti	Coarse	Bruce
dg	Ti	Fine	Sphere	Electrode	Ti	Coarse	Sphere
acd	Cu	Coarse	Sphere	Electrode	Cu	Coarse	Sphere
abce	Cu	Coarse	Bruce	System	Cu	Coarse	Bruce
aeg	Ti	Fine	Sphere	System	Cu	Coarse	Bruce
abcefg	Cu	Fine	Bruce	System	Cu	Fine	Bruce
bcdfg	Cu	Fine	Bruce	Electrode	Ti	Fine	Sphere
acg	Cu	Fine	Sphere	System	Cu	Coarse	Sphere
aef	Ti	Coarse	Sphere	System	Cu	Fine	Bruce
(1)	Ti	Coarse	Sphere	System	Ti	Coarse	Sphere
cdef	Cu	Coarse	Sphere	Electrode	Ti	Fine	Bruce
acdfg	Cu	Fine	Sphere	Electrode	Cu	Fine	Sphere
abcdef	Cu	Coarse	Bruce	Electrode	Cu	Fine	Bruce
cefg	Cu	Fine	Sphere	System	Ti	Fine	Bruce
df	Ti	Coarse	Sphere	Electrode	Ti	Fine	Sphere
bcg	Cu	Fine	Bruce	System	Ti	Coarse	Sphere

4.5.3 Voltage Application

The gap was initially set at 1.0 cm and the voltage increased in 10 kV increments every 2 minutes up to breakdown. The voltage was not switched off and was further increased at the same rate to a second breakdown after which the supply was switched off. This gave points 1 and 2 on Figure 4-6. The voltage was then increased rapidly to within 10 kV of the first breakdown voltage and then in 10 kV steps every 2 minutes until breakdown (point 3 of Figure 4-6). The gap was then set successively at 1.5, 2.0, 2.5, 3.0 and 0.5 cm, and the voltage increased rapidly to within 10 kV of the previous breakdown and then in 10 kV increments to breakdown, except in the 0.5 cm case when it was increased rapidly to 60 kV. This gave points 4, 5, 6, 7 and 8 of Figure 4-6. The gap was then re-set to 1.0 cm, the breakdown voltage checked (point 9) and the gap conditioned by sparking until the voltage was increased by about 25%. The voltage was then switched off and conditioned breakdown voltages obtained for all gaps (points 10 through 16).

During these operations, the following parameters were continuously recorded: total and collimated X-radiation, visible radiation, H_2 partial pressure and gap current.

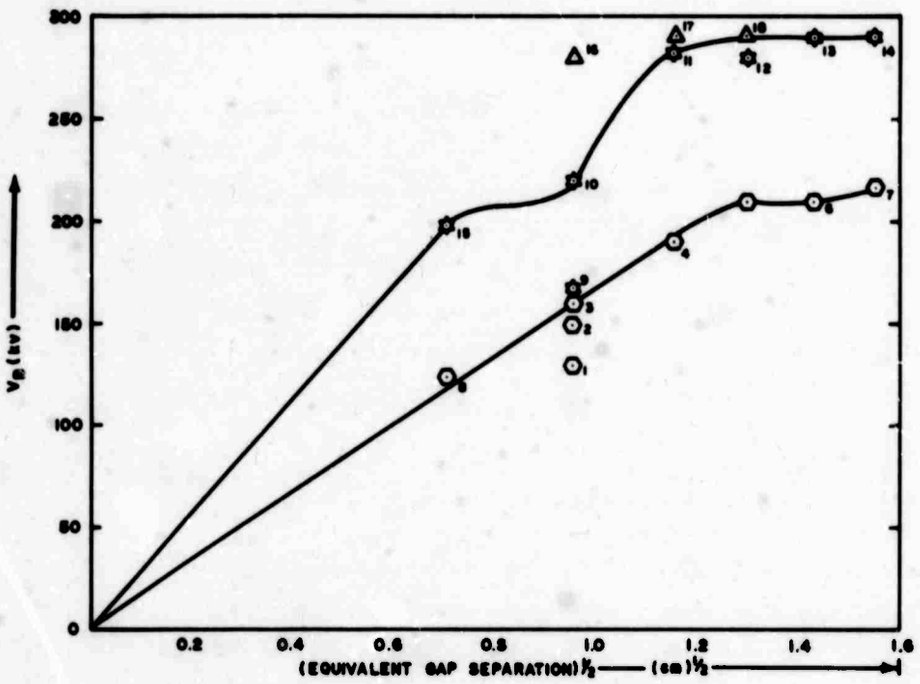

Figure 4-6. Sequence of Breakdowns for Treatment 'acg'

4.5.4 Current Monitoring

Figure 4-7 shows an electrical schematic of the voltage control and current monitoring apparatus. Charging current is fed to the Van de Graaff generator from a 20 kV power supply and is divided into a variety of paths. Two steady loads are those currents flowing through the grading

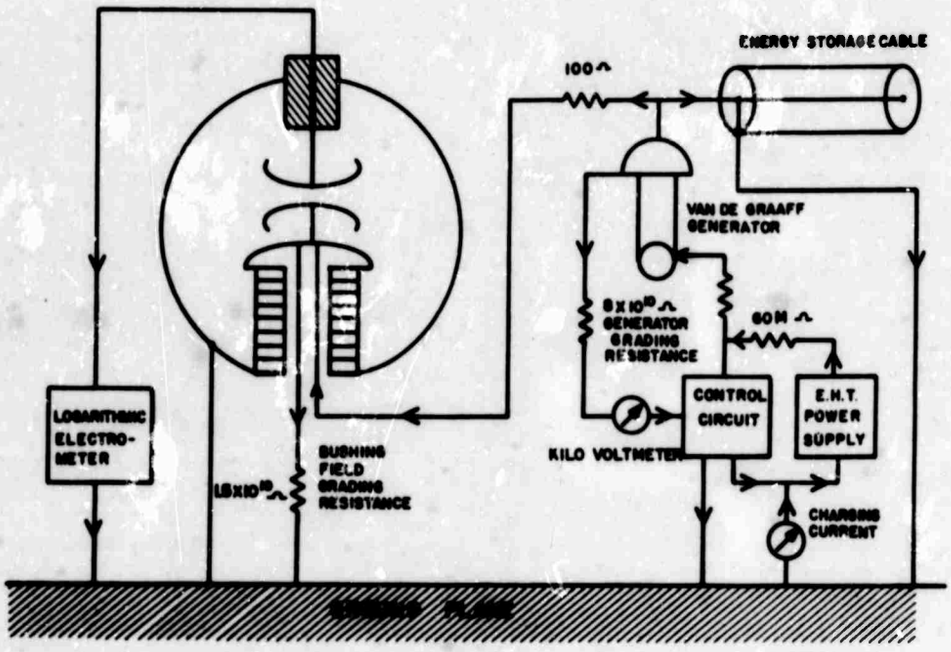

Figure 4-7. Electrical Schematic for Current Monitoring and Control

resistors of the Van de Graaff column and the feedthrough bushing which are 8×10^{10} ohm and 1.5×10^{10} ohm, respectively. In addition, there will be both breakdown and prebreakdown currents through the gap and a cable charging current after each vacuum discharge. This cable is standard 300 kV cable and serves both to provide a capacitance of about 400 pF and also to improve the generator stabilization.

The sum of all these currents was measured at the negative terminal of the 20 kV power supply. In addition, the gap current was measured and recorded using a logarithmic electrometer with a pen recorder. Finally, the Van de Graaff column current was measured and calibrated to yield terminal voltage.

4.6 Results

The results of the experiment have been presented graphically on half normal plots in Figures 4-8 through 4-14 for unconditioned electrodes in the gap range from 0.5 to 3.0 cm. In Figures 4-15 through 4-17 the remaining plots are presented for 1.0, 1.5 and 2.0 cn gaps after conditioning.

There is very little deviation from straight line plots in the first group except at 2.0 cm signifying that the estimates were small and masked by random influences. For the conditioned gaps, however, there appeared to be a little more effect. In an attempt to smooth out the random influences, a breakdown law of the form:

$$V_B = K d^{1/2} \qquad (4\text{-}1)$$

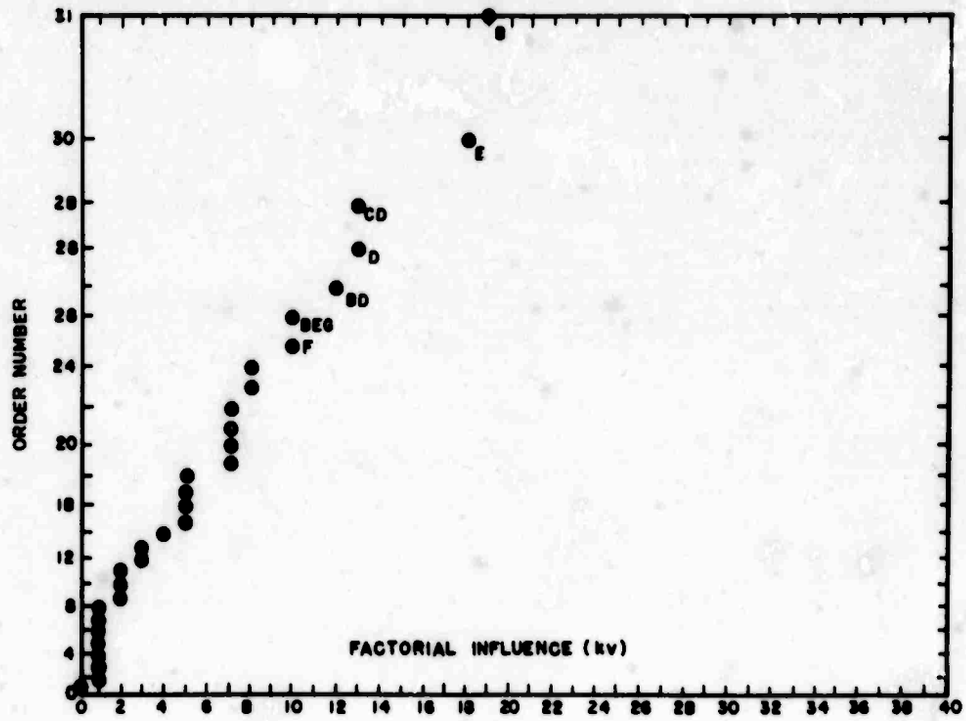

Figure 4-8. Half Normal Plot for 0.5 cm Unconditioned Gap

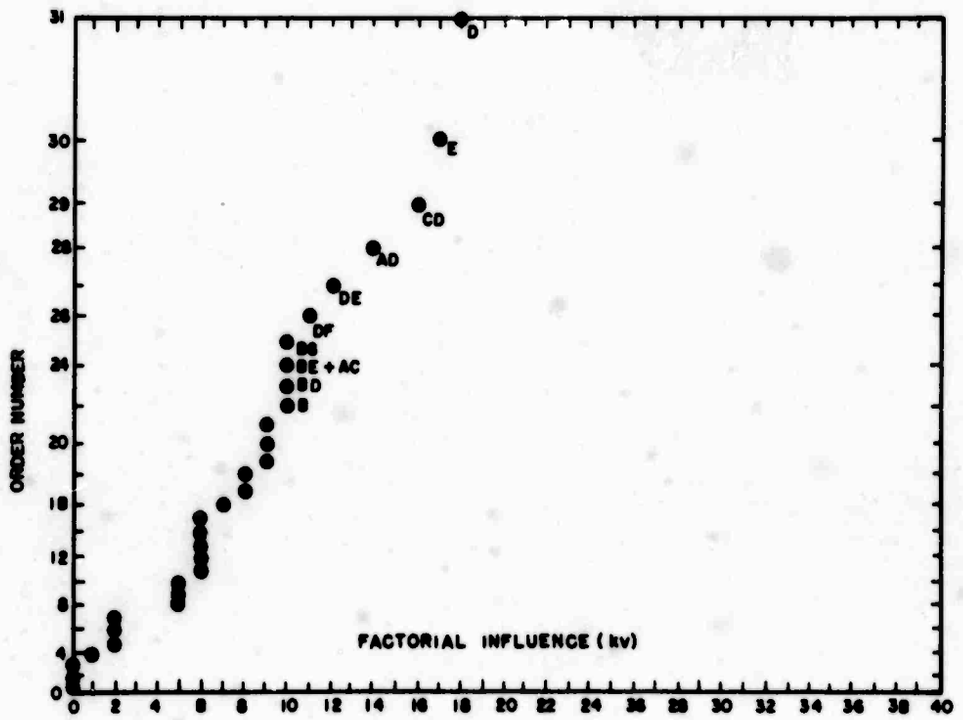

Figure 4-9. Half Normal Plot for 1.0 cm Unconditioned Gap, First Breakdown

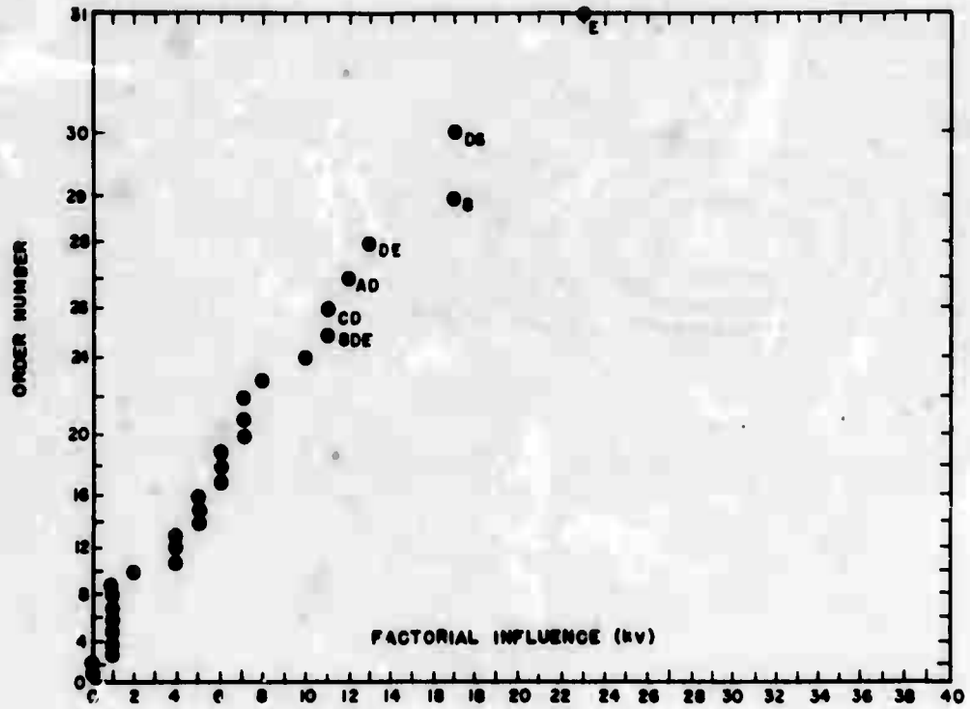

Figure 4-10. Half Normal Plot for 1.0 cm Unconditioned Gap, Third Breakdown

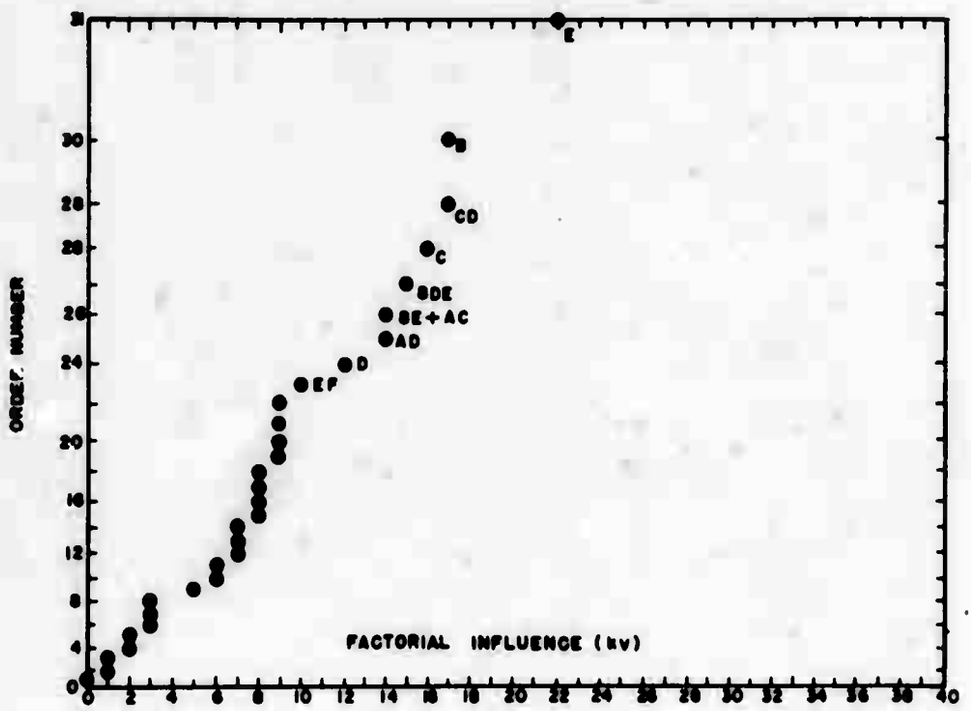

Figure 4-11. Half Normal Plot for 1.5 cm Unconditioned Gap

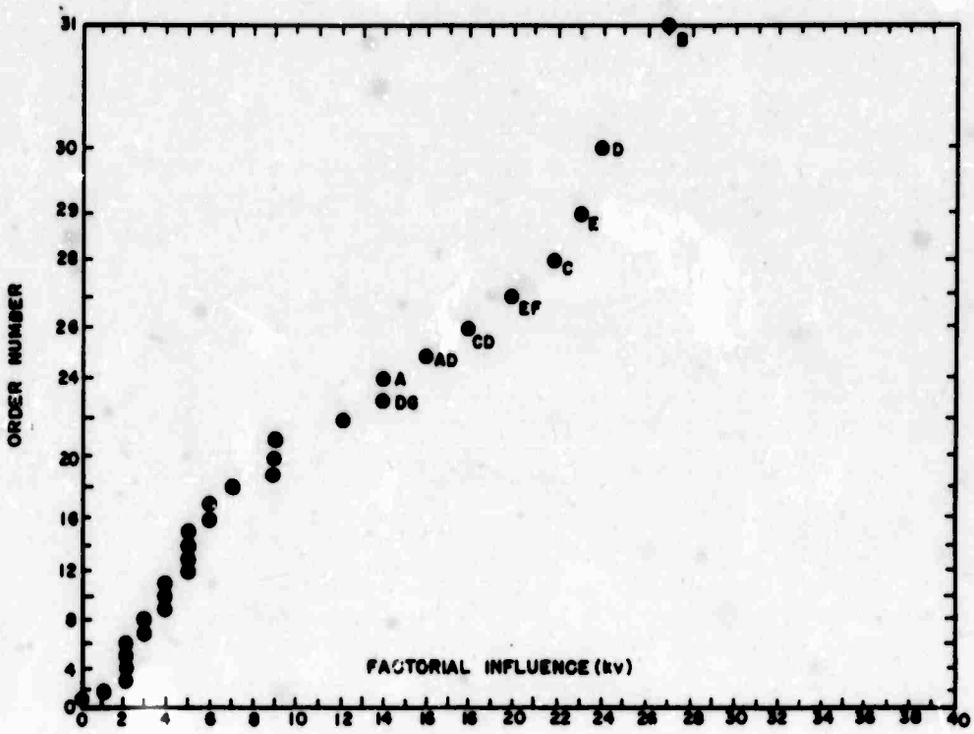

Figure 4-12. Half Normal Plot for 2.0 cm Unconditioned Gap

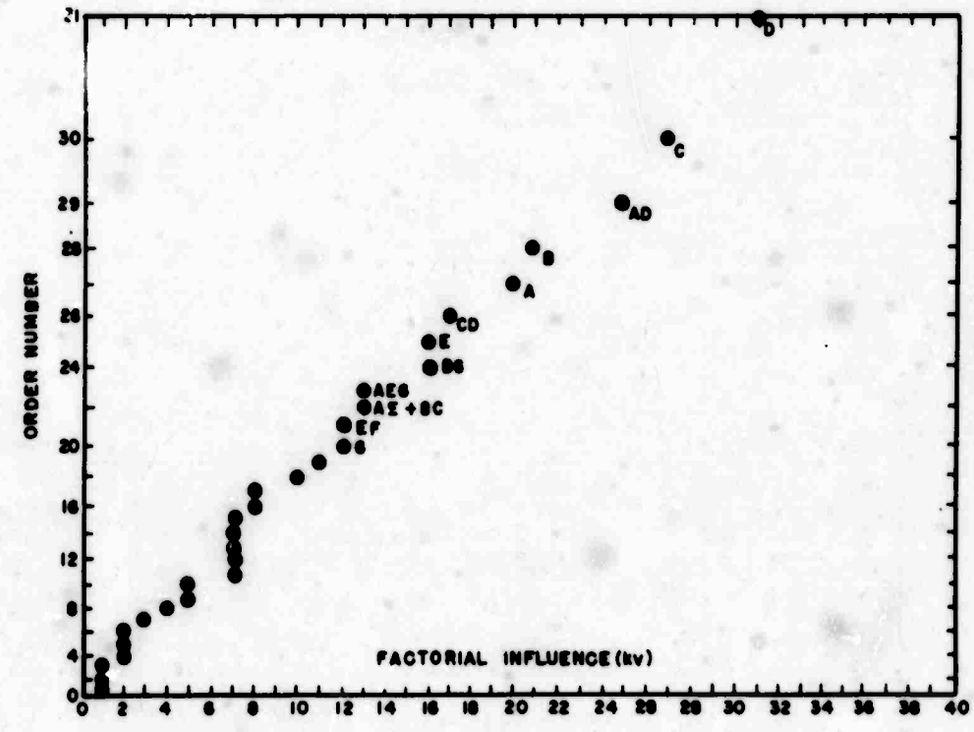

Figure 4-13. Half Normal Plot for 2.5 cm Unconditioned Gap

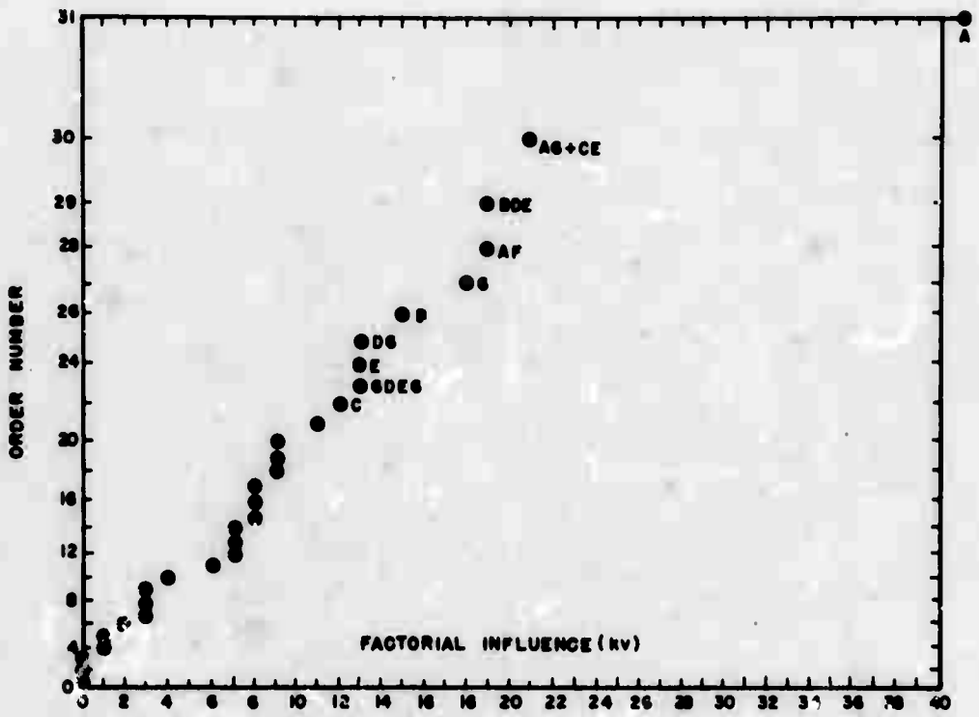

Figure 4-14. Half Normal Plot for 3.0 cm Unconditioned Gap

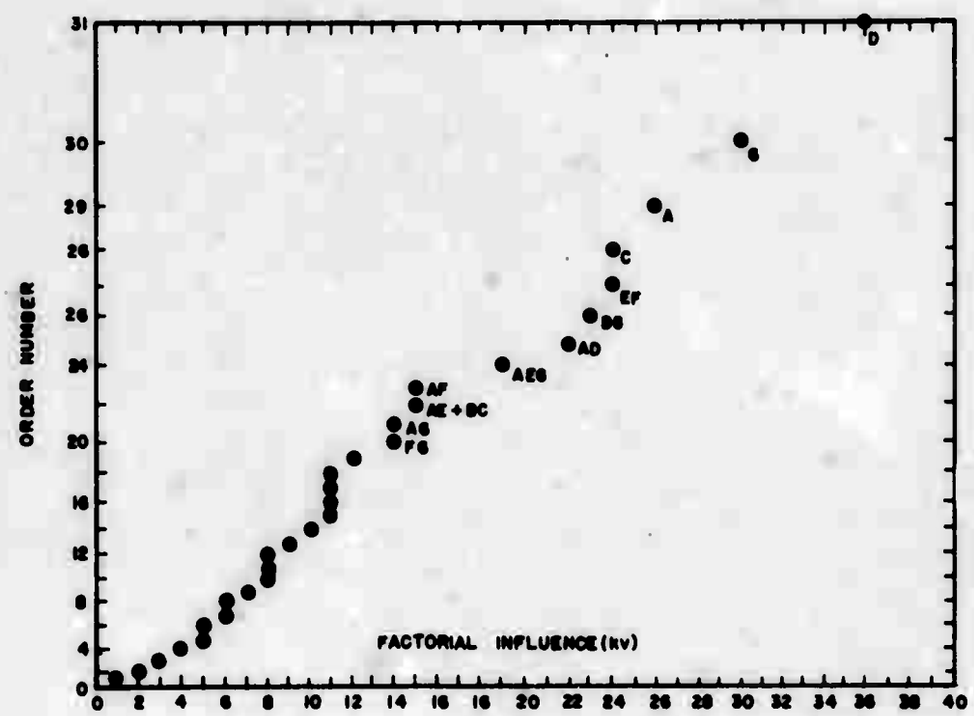

Figure 4-15. Half Normal Plot for 1.0 cm Conditioned Gap

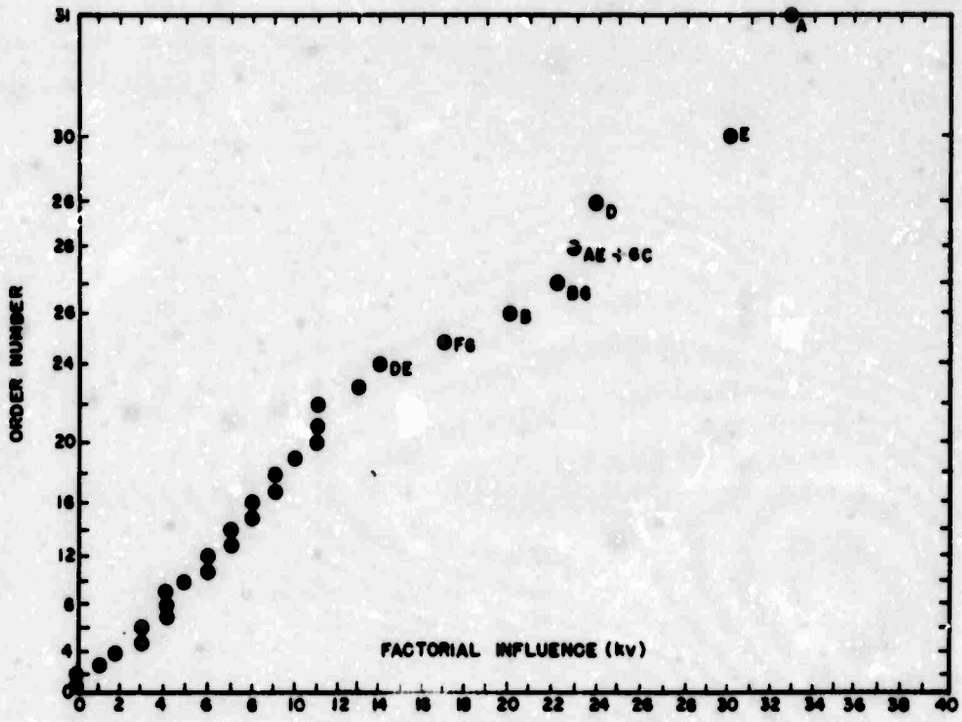

Figure 4-16. Half Normal Plot for 1.5 cm Conditioned Gap

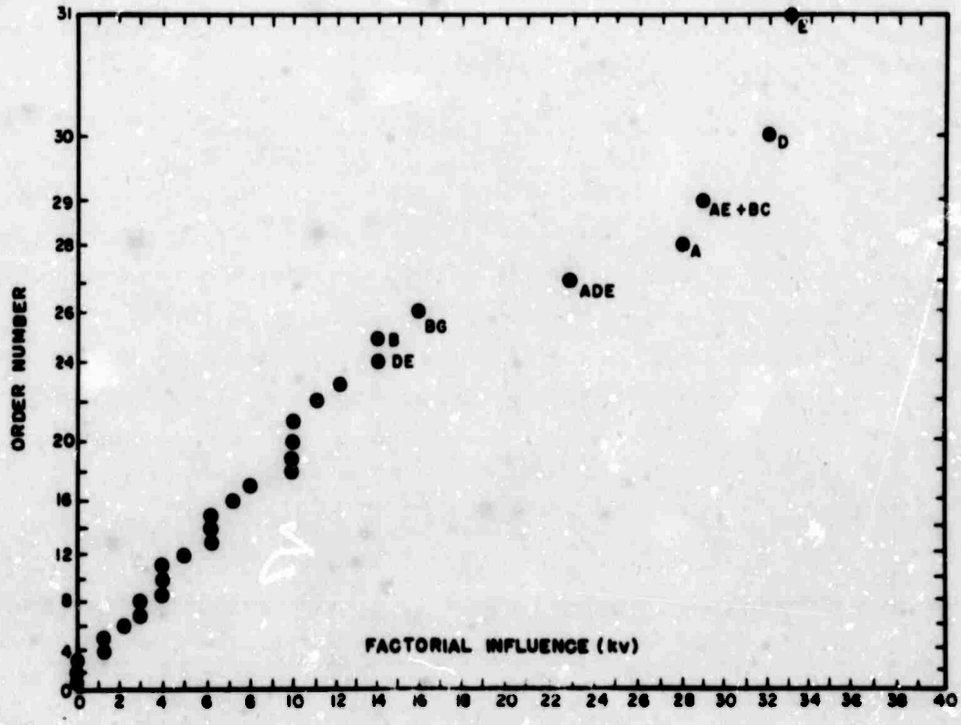

Figure 4-17. Half Normal Plot for 2.0 cm Conditioned Gap

was assumed and values of the slope K were calculated from the conditioned results at 1.0, 1.5 and 2.0 cm. The slopes obtained averaged out the random influences and are presented on a half normal plot in Figure 4-18 which is encouragingly non-linear. The deviations from linearity show that the anode material A, anode shape E, cathode shape B, bakeout D, and the interaction AE + BC are the most significant.

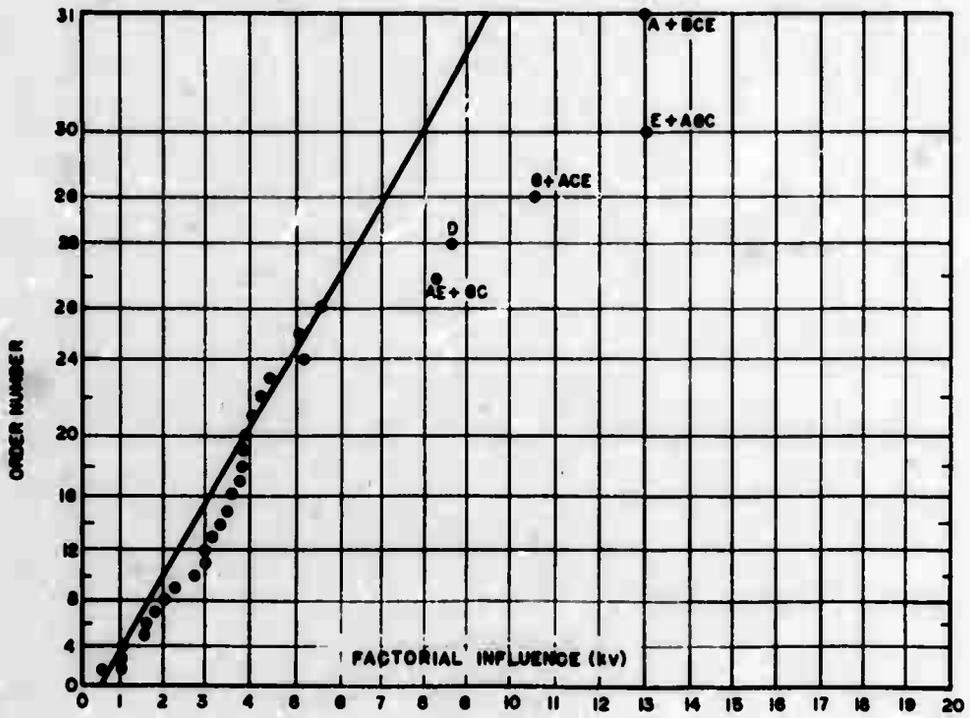

Figure 4-18. Half Normal Plot for the Smoothed Results for Conditioned Electrodes

In Table 4-4, the estimates have been presented according to their reverse rank of importance (31 representing the most important effect) and the same factors appear.

Previous to conditioning, however (sequence 1-7 in Table 4-4), the anode material assumes less importance and after conditioning (sequence 8-10) the cathode material C is less important as are the interactions AD and CD representing the influence of system bakeout on the effects of anode and cathode material.

Throughout the whole experiment, the anode shape E, cathode shape B, and system bakeout D, occupy positions of high rank in the hierarchy of significant influences. The cathode shape B and anode shape E have average positions of 28 ± 3 and 29 ± 3 respectively and system bakeout D has an average of 30 ± 3. These are consistently the most important influences and the relatively small scatter around the averages testify to their reliability as explained in Section 3.2.

Table 4-4. Significant Estimates Presented in Reverse Rank as a Function of Gap Separation and Time Sequence

	Sequence									
	1	2	3	4	5	6	7	8	9	10
	Gap									
	1.0	1.0	1.5	2.0	2.5	3.0	0.5	1.0	1.5	2.0
A				24	27	29		31	31	28
B	22	29	30	31	28	30	31	26	26	25
C			28	28	30	28		22		
D	31		24	30	31	31	28		29	30
E	30	31	31	29	25		30	24	30	31
AD	28	27	25	25	29	25				
CD	29	26	29	26	26		29			

4.7 Prebreakdown Phenomena

Throughout the experiment, the prebreakdown current was measured at every voltage step up to breakdown. The logarithm of the current as a function of voltage indicated that not only did it deviate from behavior expected from the simple Fowler-Nordheim law but that the characteristics (Figures 4-19 through 4-21) varied according to the amount of conditioning (i.e., number of previous breakdowns). A most significant measurement was the logarithm of the current immediately preceding breakdown.

Early in the program, difficulty was encountered in detecting the initially very feeble breakdowns and a procedure was developed in which the voltage was raised until they appeared in rapid succession. Using this as the breakdown voltage, it was found to increase quite accurately with the square root of gap separation and the corresponding logarithm of the ultimate prebreakdown current decreased linearly with the same variable (Figures 4-22 and 4-23). This, however, proved not to be the general case and the current was almost constant for low gap separations.

The appearance of this follows readily from the Fowler-Nordheim law:

$$I = A \left(\beta \frac{V}{d} \right)^2 \exp \left(- \frac{B d}{\beta V} \right) \qquad (4\text{-}2)$$

where A includes the area of the emitting site. If the breakdown voltage obeys a law:

$$V_B = K d^{1/2} \qquad (4\text{-}1)$$

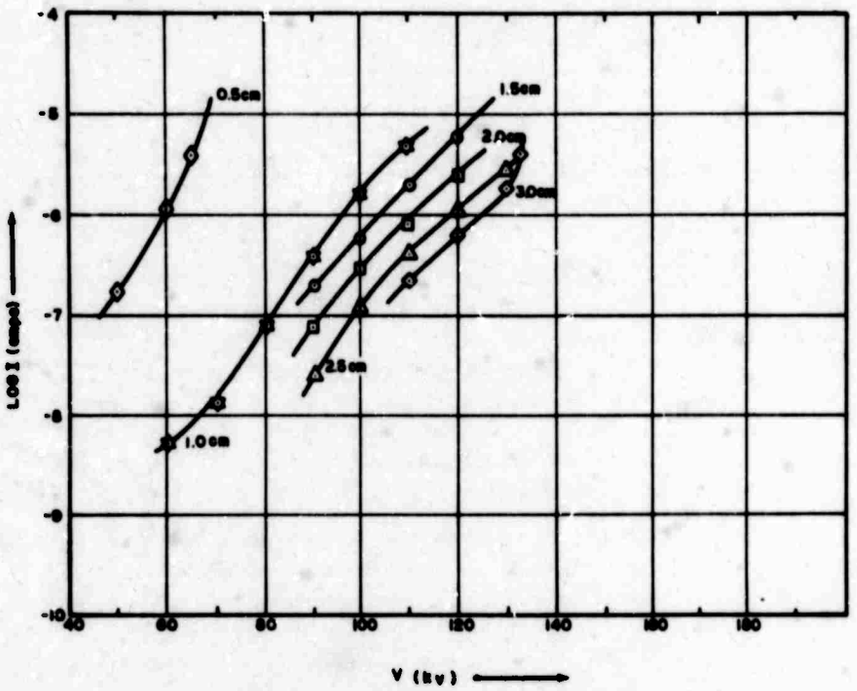

Figure 4-19. Current Variation up to Breakdown at Different Gap Separations (Test Sequence 1)

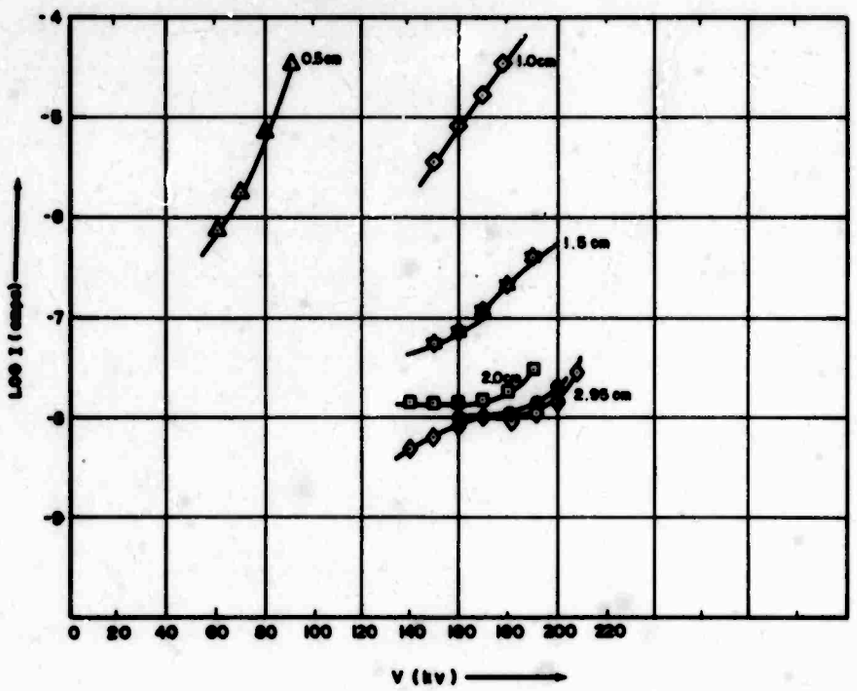

Figure 4-20. Current Variation up to Breakdown at Different Gap Separations (Test Sequence 2)

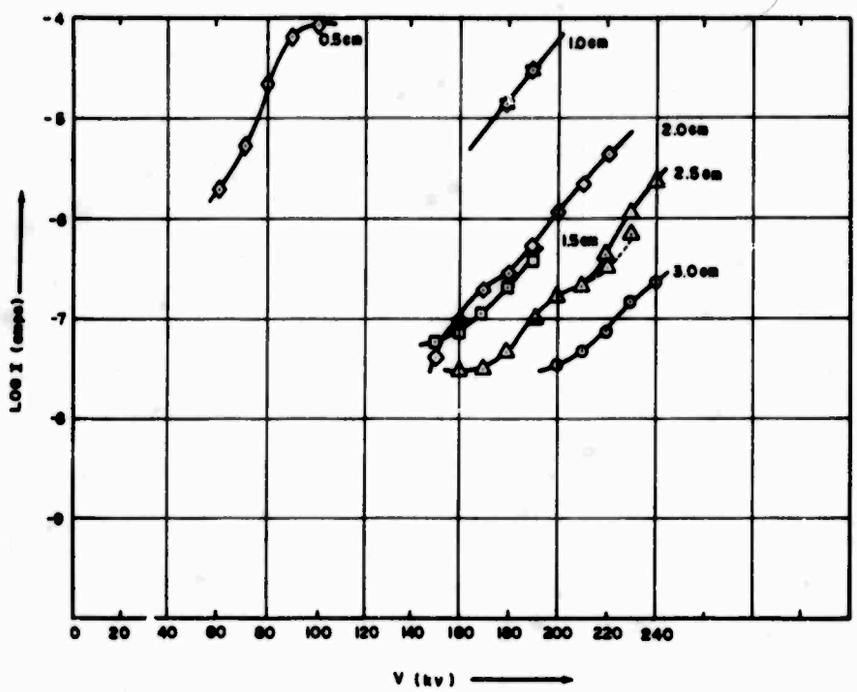

Figure 4-21. Current Variation up to Breakdown at Different Gap Separations (Test Sequence 3)

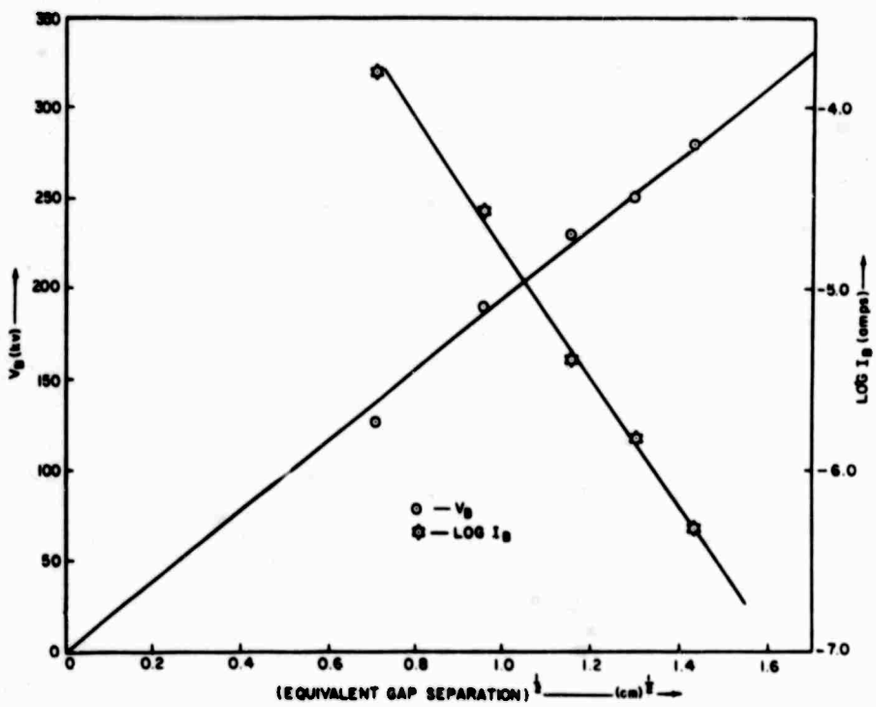

Figure 4-22. The Square Root Law for Treatment acf (Cu Sphere-Cu Sphere)

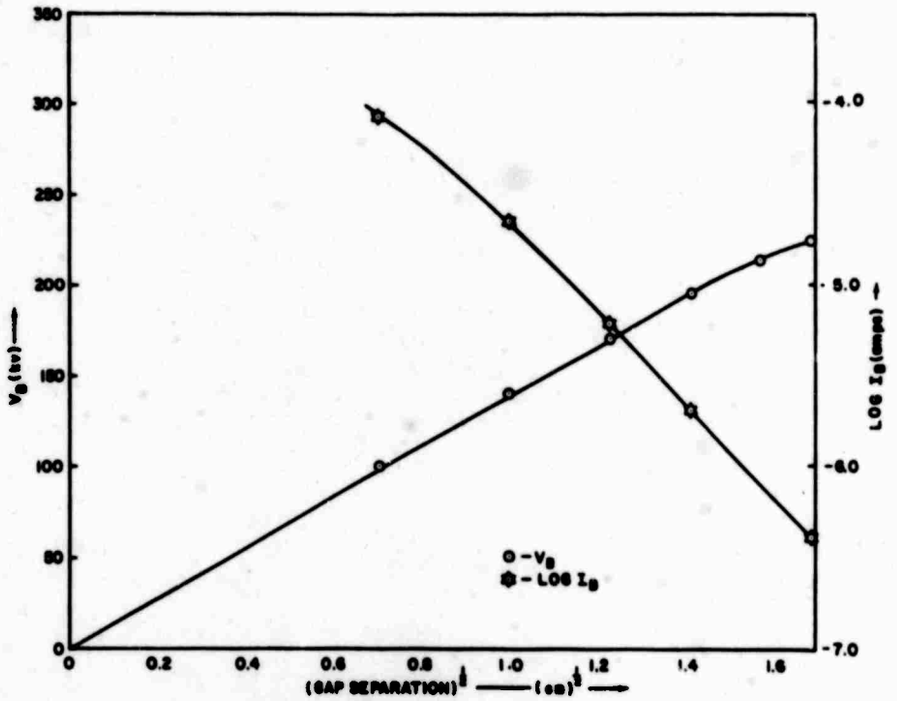

Figure 4-23. The Square Root Law for Treatment abcdeg (Cu Bruce-Cu Bruce)

then it follows that:

$$\log I = \log A + 2 \log \left\{ \frac{\beta^2 K^2}{d} \right\} - \frac{B d^{1/2}}{\beta K} \qquad (4\text{-}3)$$

Thus log I decreases linearly with $d^{1/2}$ provided that the second term on the right of Equation (4-3) can be neglected and if B, governed by the electron tunneling probability, is constant. At sufficiently low values of d this relative dominance of terms is reversed, but if then the breakdown voltage obeys a linear dependence on gap separation log I will be constant.

In most of the experimental treatments, the electric field was not uniform because spherical and pianar electrodes were employed according to the requirements of the design. A correction could be applied, however, to the value of d so that the cathode field strength could still be represented by E = V/d. This correction had the effect of linearizing the curves of log I vs $d^{1/2}$ as would be expected, but it also linearized the law of V_B vs $d^{1/2}$ (Figure 4-23). This evidence is consistent with the influence of cathode shape on the breakdown voltage. It, therefore, appears that the breakdown voltage is influenced by cathode curvature through the effect of this upon prebreakdown current.

Subsequent to this the experimental technique was changed and only one individual breakdown voltage and its corresponding current were measured. The above mentioned behavior was not observed until the test sequence over the whole range of gap separations had been repeated several

times (Figures 4-24 through 4-28). Deviations from linearity could be attributed to variations in the tunneling probability due to chemisorbed layers or thin oxide films.

During the stepwise approach to breakdown the mass spectrometer recorded weak pressure surges at a specific threshold value of the voltage which increased as the square root of the gap separation (Figure 4-29). The significance of this phenomenon is that gas evolution seems somehow related to breakdown because they both vary in the same functional manner with gap separation.

4.8 Conclusions

Gas or vapor evolution and its subsequent ionization is an essential prerequisite for voltage breakdown and arc formation. Breakdown theories so far have proposed that gas may enter the gap either suddenly as when a metal clump evaporates on impact, or if a cathode microprotrusion explodes by overheating. On the other hand, gas can enter the gap gradually by electron beam heating of the anode. In the latter case, the concentration of gas dissolved in the anode would be reduced by bakeout and upon electron beam heating the anode would give up its gas readily, thus accounting for prebreakdown gas evolution and its relationship with breakdown.

It is easy to see from Equation (4-2) that the linearity of the log I vs $d^{1/2}$ plots at breakdown follow from the square root law, Equation (4-1). If, however, there is distortion of the macroscopic cathode field due to electrode curvature, then the field enhancement factor must be redefined at each gap setting. The log I vs $d^{1/2}$ plot would then become non-linear if V_B remained the same function of $d^{1/2}$. This does not occur, however, so the changes in V_B vs $d^{1/2}$ due to electrode curvature is somehow associated with the corresponding change in current.

A theory consistent with these facts must take account of gas evolution and field emission current. It, therefore, appears that field emission current ionizes the evolved gas by impact and that the growth of this ionization leads to breakdown.

If gas evolution were to be a significant factor, then it should be influenced by the area of the electrodes since this restricts radial streaming because of the low pumping conductance and controls the gas density on the axis. This would account for the well-known area effect. The factorial experimentation technique is ideally suited for demonstrating an interaction between area and anode gas content which would confirm this proposal.

4.9 References

(1) Watson, A., Denholm, A. S. and Mulcahy, M. J., "Prebreakdown Phenomena in Vacuum Gaps", Proceedings of Second International Symposium on High Voltage Insulation in Vacuum (1966). (Also Section 2 of this report.)

(2) Bruce, F. M., "Calibration of Uniform Field Spark Gaps for High Voltage Measurement at Power Frequencies", Proc. IEEE 94, Pt. 2, 138 (1947).

(3) Chrepta, M. M., Weinstein, J., Taylor, G. W. and Zinn, M. H., "The Design of a High-Voltage Breakdown-in-Vacuum Experiment", Conference on Design of Experiments Sponsored by Army Research Office (1965).

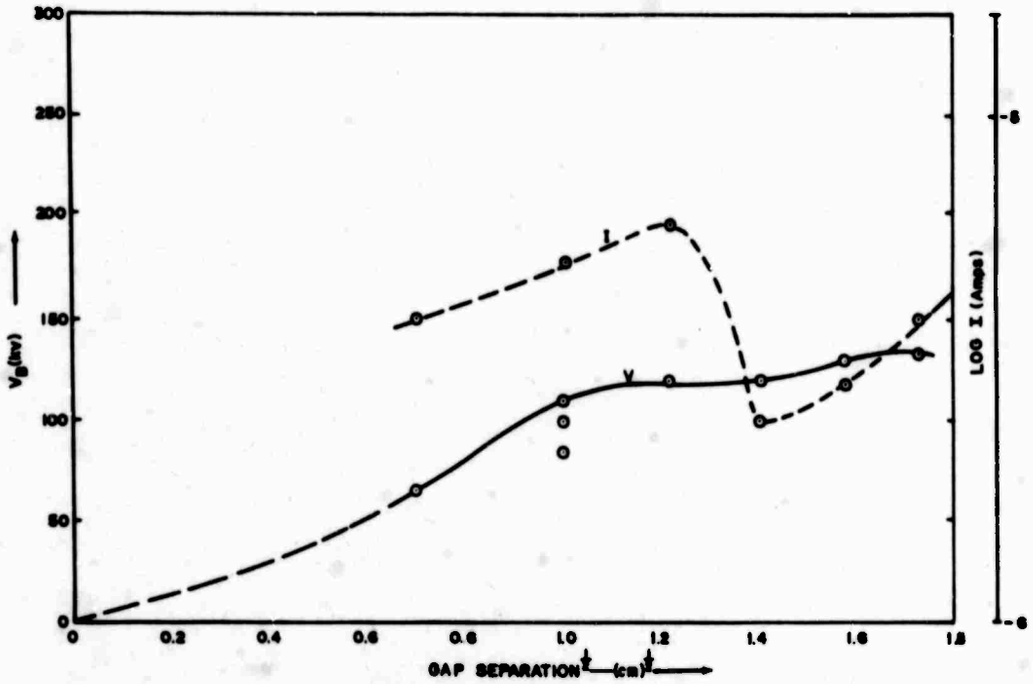

Figure 4-24. Breakdown Voltage and Penultimate Gap Current as Function of Gap Separation (Treatment abcefg, Test Sequence 1, Fresh Electrodes)

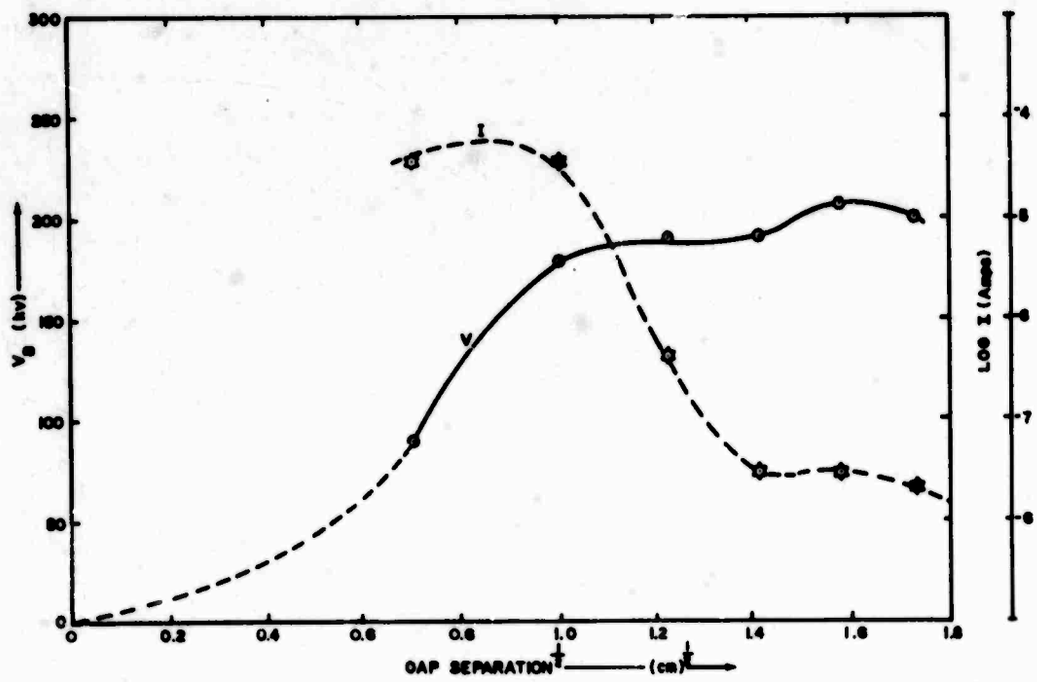

Figure 4-25. Breakdown Voltage and Penultimate Gap Current as Function of Gap Separation (Treatment abcefg, Test Sequence 2, After Conditioning)

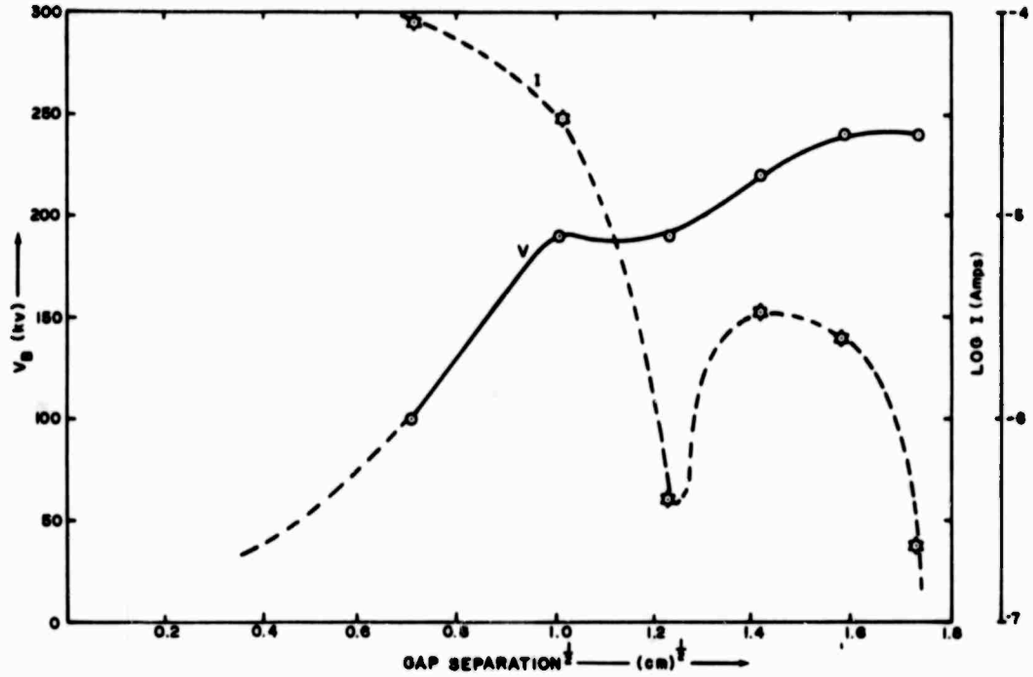

Figure 4-26. Breakdown Voltage and Penultimate Gap Current as Function of Gap Separation (Treatment abcefg, Test Sequence 3, After Further Conditioning)

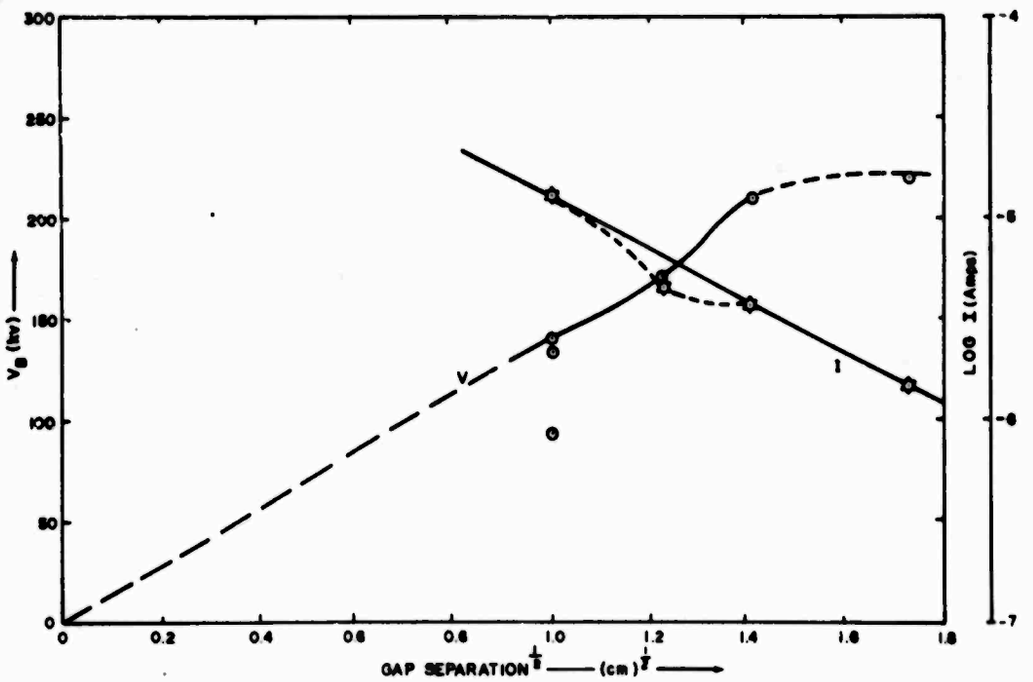

Figure 4-27. Breakdown Voltage and Penultimate Gap Current as Function of Gap Separation (Treatment abcefg, Test Sequence 4, After Deconditioning)

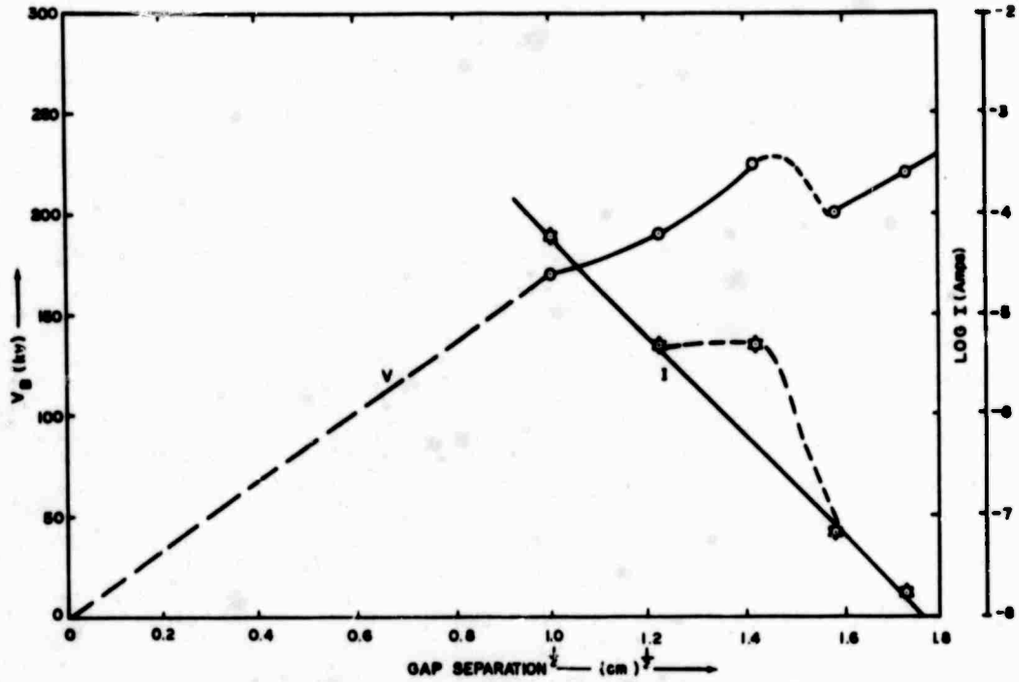

Figure 4-28. Breakdown Voltage and Penultimate Gap Current as Function of Gap Separation (Treatment abcefg, Test Sequence 5, Conditioned After Deconditioning)

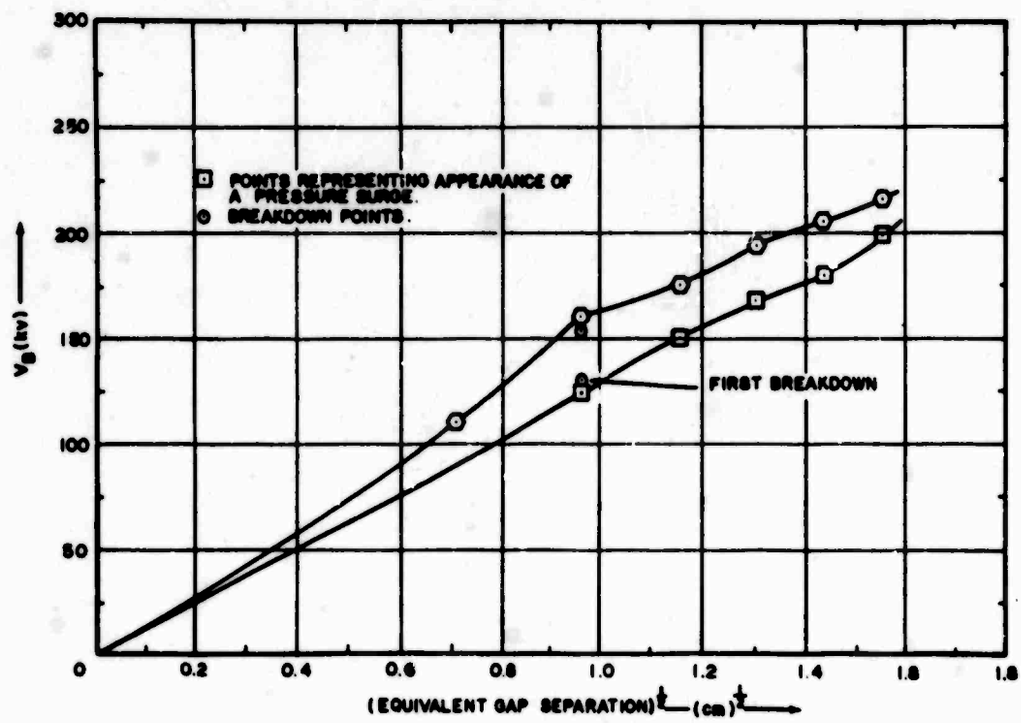

Figure 4-29. Threshold Voltage for Pressure Surges as a Function of Gap Separation

SECTION 5
FULL FACTORIAL EXPERIMENTS

5.1 Abstract

Breakdown voltage was studied as a function of gap separation in three consecutive three factor, two level, full factorial experiments. In the first two, the gap was tested in two consecutive sequences of gap separations to study the influence of spark conditioning on the factorial estimates. Following this, the experiment was repeated with a weak transverse magnetic field superimposed to measure its influence. Each measurement was immediately preceded and followed by measurements without magnetic field to act as controls against which to compare magnetic influences and any short time history effects which they might possibly introduce.

Either cathode or anode could be baked out in vacuum or saturated with hydrogen by prefiring. Large or small area uniform field electrodes comprised two levels of pumping conductance as a third factor without introducing non-uniformity of the interelectrode field. The proposed interaction of anode gas content and electrode area was confirmed and new data on the influence of weak magnetic fields on breakdown voltage and prebreakdown current was gathered.

A final experiment on the variation of breakdown voltage with magnetic field strength gave estimates of the various factors and interactions under these conditions.

5.2 Introduction

The results of a quarter replicate partial factorial experiment have indicated that consistently throughout the conditioning history of a pair of electrodes the decisive factors in determining voltage breakdown were the electrode materials, shapes and system bakeout. Statistical scatter of the results was poor, however, and thought to be from two causes. Firstly, there was no guarantee of similar previous heat treatment of the electrode materials and, therefore, no control of gas content. Secondly, there was a conditioning period between test sequences during which the breakdown voltage was arbitrarily raised by 25%.

The reason for the results was thought to be that gas evolved from the anode was concentrated on the gap axis by electrodes with a low vacuum pumping conductance and ionization took place there more readily. Bakeout would then be expected to appear significantly among the important factors along with anode material and electrode shapes which would control the electric field as well as the pumping conductance.

A new experiment has therefore been designed to investigate and control these factors as well as to provide data on magnetic influences on breakdown.

There has been very little reported work on the influence of magnetic fields upon vacuum breakdown voltage. This was perhaps largely due to the supposition that no great influence should be detectable for an electron beam mechanism unless it could be deflected outside of the gap. An investigation at such high field strengths was carried out by Pivovar and Gordienko.[1]

There has been interest in the effect of transverse magnetic fields upon vacuum breakdown voltage from the standpoint of particle separators. In this case, a weak magnetic field is crossed with a high electric field in such a way as to permit certain high energy particles to be transmitted selectively. It was found by Sanford[2] that field strengths as low as 175 gauss could reduce the breakdown voltage significantly. The data, however, were obtained largely at higher pressures and gap separations large enough for electrons to have cycloidal interelectrode paths which caused increased ionization and ultimately a glow discharge.

It was, therefore, particularly appropriate that the following experiment should study the interactions of a magnetic field with electrode gas content.

5.3 Experimental Design

Gas content was fixed at either of two levels by baking in vacuum or hydrogen. Only copper was investigated to eliminate the material as a factor, and large or small diameter Bruce profile electrodes gave the gap two levels of pumping conductance for each separation (Tables 5-1 and 5-2). The use of identical Bruce profile electrodes eliminated the possibility that variations of electric field configuration would influence the results over a range of gap separation.

Table 5-1. Factors and Levels for Block Experiment Without Magnetic Field

Factor	Letter	Level	
		High	Low
Anode Processing	A	a - Vacuum Baked	1 - Hydrogen Baked
Cathode Processing	B	b - Vacuum Baked	1 - Hydrogen Baked
Electrode Size	C	c - Large	1 - Small

Table 5-2. Factors and Levels for Block Experiment With Magnetic Field

Factor	Letter	Level	
		High	Low
Anode Processing	A	a - Vacuum Baked	1 - Hydrogen Baked
Cathode Processing	B	b - Vacuum Baked	1 - Hydrogen Baked
Electrode Size	C	c - Large	1 - Small
Transverse Magnetic Field	E	d - Present	1 - Absent

A three factor full factorial experiment was planned so as to avoid any confounding of factors and interactions. Four parallel experiments were carried out with magnetic field as a flexible

factor. Two sequences of tests were made immediately following each other and are referred to as "unconditioned" and "conditioned", respectively. Following this, the testing was repeated with a 250 gauss transverse magnetic field over a range of gap separations. After standing for about 10 hours, the influence of a variable magnetic field strength on breakdown voltage at fixed gap separation was investigated. Thus, four independent sets of three factor, two level experiments were carried out with controlled time intervals and the same number of sparks had been passed at each stage of the experiment.

5.4 Introductory Operating Experience

The experiment was begun with the equipment described in Section 4, but heavy prebreakdown current levels prevented the Van de Graaff generator from charging up to the breakdown voltage in some cases. It was, therefore, necessary to begin again with a 2.0 ma, 300 kV rectified ac power supply connected to the cable.

It was also intended to study the effects of an axial as well as a transverse magnetic field. An axial magnetic field was, however, found to induce a heavy current load on the source, preventing it initially from applying more than 10 kV to the system. Gas was evolved copiously into the chamber which was filled with a purple glow and as it gradually abated, it was possible to raise the voltage. It was not, however, considered satisfactory to submit the electrode system to such a contaminating influence and this part of the experiment was accordingly abandoned.

The cause of the phenomenon is believed to be due to the failure of voltage grading on the bushing by some conducting mechanism.

The effect was studied at various magnetic field strengths which progressively intensified it. Measurements were made of the ion pump current and total charging current as a function of voltage and magnetic field strength. A hysteresis of the current-voltage characteristic was always observed as well as of the pressure as revealed by the ion pump current (Figures 5-1 and 5-2).

The cause of the gas evolution is probably that electrons are emitted from the dielectric (alumina) surface of the bushing and are returned by the magnetic field to bombard it, causing gas evolution and some surface conduction. The appearance of this in any one section would cause current to be shunted across the grading resistors disturbing the uniformity of the voltage distribution. On reducing the voltage, the low resistance persists, maintaining the charging current at a higher level than when the voltage is being raised from zero.

Electron emission from dielectrics has been proposed by Watson[3] as a precursor to flashover in vacuum and gas evolution in high electric fields was reported by Avdienko and Kiselev.[4] This effect is considered important because it is an indicator of a possible influence determining the manner in which a dielectric envelope would be expected to affect breakdown phenomena in vacuum.

5.5 Experimental Procedure

Copper electrodes were machined and polished with successively smooth grades down to 600 grade of emery paper. After degreasing, they were fired for 6 hours at 900°C in either vacuum at

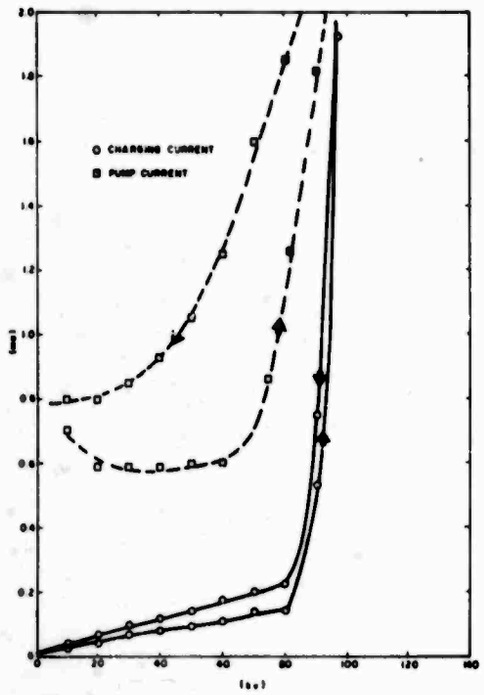

Figure 5-1. V-I and Pressure Characteristics of System with 155 Gauss Axial Magnetic Field

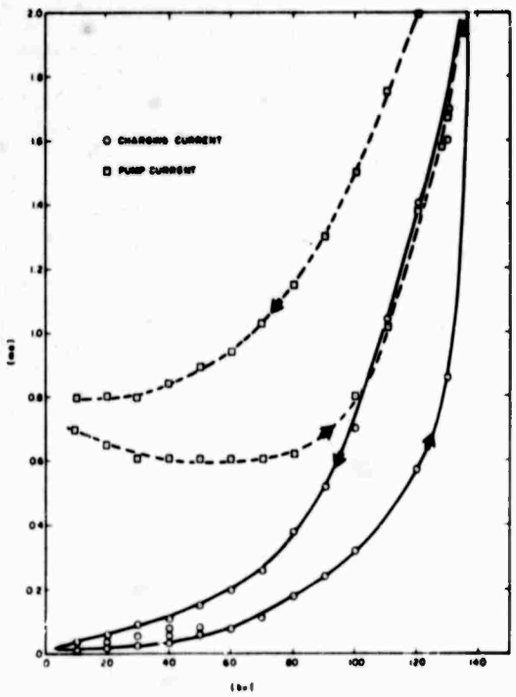

Figure 5-2. V-I and Pressure Characteristics of System with 250 Gauss Axial Magnetic Field

$< 10^{-6}$ torr or in hydrogen at atmospheric pressure. They cooled at 200°C in their respective environments and dry nitrogen was admitted for transferring to the vacuum test chamber where a complete system bake at 400°C was carried out for 6 hours. Gas analysis of test samples showed that the hydrogen baked into them was 0. 35 ppm and fell to 0. 14 ppm after the second bakeout.

A sequence of breakdown tests over a range of gap separation from 0. 5 to 3. 0 cm in 0. 25 cm increments was performed without any previous conditioning. Immediately following this, the procedure was repeated. These tests are arbitrarily referred to as "unconditioned" and "conditioned" simply because in the second series a fixed greater number of sparks (twelve) precedes each test than in the corresponding test in the first series. Following this, the magnets were assembled and the breakdown observed at 0. 5 cm intervals from 0. 5 to 3. 0 cm. At each separation the measurement was made without, with and again without the magnetic field. Comparison was made between these results to observe the magnetic effect.

After standing about 10 hours overnight, the breakdown voltage was measured again without magnetic field and at approximately 50 gauss intervals up to 250 gauss, then at zero gauss once more. This was carried out at 2 and 3 cm gap separations as an exploratory investigation. By expressing the breakdown voltage changes as percentages of the zero magnetic field values, however, and neglecting the influence of gap separation in this regime, it is possible to treat them in the factorial manner as though the gap were fixed.

5. 6 Discussion of Factors and Interactions

The results of the first two experiments, that is the unconditioned and conditioned test sequences, are presented in Figures 5-3 through 5-17. In the first figure, the points on the graphs are numbered sequentially for the average breakdown voltages in the two experiments. Measurements below 1 cm were carried out at the end of each sequence because the primary aim of the investigation was to study the high voltage regime above 100 kV. The sixth and seventh results thus appear more naturally on the upper curve due to conditioning. This tendency had disappeared when the third experiment was performed with the magnetic field.

In the figures following Figure 5-3, the magnitudes of the various effects and interactions are superimposed upon the average breakdown voltage as a function of gap separation for comparison.

Inspection of the figures shows that the main effects A, B and C all contribute negatively to the breakdown voltage before conditioning. That is to say that bakeout of either the anode or cathode in vacuum (high levels) gives a lower breakdown voltage than a preliminary bake in hydrogen (low levels) and large electrodes (high level) give lower breakdown voltages. After some conditioning, however, the effect of anode pretreatment on breakdown voltage diminishes but this is not so for cathode pretreatment. In this case, the effect remains strongly negative but only above about 0. 75 cm gap separation. Large area electrodes always reduce the breakdown voltage, particularly after conditioning.

The AB interaction before and after conditioning behaves similarly to the A effect, indicating that cathode pretreatment influences the effect of anode pretreatment on breakdown voltage only

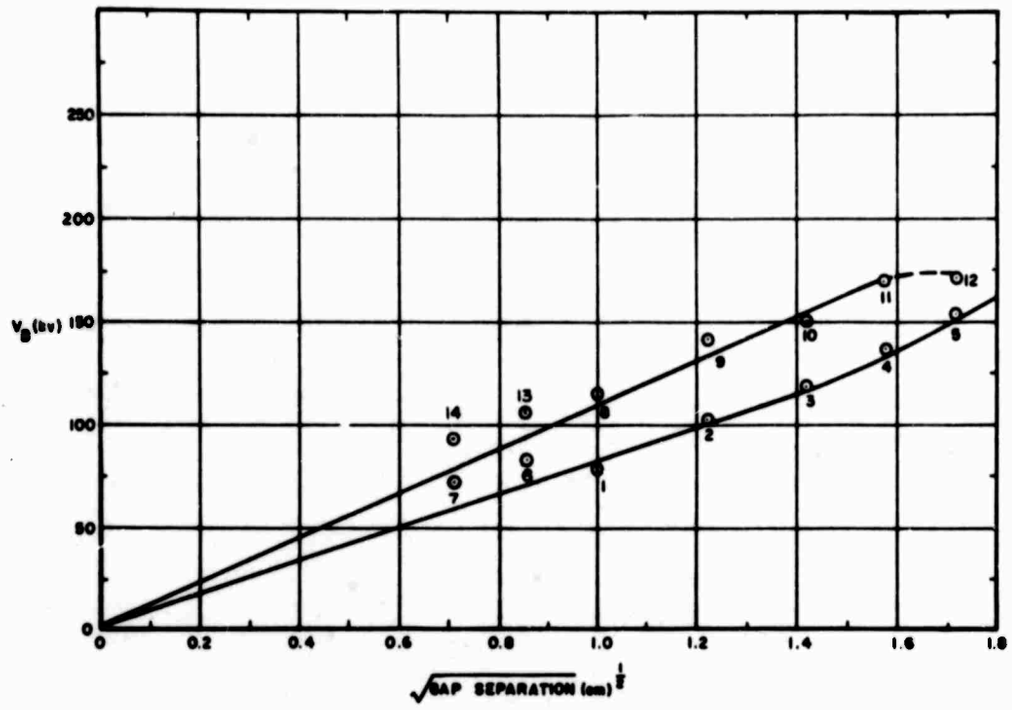

Figure 5-3. The Mean Breakdown Voltages and Test Sequence

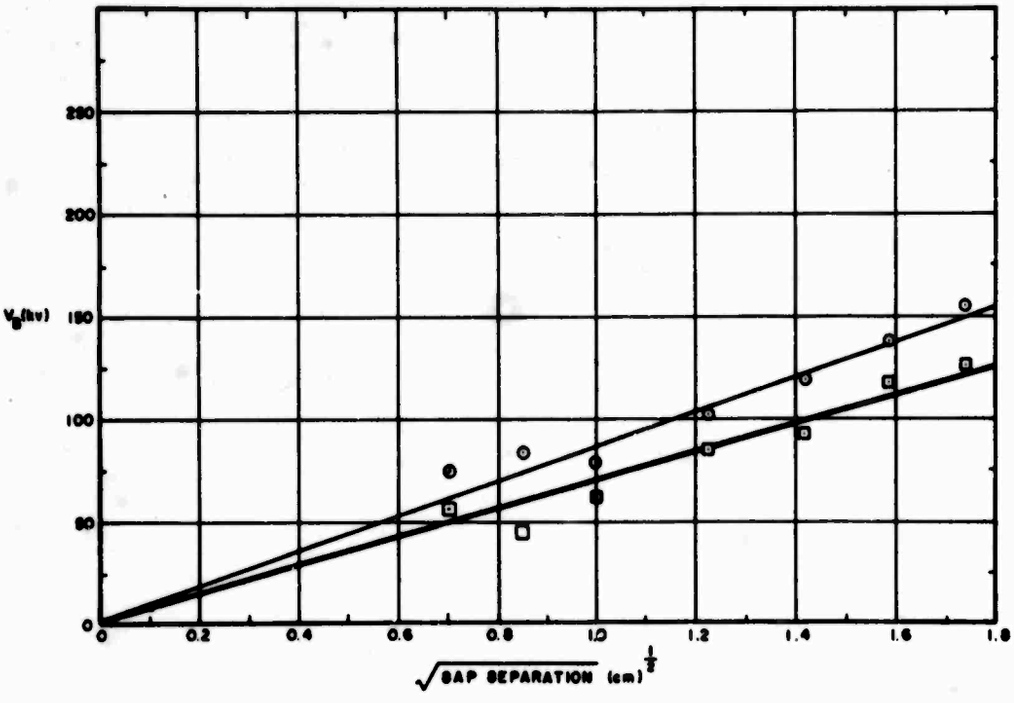

Figure 5-4. A Effect (Unconditioned)

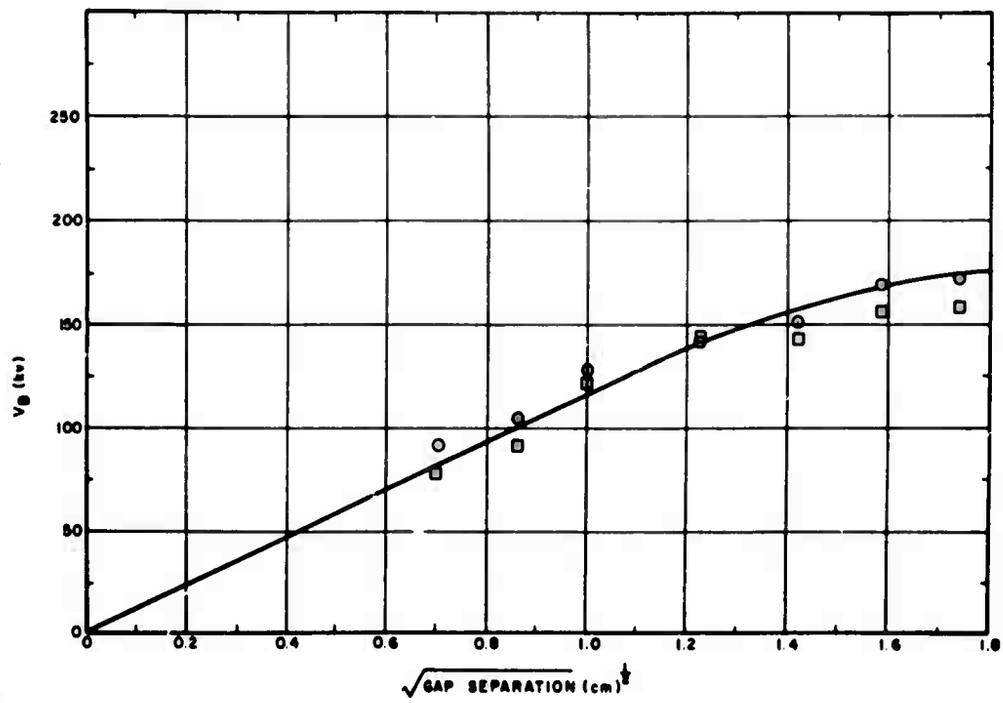

Figure 5-5. A Effect (Conditioned)

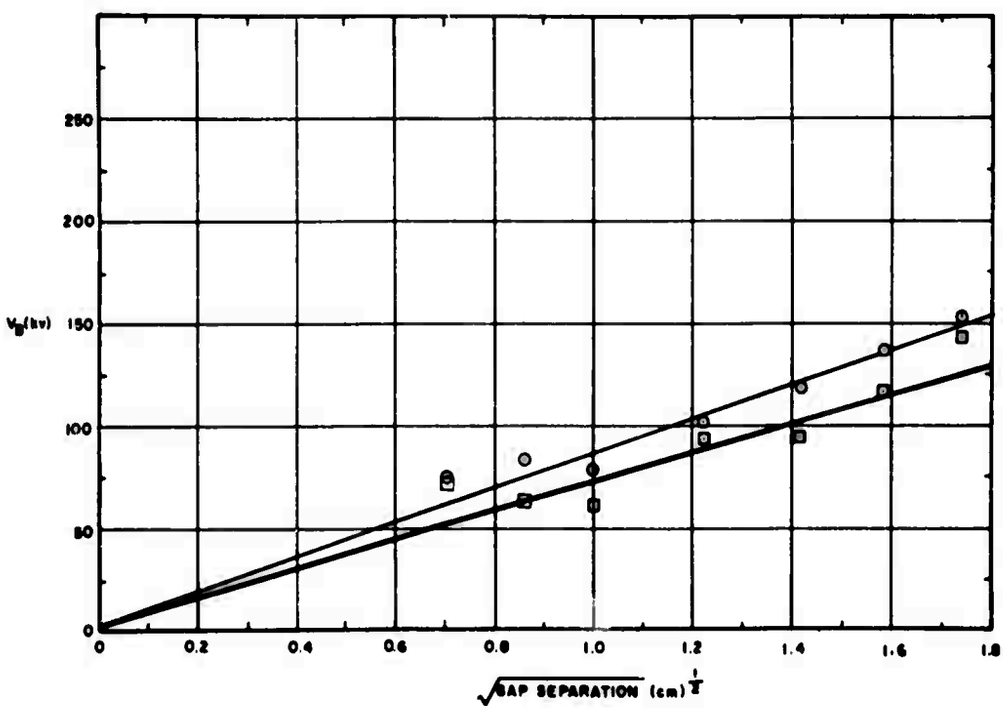

Figure 5-6. B Effect (Unconditioned)

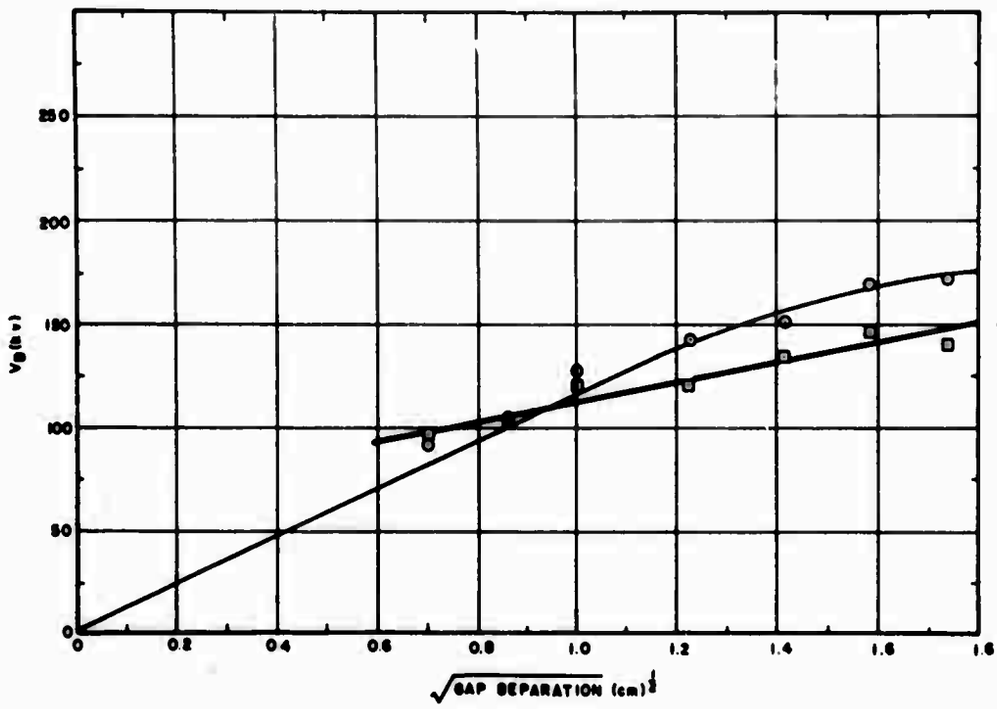

Figure 5-7. B Effect (Conditioned)

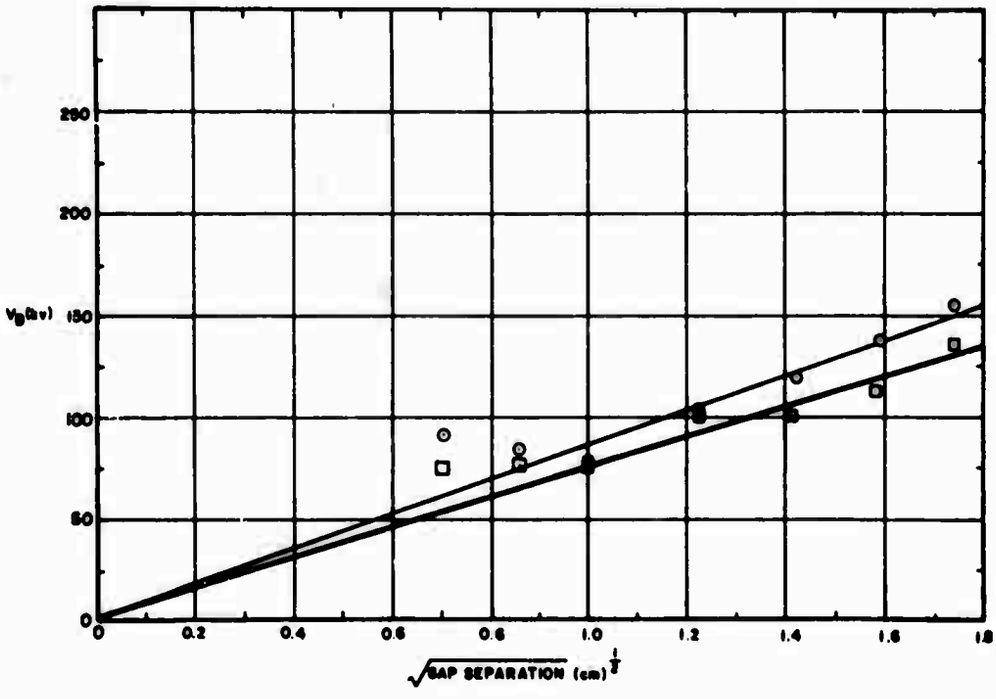

Figure 5-8. AB Effect (Unconditioned)

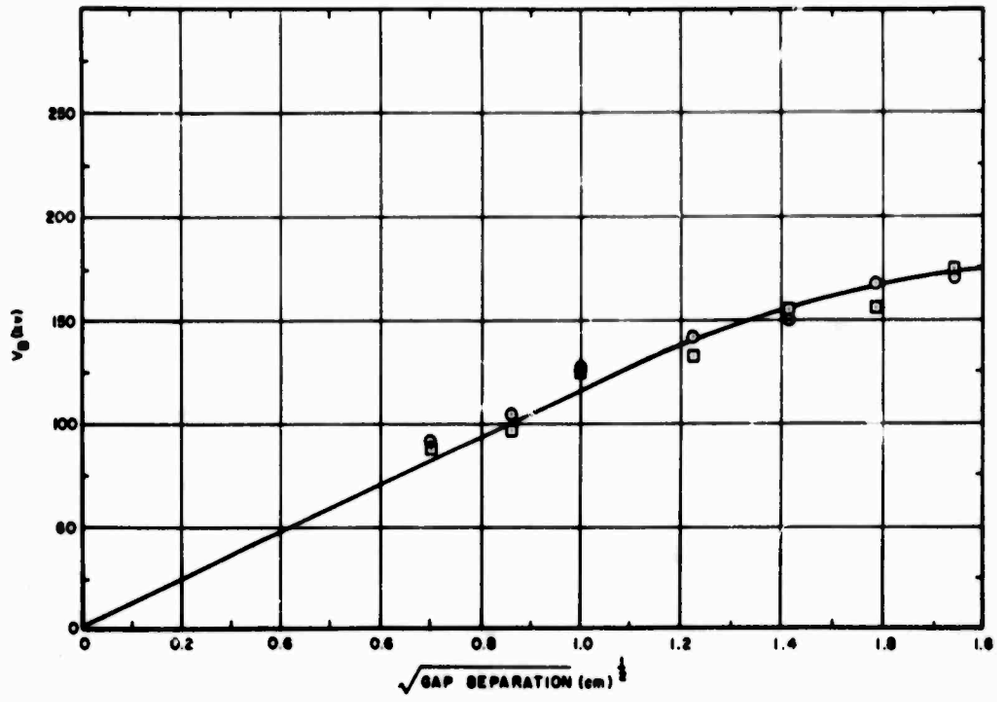

Figure 5-9. AB Effect (Conditioned)

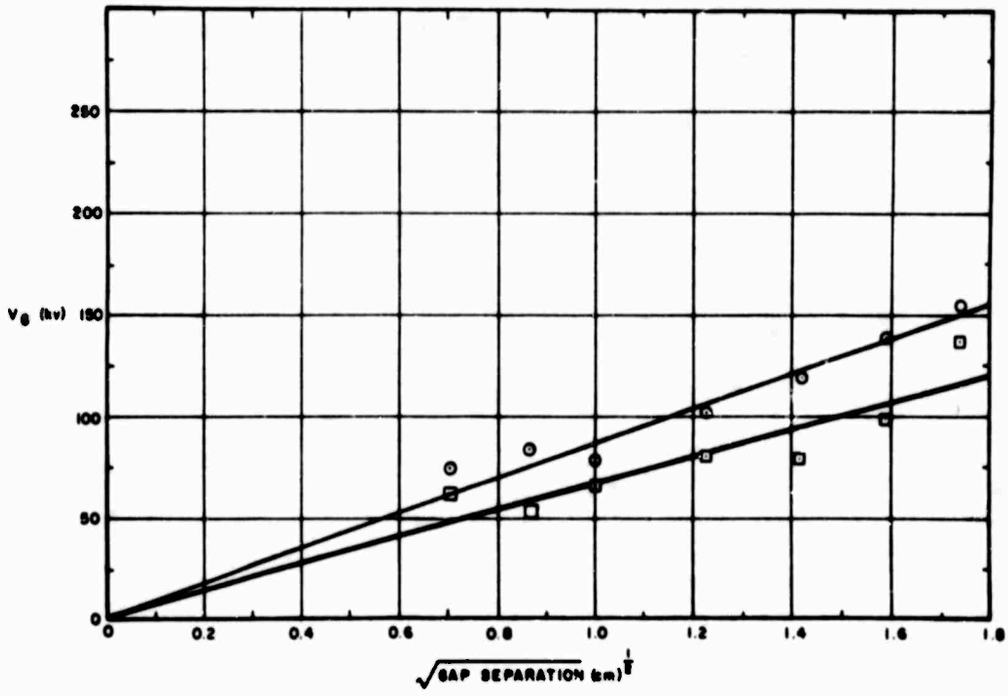

Figure 5-10. C Effect (Unconditioned)

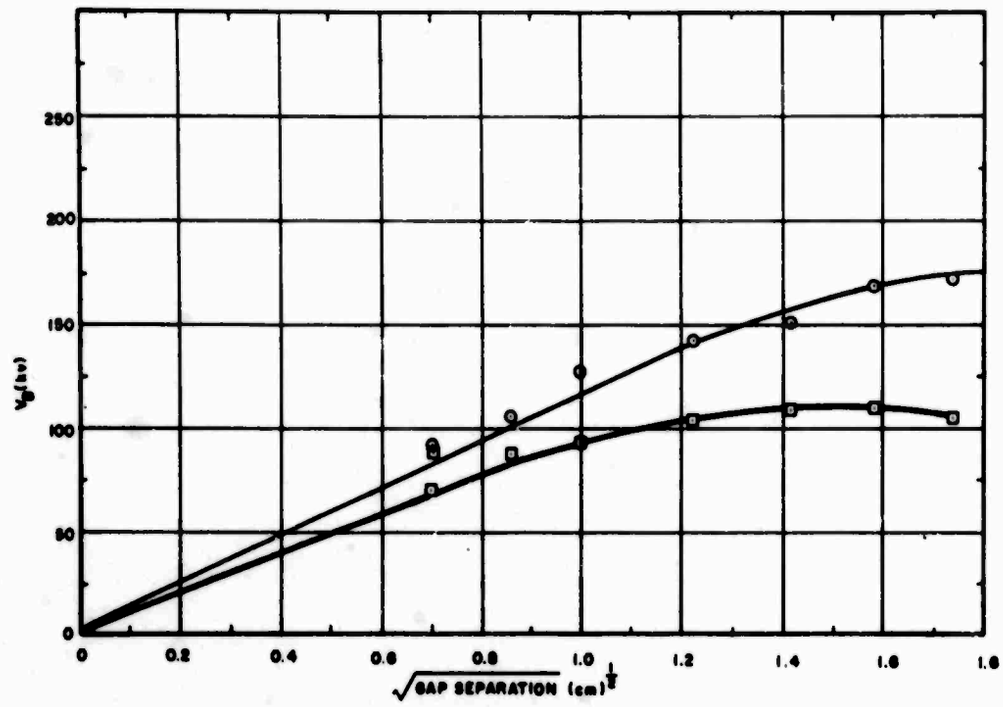

Figure 5-11. C Effect (Conditioned)

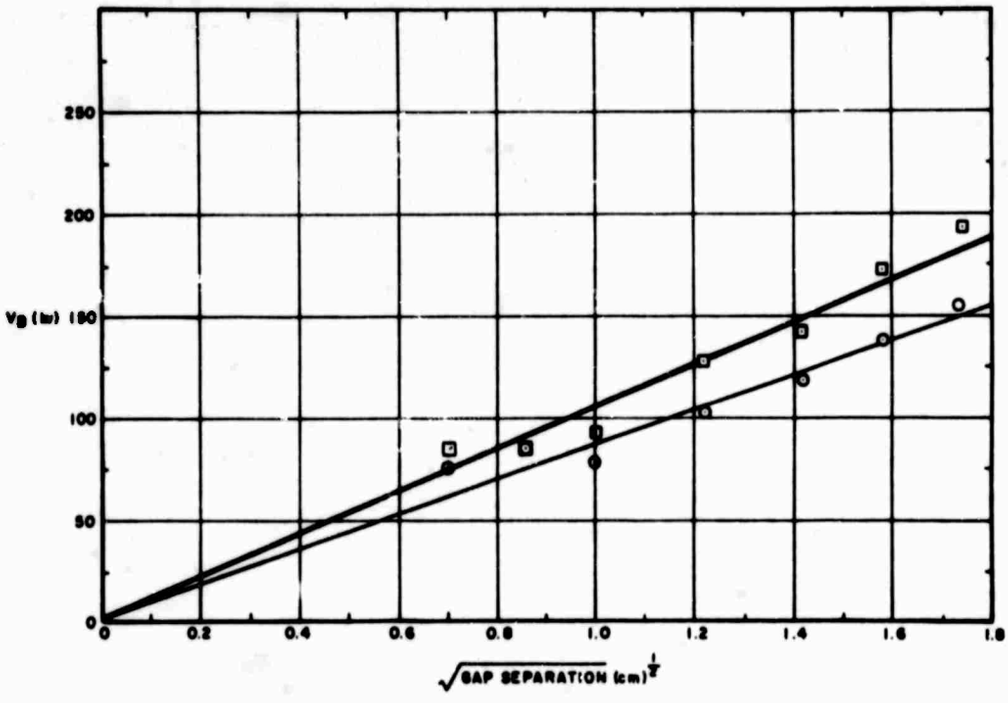

Figure 5-12. AC Effect (Unconditioned)

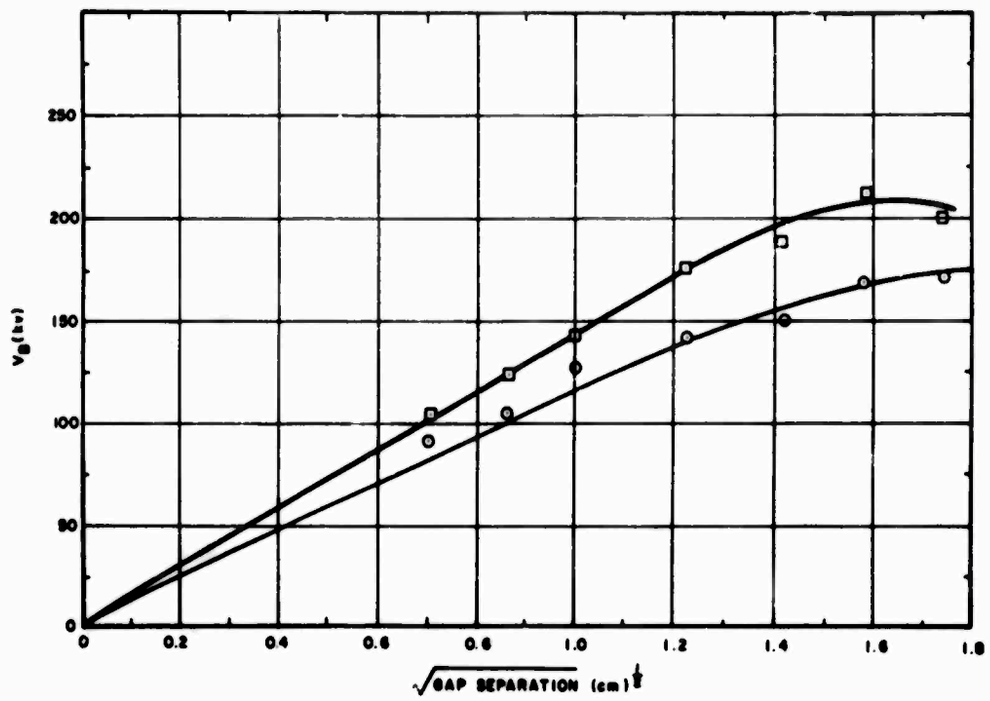

Figure 5-13. AC Effect (Conditioned)

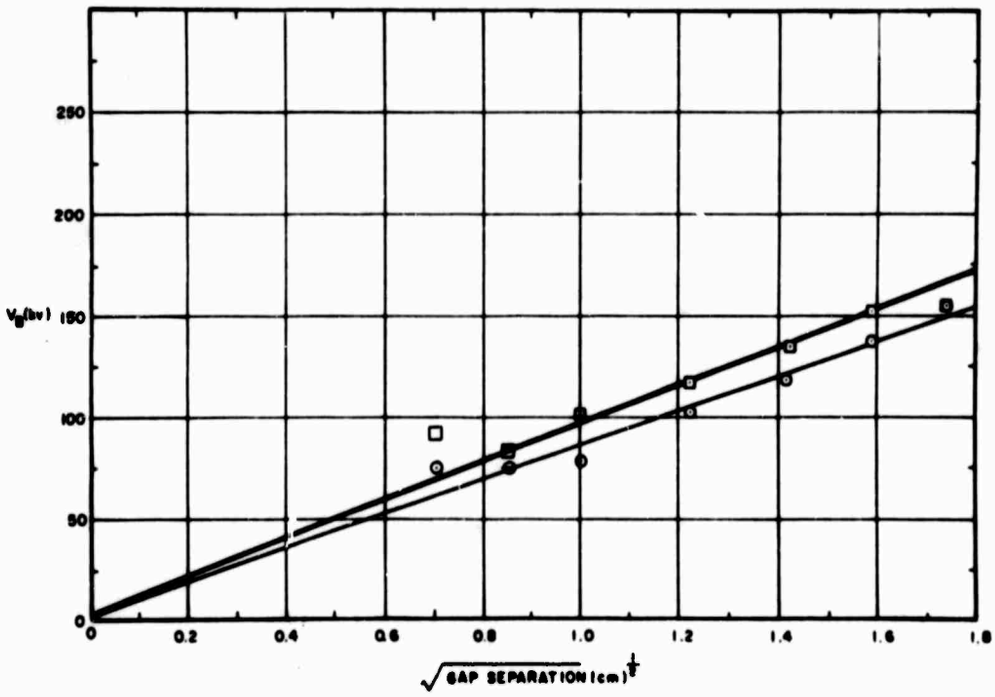

Figure 5-14. BC Effect (Unconditioned)

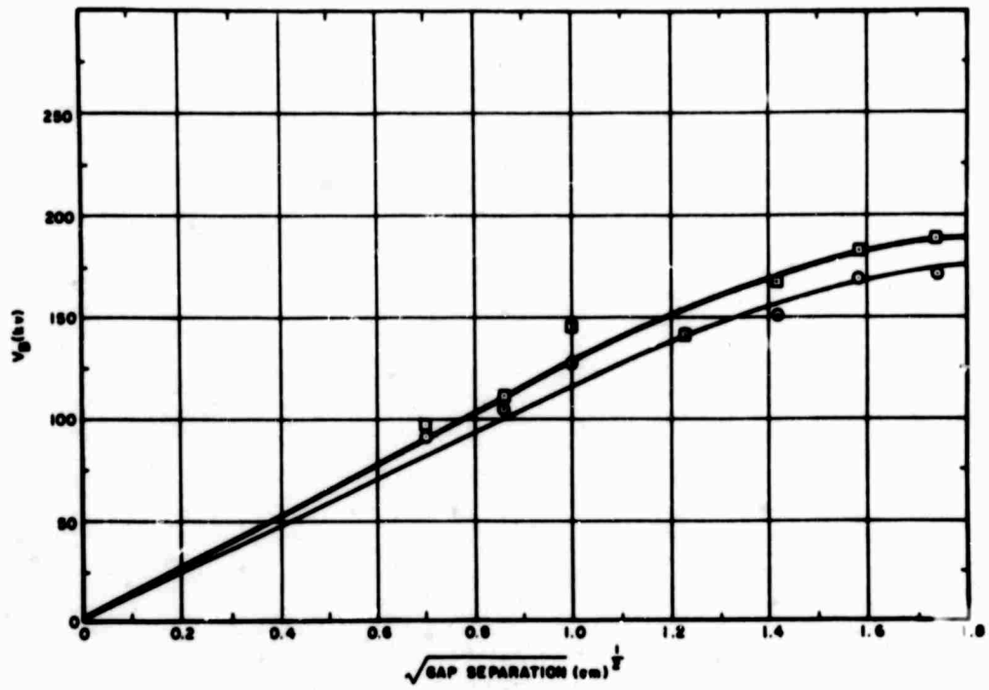

Figure 5-15. BC Effect (Conditioned)

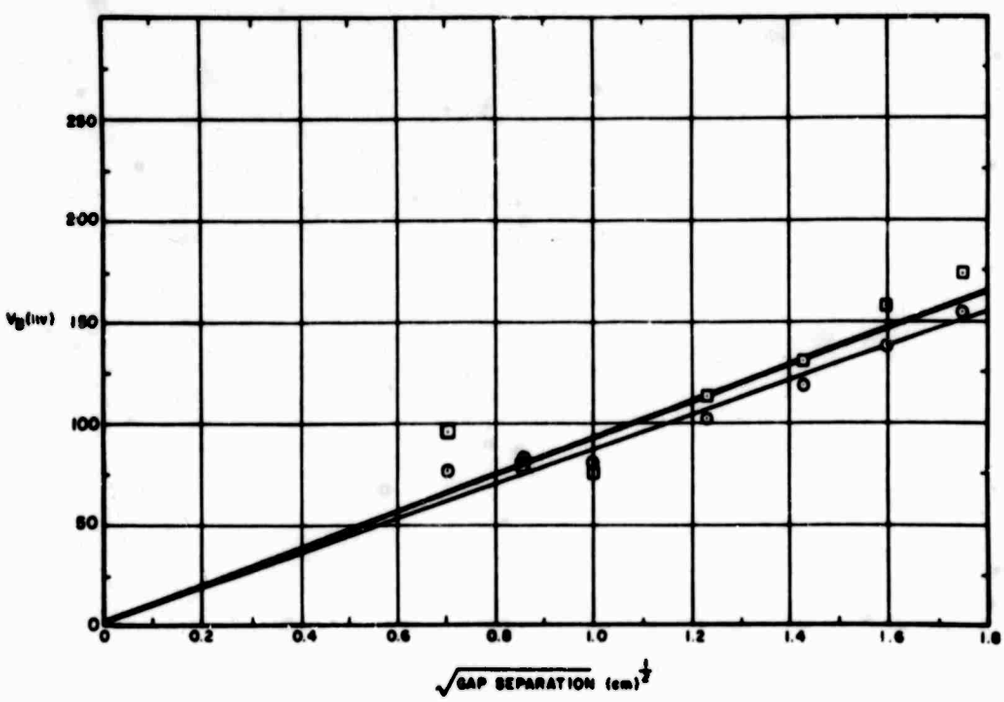

Figure 5-16. ABC Effect (Unconditioned)

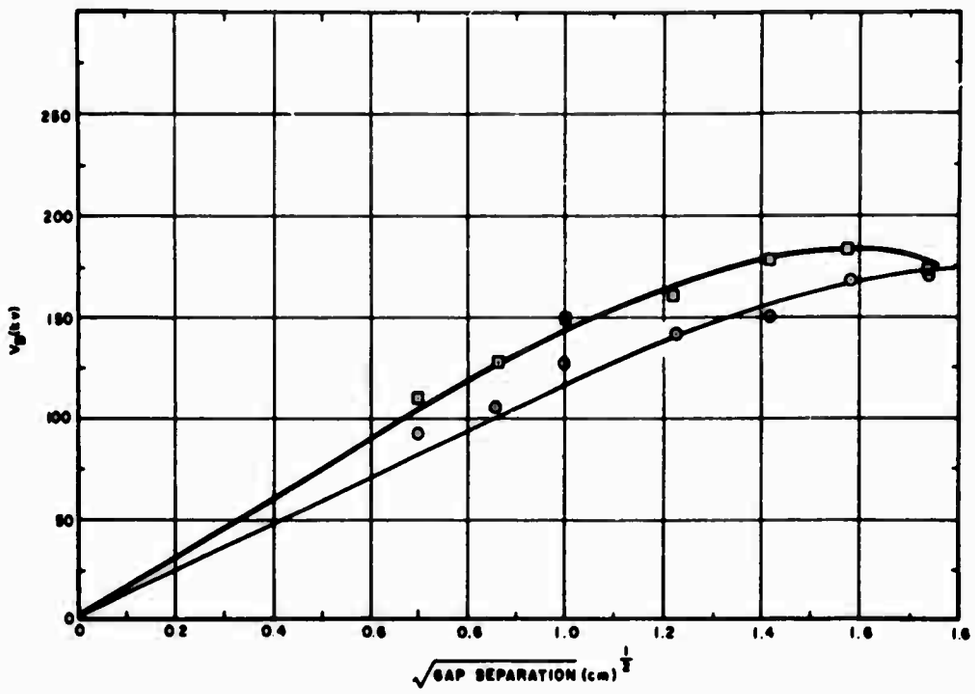

Figure 5-17. ABC Effect (Conditioned)

when it is large enough itself. Cathode pretreatment cannot enhance a zero value of the anode pretreatment effect.

The BC interaction is small, undiminished by conditioning, and consistently opposite in sign to both the B and C effects for all gap separations.

The AC interaction is similar but much more pronounced particularly after conditioning. Thus, large area electrodes will concentrate the effect upon breakdown voltage of pretreatment of either electrode, but will reverse the sign. Alternatively, small area electrodes concentrate pretreatment effects.

Finally, the ABC and AC interactions are similar in that they intensify somewhat after conditioning and have the same sign.

The results of the third experiment are presented graphically in Figures 5-18 through 5-25 in the same manner as before. Each factorial effect and interaction is shown by comparison with the average breakdown voltage by subtracting the estimates of the influences of A, B, AB, C, AC, BC, ABC at their high levels from the corresponding overall average breakdown value μ. This has been done for each gap separation and the results plotted as functions of its square root to demonstrate the validity of the breakdown law:

$$V_B \propto d^{1/2}$$

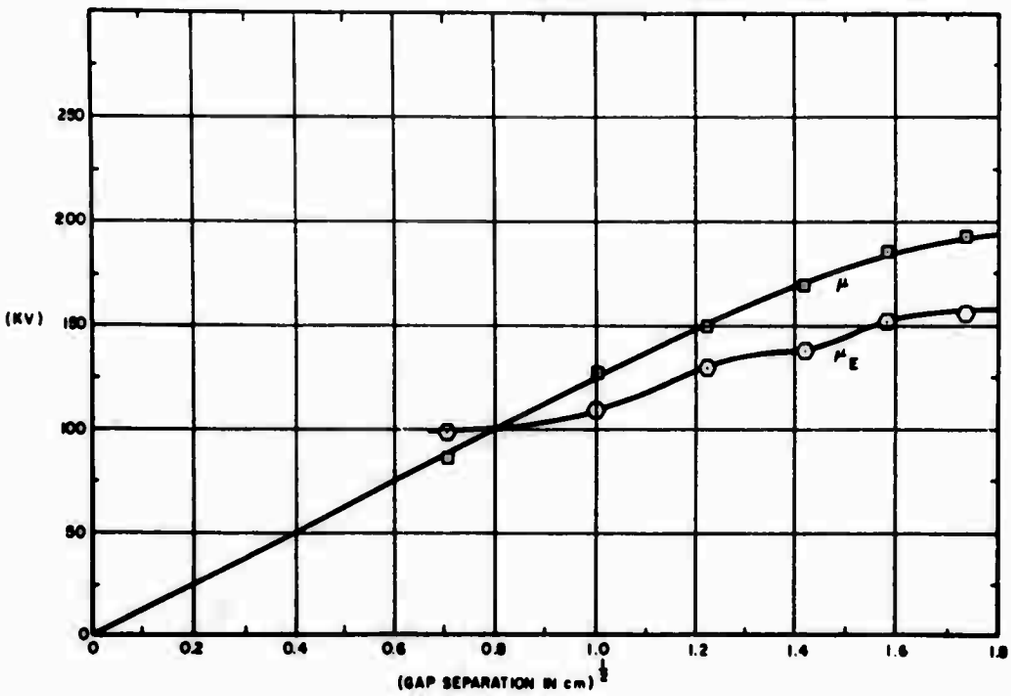

Figure 5-18. The Average Effect (μ)

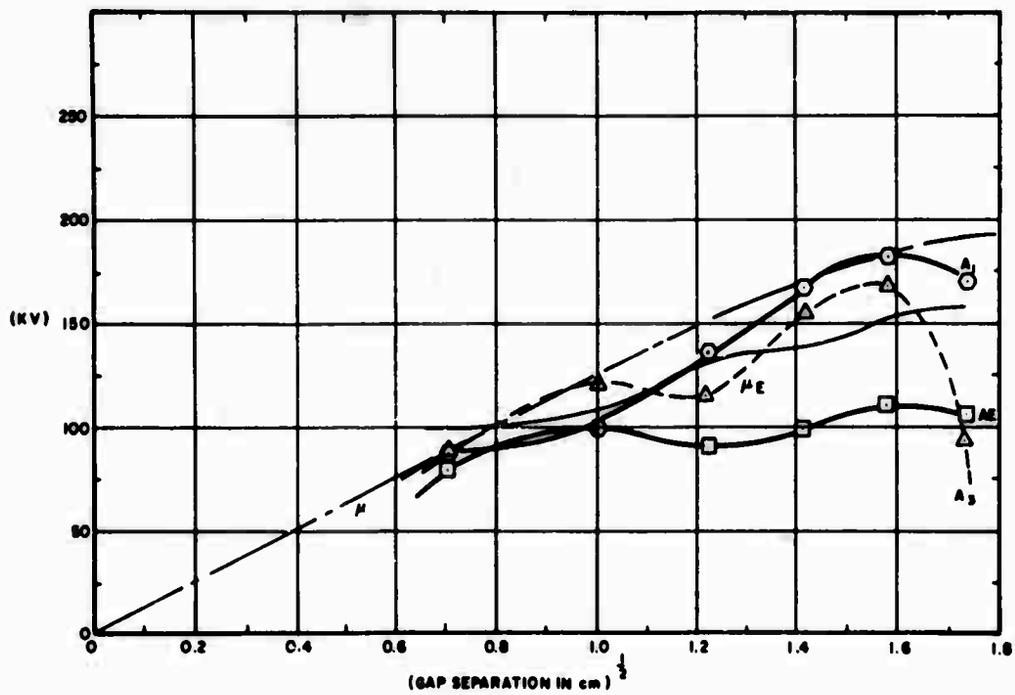

Figure 5-19. Anode Processing (A)

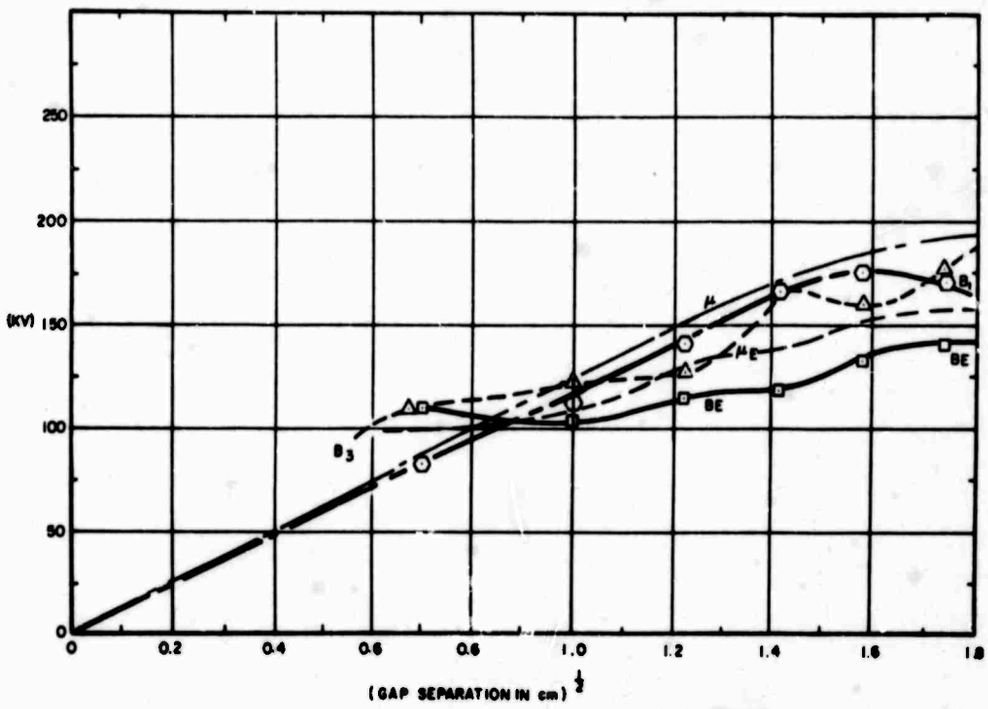

Figure 5-20. Cathode Processing (B)

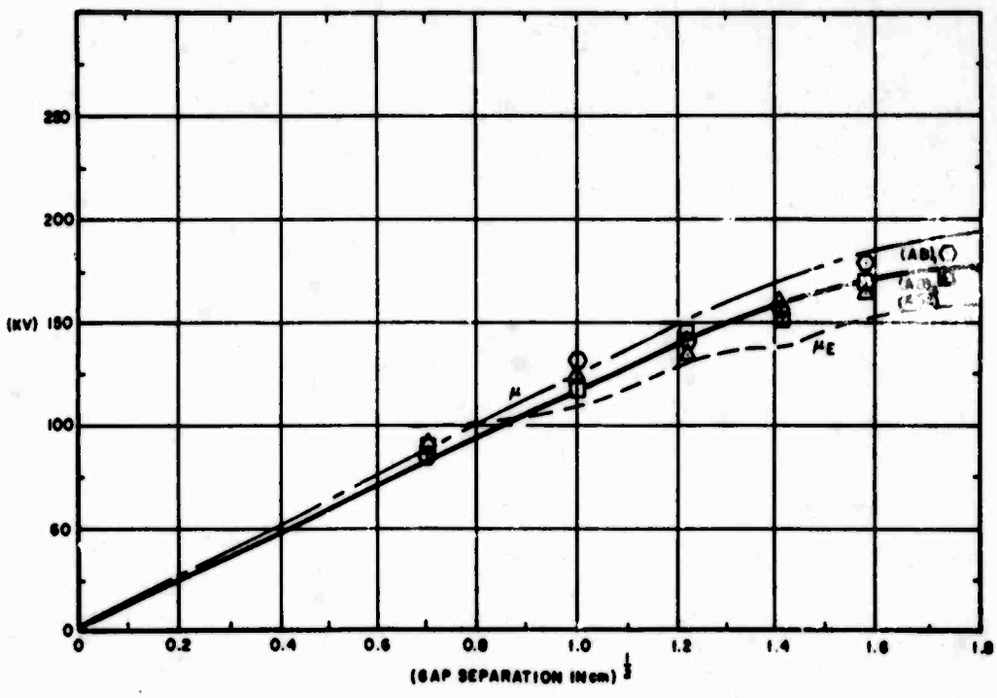

Figure 5-21. Anode Processing x Cathode Processing (AB)

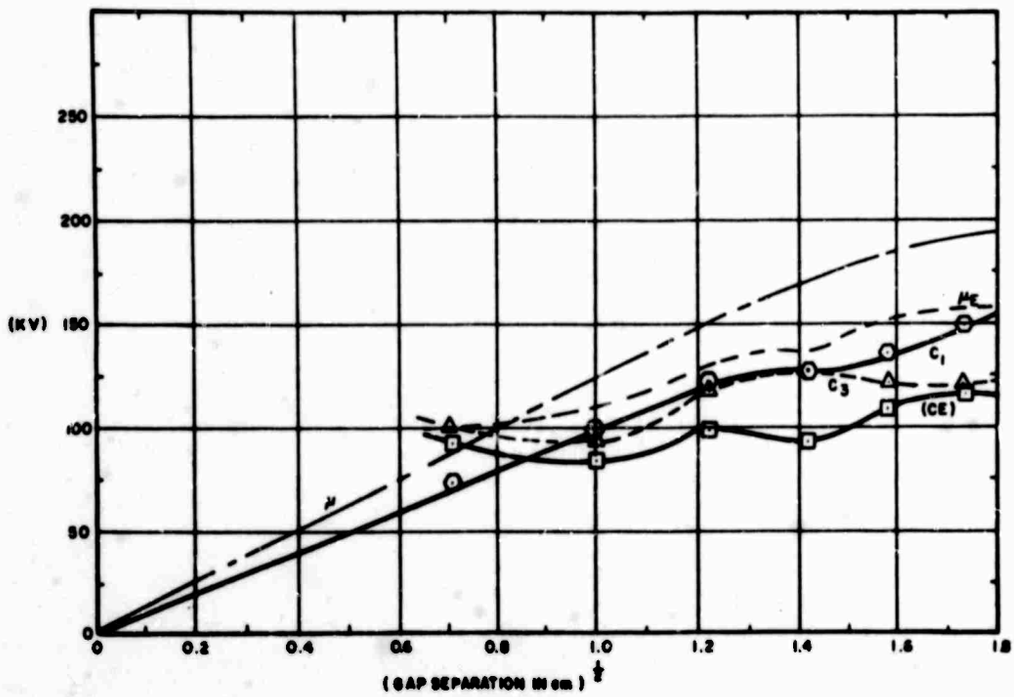

Figure 5-22. Electrode Size (C)

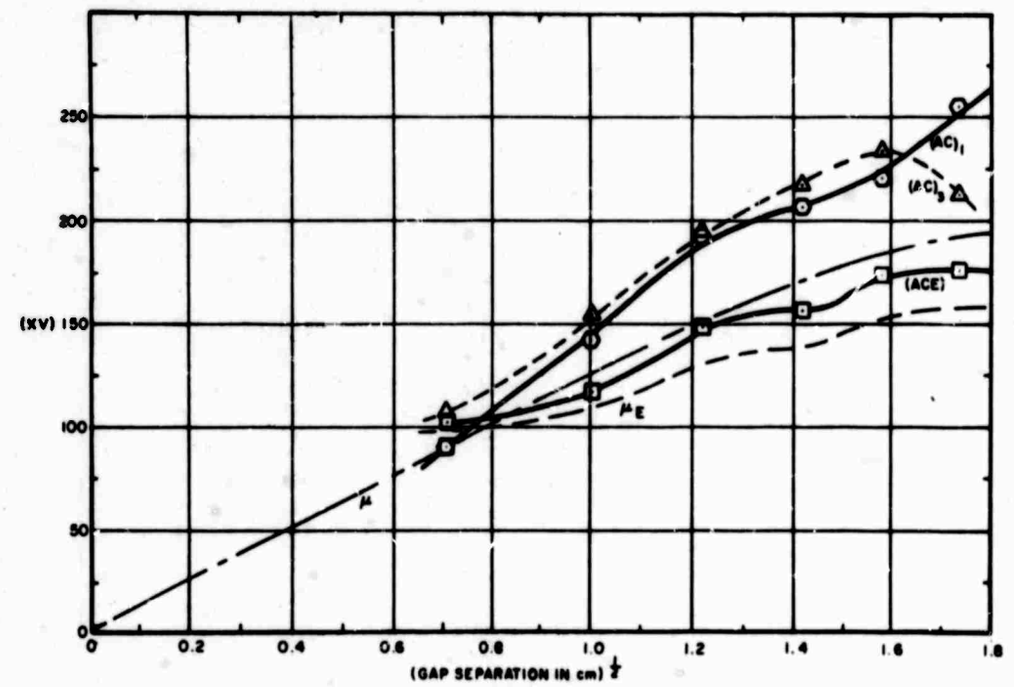

Figure 5-23. Anode Processing x Electrode Size (AC)

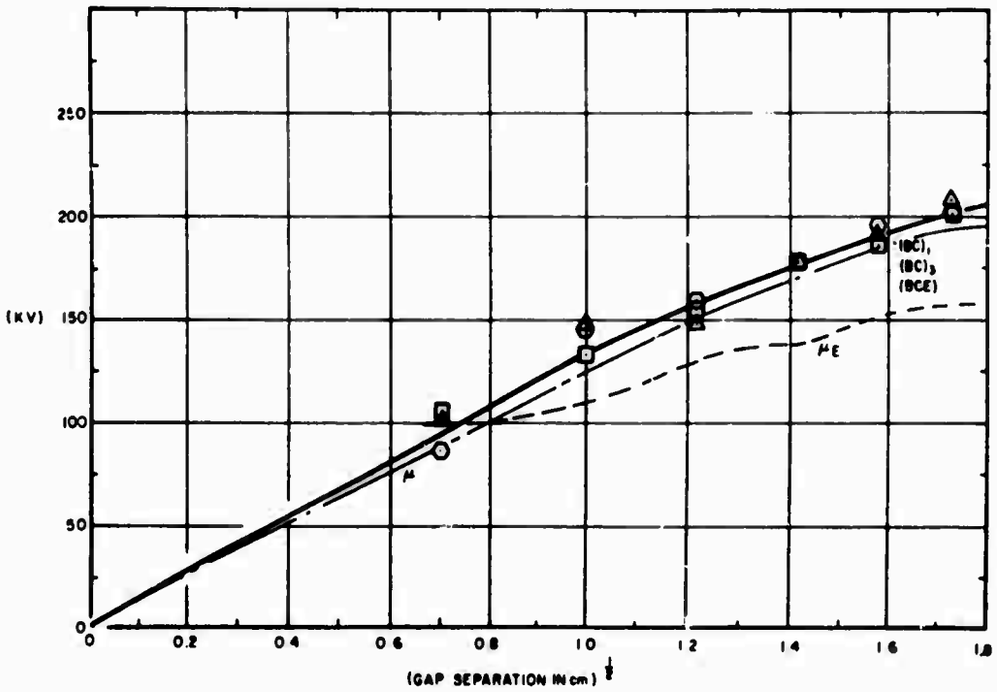

Figure 5-24. Cathode Processing x Electrode Size (BC)

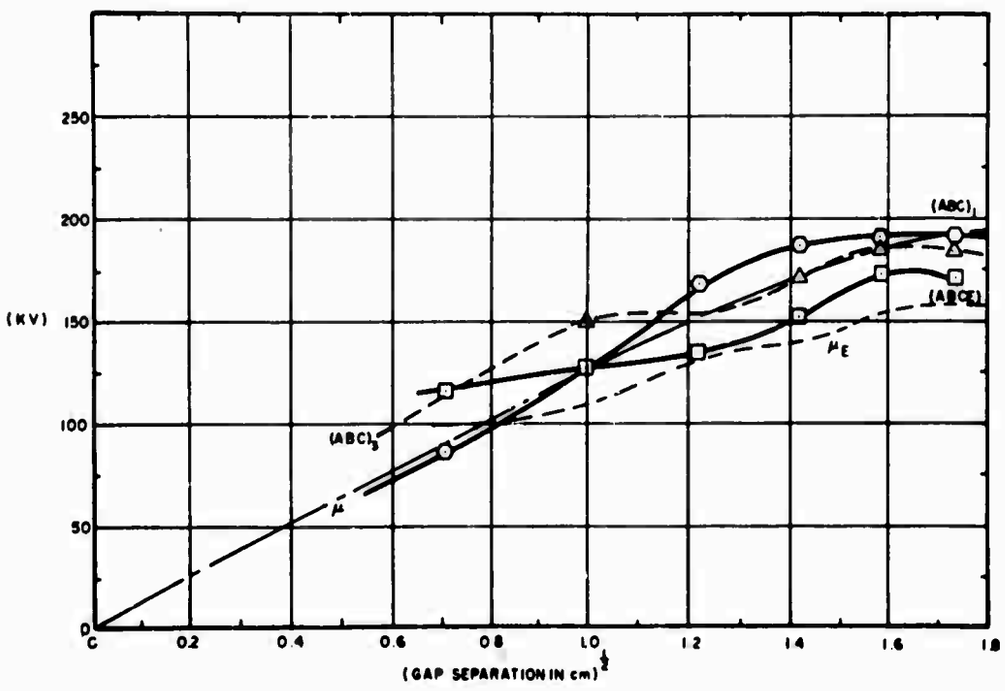

Figure 5-25. Cathode Processing x Anode Processing x Electrode Size (ABC)

The corresponding factors and interactions (denoted as AE, BE, ABE, CE, ACE, BCE, ABCE) in the presence of a transverse 250 gauss magnetic field have also been plotted for comparison.

The subscripts 1 and 3 labeling the curves refer to the first and third breakdown in each case. These took plate respectively before and after the breakdown measurement in the presence of the magnetic field and were meant to be indicative of any possible memory effects.

All factors and interactions without the magnetic field present reproduced remarkably well the trends already described. The contribution of the magnetic field is readily seen in each case by comparing the magnetic factorial effect with the non-magnetic case. Thus the magnetic A effect (AE) reduces the breakdown voltage much further below the magnetic average μ_E than A is below μ except below 0.75 cm. Thus the AE effect is negative. Similarly, the magnetic field enhances the effect of cathode pretreatment but scarcely influences the electrode size effect except below the crossover gap separation of 0.75 cm. It also reverses the sign of the combined electrode pretreatment interaction (AB) and reduces the AC interaction, while amplifying the BC interaction. Finally, it has a slight effect only on the ABC interaction except in shifting the crossover gap to 1.0 cm.

More detailed information on the nature of the magnetic interactions may be obtained by studying the curves of them as functions of magnetic field strength. Each one has been plotted along with the average magnetic field effect for comparison (Figures 5-26 through 5-33). The average effect is significant in that there is an increase in breakdown voltage below about 85 gauss but a much greater reduction for higher field strengths. The BE effect as a function of field strength is remarkably similar in shape except that it is always positive. The A effect becomes steadily more strong as magnetic field strength increases and has oscillations superimposed. On the other hand, the electrode size effect oscillates in sign. It must be borne in mind, however, that since in this case we are studying the percentage variation of an effect, a change in sign merely indicates that there is a swing from the effect getting weaker to getting stronger.

Not surprisingly, all other interactions which include A or C show the same oscillatory variation.

5.7 Prebreakdown Current

Measurements made during exploratory experiments showed that both the breakdown voltage, V_B, and $\log I_B$, the logarithm of the ultimate prebreakdown current, have a linear dependence on the square root of gap separation. It has furthermore been proposed from those results that the increased prebreakdown current induced by the greater macroscopic field at a curved cathode is responsible for corresponding increases in V_B. With this in mind, therefore, it is natural to inquire whether each factor influences V_B and $\log I_B$ in the same way and the last mentioned variable has, therefore, been studied using the factorial method. The value of $\log I_B$ was recorded for each gap separation and the averages (I and E rows in Table 5-3) and various factors were calculated with and without the magnetic field imposed.

The data are presented graphically as functions of $d^{1/2}$ in Figures 5-34 through 5-41 in the same way as the corresponding V_B data. In Figure 5-34 the average value of $\log I_B$ is shown to

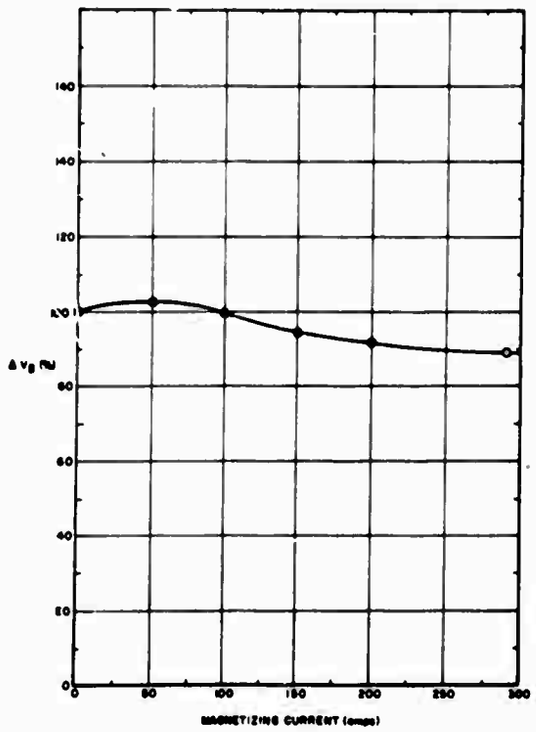

Figure 5-26. The E Effect

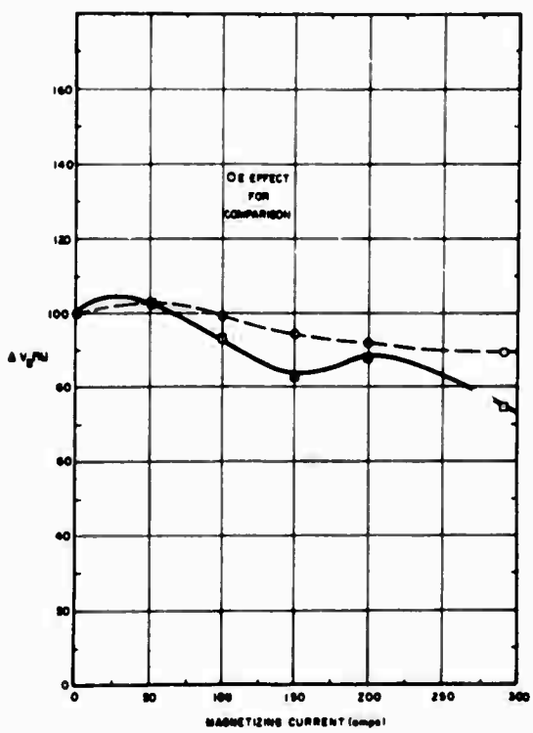

Figure 5-27. The AE Effect

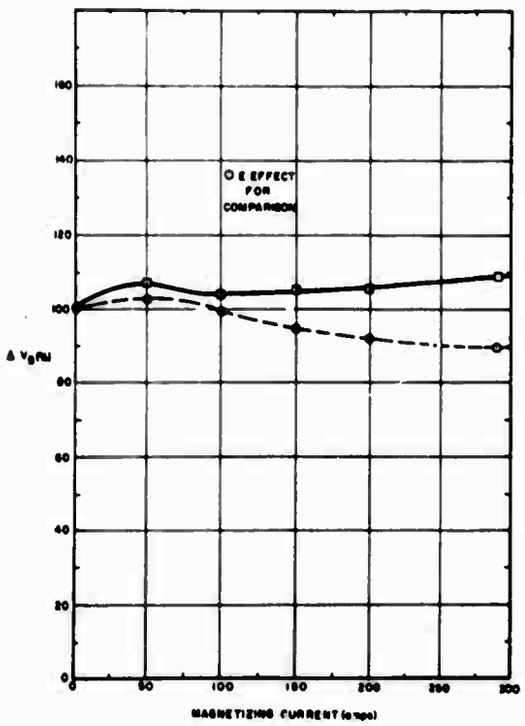

Figure 5-28. The BE Effect

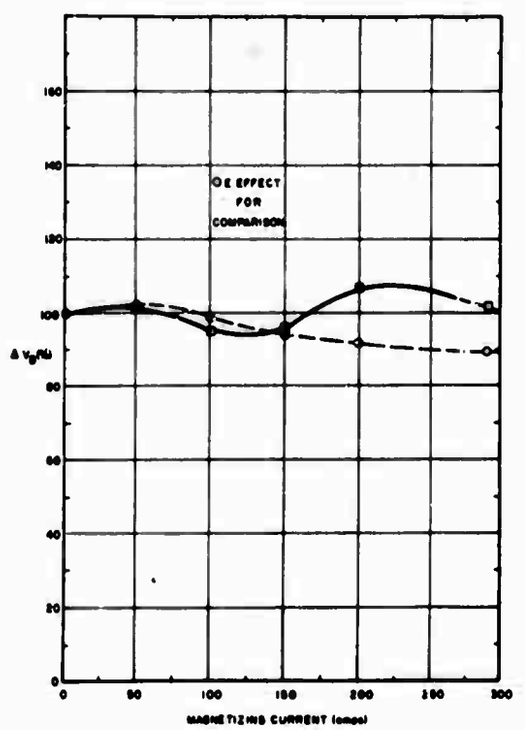

Figure 5-29. The ABE Effect

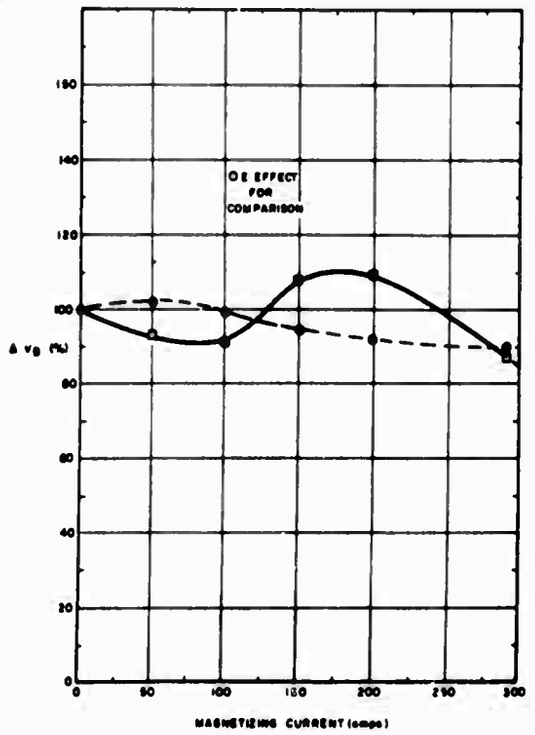

Figure 5-30. The CE Effect

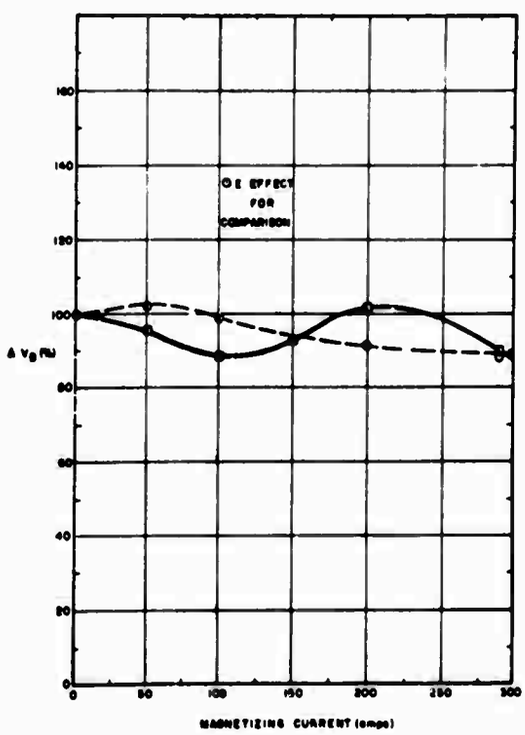

Figure 5-31. The ACE Effect

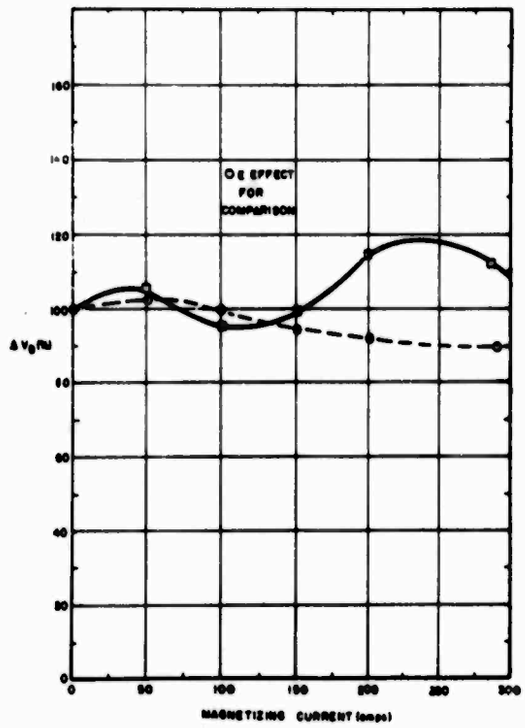

Figure 5-32. The BCE Effect

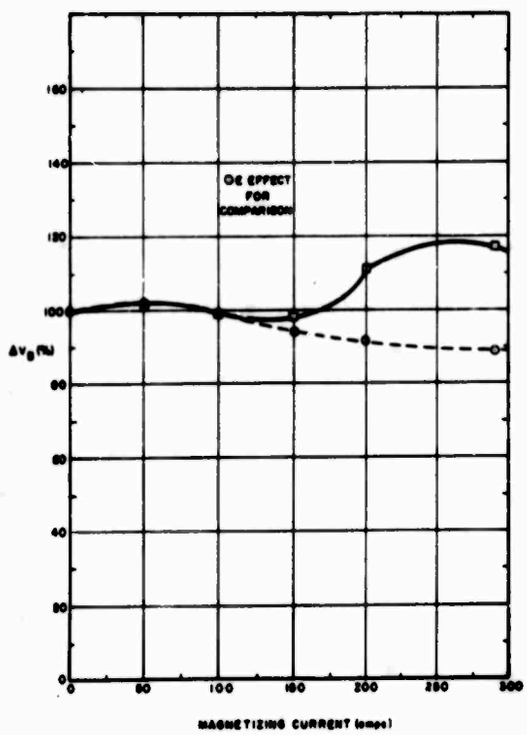

Figure 5-33. The ABCE Effect

Table 5-3. Yates Algorithm Estimates for Log I_B Without and With Magnetic Field (Conditioned Data)

	0.5 cm			1.0 cm			1.5 cm			2.0 cm			2.5 cm			3.0 cm		
	No	Yes	No	No	Yes	No	No	Yes	No	No	Yes	No	No	Yes	No	No	Yes	No
I	-6.29		-5.33	-7.48		-7.48	-8.55		-7.73	-8.30		-7.36	-8.82		-7.67	-7.19		-5.89
E		-5.53			-9.39			-9.67			-9.04			-8.66			-7.64	
A	-0.75		2.12	0.98		-3.06	-3.46		-2.76	-0.50		2.75	0.69		1.43	2.39		0.49
AE		1.78			-1.37			-4.43			1.91			2.44			1.13	
B	0.62		1.54	-0.48		0.49	0.17		1.32	2.65		0.25	-0.03		2.42	2.75		-1.25
BE		1.67			0.87			+0.93			-0.06			0.86			2.22	
AB	2.89		-1.69	-2.13		-1.29	-2.00		1.02	-2.76		-0.69	-0.22		0.78	-1.63		1.01
ABE		-1.73			-0.02			-1.17			-4.06			-2.68			-5.37	
C	-2.52		-2.06	-2.14		-2.60	-2.52		-3.09	-3.50		-2.75	-1.51		-3.82	-0.53		2.84
CE		-1.93			0.72			-0.47			0.74			1.21			1.63	
AC	-1.99		1.91	-1.09		-1.68	-1.91		-1.91	-2.91		2.31	-4.69		0.72	0.40		-2.90
ACE		1.95			0.13			+0.23			-3.26			2.97			1.22	
BC	1.56		1.75	1.59		2.47	2.17		7.65	1.24		-0.01	1.88		2.4	1.64		-1.16
BCE		1.88			5.07			2.58			1.41			0.33			2.13	
ABC	1.13		-2.30	-3.76		0.03	-0.37		-1.17	-0.65		-0.55	-0.78		1.37	-0.29		1.10
ABCE		-2.04			-1.22			-2.37			-2.59			2.79			1.72	

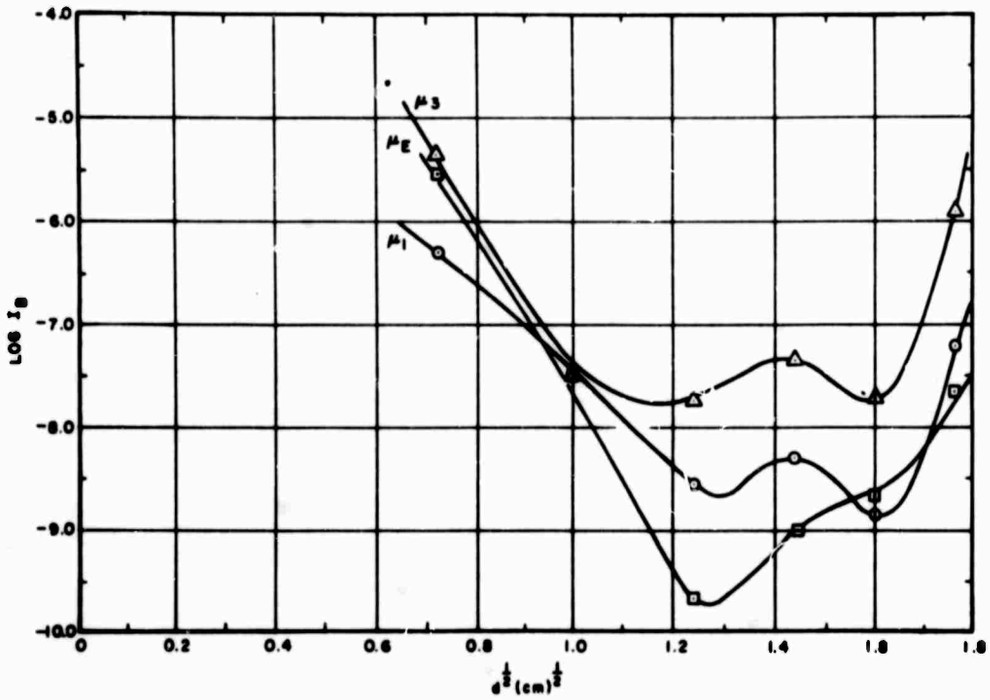

Figure 5-34. The μ Effect on Current

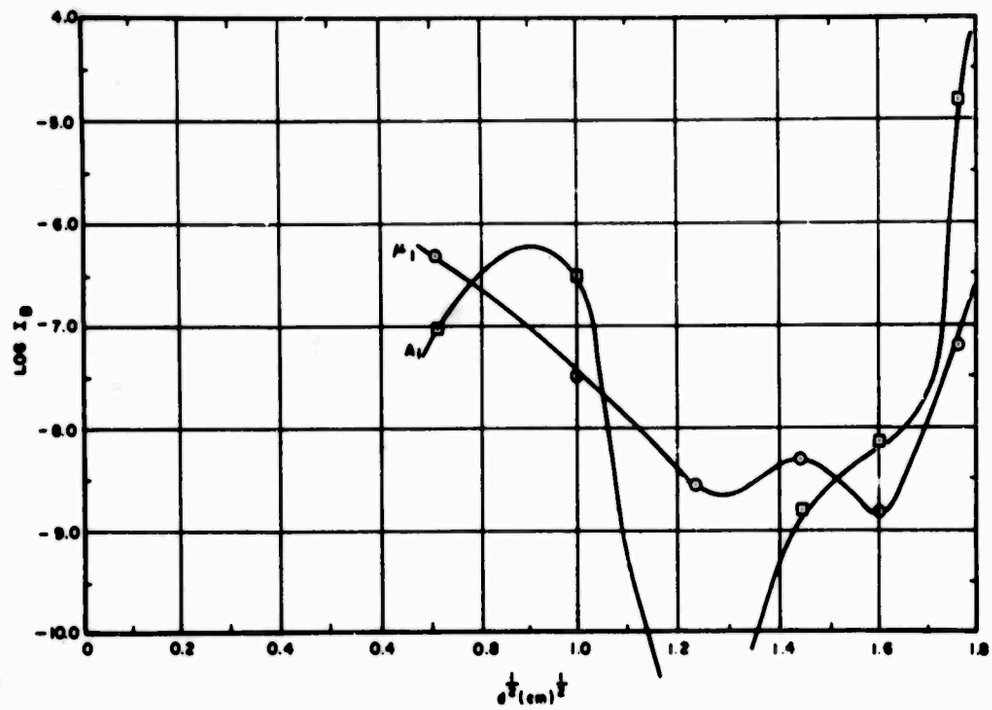

Figure 5-35. The A Effect on Current

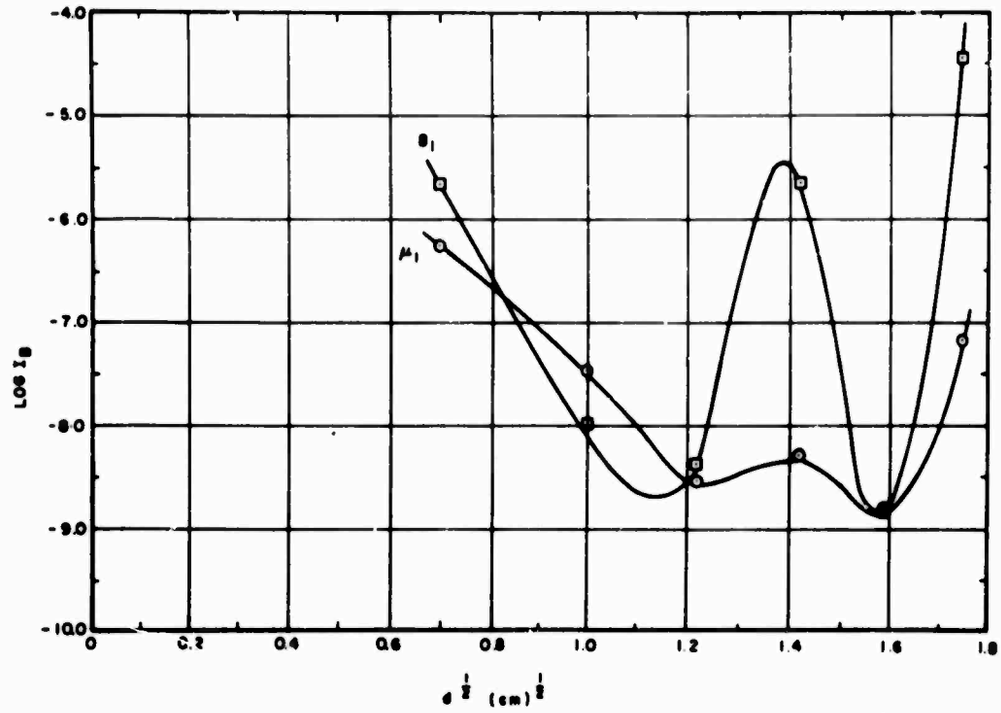

Figure 5-36. The B Effect on Current

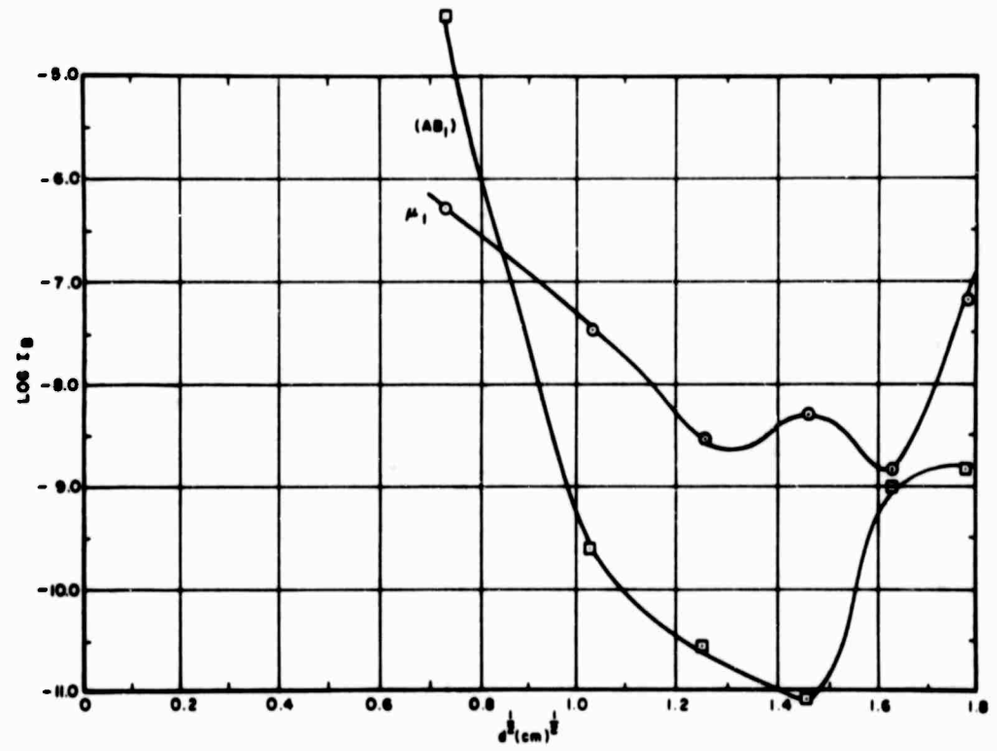

Figure 5-37. The AB Effect on Current

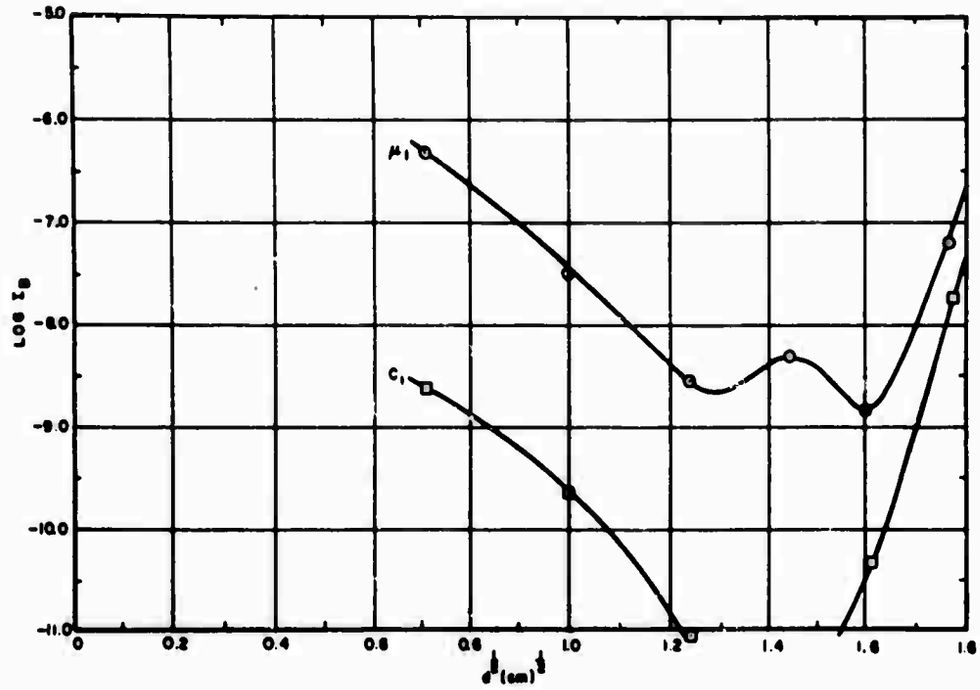

Figure 5-38. The C Effect on Current

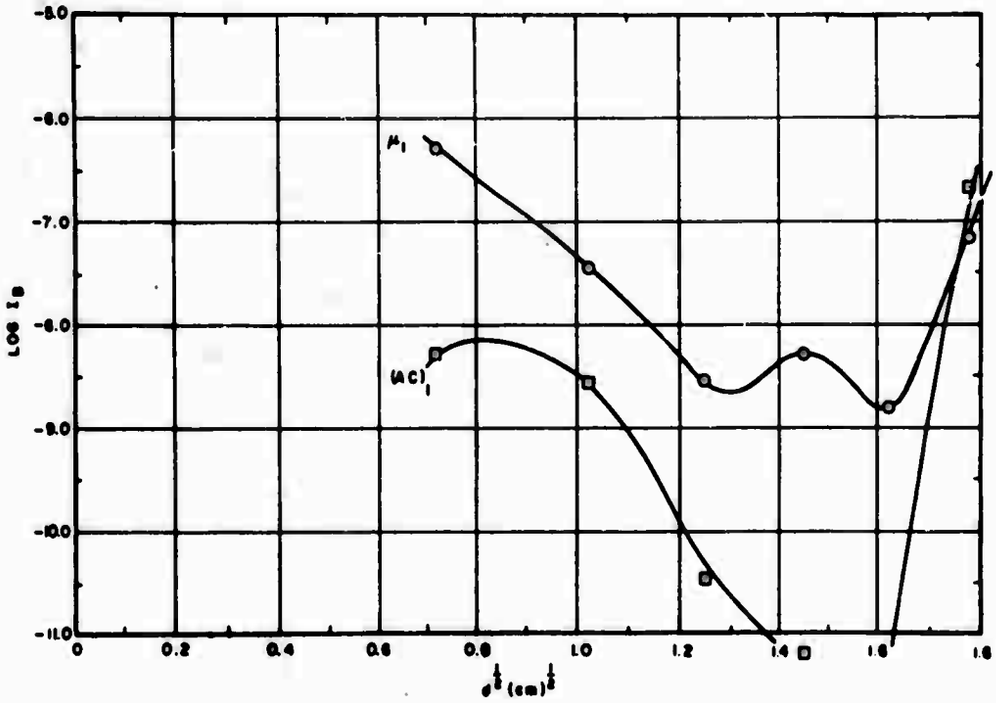

Figure 5-39. The AC Effect on Current

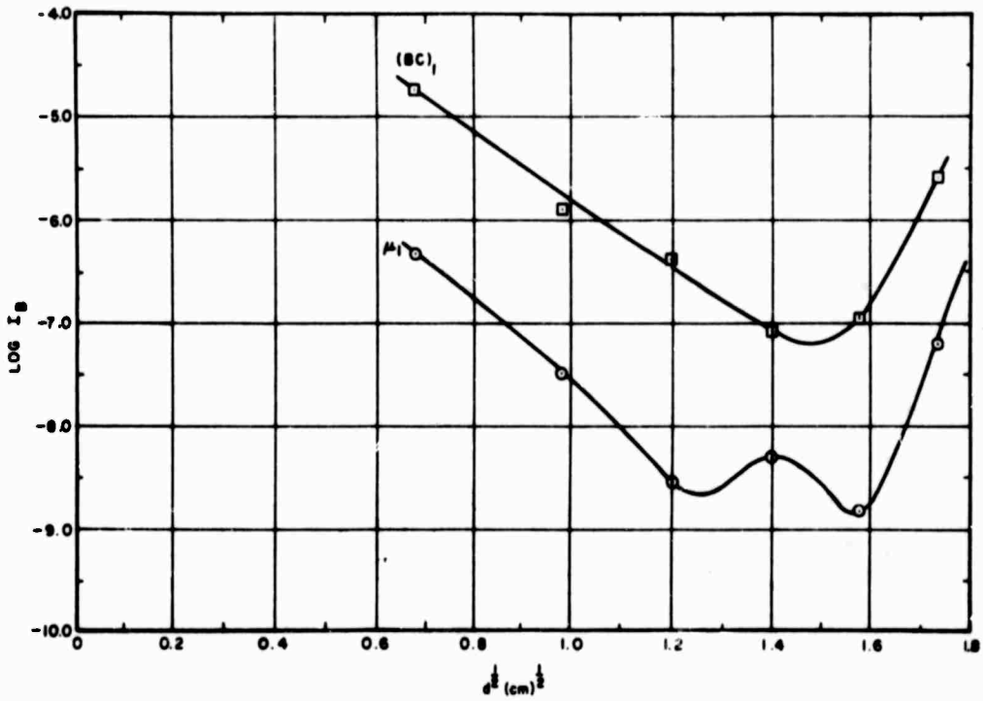

Figure 5-40. The BC Effect on Current

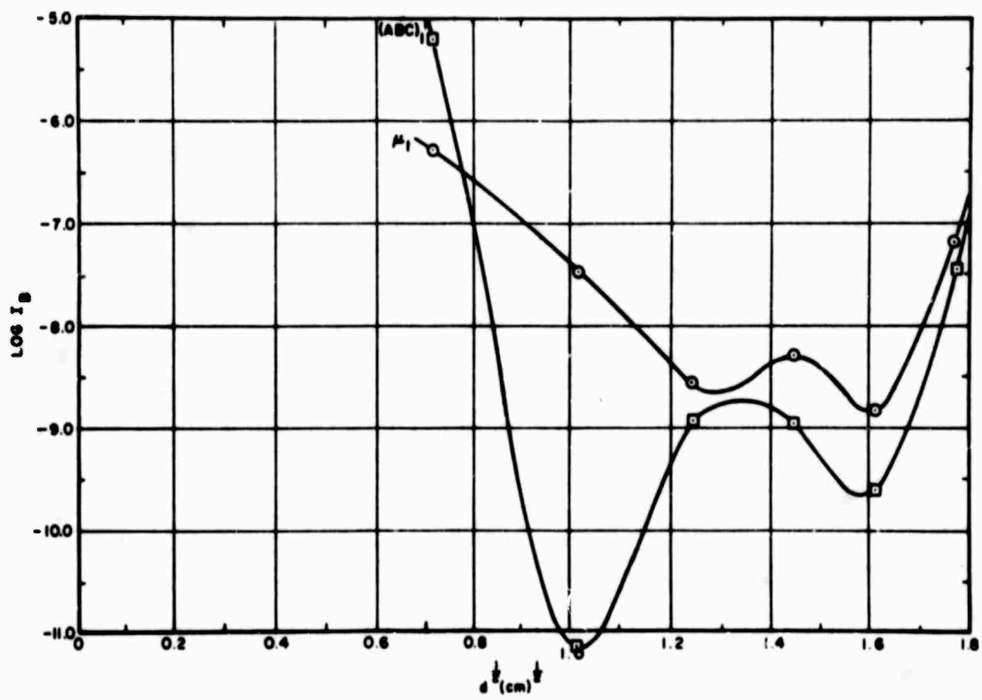

Figure 5-41. The ABC Effect on Current

be reduced by a 250 gauss transverse magnetic field except for currents above about 5×10^{-8} amp (compare the μ_i and μ_E curves). After the magnetic field is switched off, the value of log I_B increases to above the initial value at all gap separations so there appears to be a magnetic history effect.

The influence of anode gas content is strong and fluctuates widely above and below the average and cathode processing in vacuum raises log I_B above the average for most gap separations. Large electrode area on the other hand reduces log I_B strongly and consistently at all gap separations just as it influences V_B.

The AC effect, however, is negative, opposite to its effect upon V_B, but the magnetic field changes this. The BC effect, on the other hand, is positive with and without the magnetic field on, just as it is for V_B.

It therefore seems that each factor influences the ultimate prebreakdown current in similar ways to the manner in which it influences V_B. Thus, it would seem that some factors tending to raise the prebreakdown current would also raise the breakdown voltage. The evidence for this, however, is not strong because of the wide range of influences on log I_B and their apparent inconsistency, which may be due to a magnetic memory effect.

5.8 Conclusions

The most significant conclusion is that the strong AC interaction between anode gas content and electrode area is consistent with the theory that gas evolution directly affects breakdown. Large area electrodes would then concentrate gas density at the electron beam.

Gas density alone has a slight effect as evidenced by the consistency of the A influence, but it acts oppositely to what was initially thought. Additional gas in the system thus raises the breakdown voltage. This fact, however, is entirely consistent with the experimental findings of other workers[5] who raised the ambient gas pressure in their systems. The influence of large area electrodes, however, is to reduce the breakdown voltage which, if it were due to the decreased pumping conductance, should have the same effect as raising the ambient gas pressure or the level of anode gas content. At 0.5 cm, however, in a 250 gauss magnetic field the area effect is very slightly positive and so there is no reason to believe that its sign is unique. A similar phenomenon is observed with the AC interaction.

From this, it must be concluded that the evolution of gas into the system has a more complicated effect on breakdown voltage than simply raising or lowering the value. The small reversals of the C and AC effects at 0.5 cm coincide with a situation for which the prebreakdown current is large and the electron impact ionization consequently strong.

The factorial influences on the ultimate prebreakdown current are often strong and powerfully influenced by the magnetic field. Very little can be said about them for sure, but the average values of log I_B as a function of gap separation preserve their shape after the magnetic tests although they are relatively displaced. The statistical scatter about each point would, therefore, appear to be small.

The data do, however, show that manipulation of the gas density in the system will influence both V_B and log I_B in a complicated way. The magnetic field, although very weak, has a strong influence on them too. In view of the complexity of the system, a theoretical model of the breakdown process has been constructed and analyzed in an attempt to see some pattern in this experimental data.

5.9 References

(1) Pivovar, L. I., et al, "The Effect of the Electron Current Component on Development of Electrical Breakdown in High Vacuum", Sov. Phys.-Tech. Phys. 2, 909 (1957).

(2) Sanford, J. R., Proceedings of the First International Symposium on Insulation of High Voltages in Vacuum (1964).

(3) Watson, A., "Pulsed Flashover in Vacuum", J. Appl. Phys. 38, 2019 (1967).

(4) Avdienko, A. A. and Kiselev, A. V., "Outgassing from Insulator Surfaces in a Strong Electric Field in Vacuum", Sov. Phys.-Tech. Phys. 12, 381 (1967).

(5) Cooke, C. M., "Residual Pressure and Its Effect on Vacuum Insulation", Proceedings of the Second International Symposium on Insulation of High Voltage in Vacuum (1966).

PART B

THEORETICAL

SECTION 6
PURPOSE OF THE THEORY

For many years, the precise mechanisms of vacuum insulation failure have evaded discovery. Indeed there has been a proliferation of theoretical mechanisms designed to satisfy narrowly defined experimental conditions, not all of which have been demonstrated to be uniquely valid. Thus the experimental discovery that the breakdown voltage increases with the square root of gap separation led to the development of the so-called "clump" theory. This being principally designed to explain that fact, it is sometimes tacitly assumed to be true whenever there is a square root law, although it fails to explain other phenomena. A transition in the functional form of the breakdown voltage versus gap separation curve from a square root to a linear dependence at low gap separations leads perhaps erroneously to the conclusion that some other mechanism becomes operative. The more widely accepted (although unverified) theories attribute the breakdown to thermal instabilities at either the cathode or anode. Two regimes of applied voltage duration and gap separation have been defined by consideration of the cathode thermal instability mechanism which is valid for short pulses and small gap separations. It has received theoretical and experimental attention and will not be considered here. On the other hand, the thermal anode instability mechanism which is supposed to lead to breakdown of long gaps under dc conditions has not been theoretically defined beyond the statement that an electron beam from the cathode can overheat an anode spot until it becomes unstable. Other unsuccessful theories pertinent to this operating regime have attempted explanations by a current multiplication instability induced by photons from the anode or by an ion exchange process occurring at both electrode surfaces.

While theories were failing to clarify experimental facts, more data appeared which obscured the underlying mechanism even further. It appeared that large area electrodes had lower breakdown voltages than smaller ones and that electrode curvature enhanced the breakdown voltage, contrary to what would be intuitively expected. Also contrary to intuition, it was found that increasing the pressure into the poor vacuum range increased the breakdown voltage.

The analytical investigations about to follow have been successful in combining previous theoretical and experimental work into one unified picture of the breakdown mechanism as an instability of the interelectrode space charge growth. The new viewpoint is successful also in describing new experimental data on magnetic field effects.

BLANK PAGE

SECTION 7

IONIC FIELD ENHANCEMENT

7.1 Abstract

A theoretical analysis of the equilibrium radius of a cathode protrusion under surface migration in an electric field indicates values inconsistent with those required to account for field emission current densities. Positive ion accumulation at the tip to supplement the geometrical field enhancement is therefore proposed to explain the difficulty. A preliminary study shows that the breakdown voltage, V_B, will increase with the square root of gap separation if the field enhancement factor becomes unstable at some critical value. Development of the Fowler-Nordheim expression for total current, I, to account for the change of emission area shows that the value of $1/V_B$ *ln* (I_B/V_B^2) should be constant at all gap separations. Experimental data is presented to confirm that this is so after some spark conditioning.

7.2 Introduction

The steady prebreakdown currents which appear when high voltages are applied to electrodes in vacuum are normally attributed to field emission by the Fowler-Nordheim mechanism. It is necessary, however, to assume that the field is enhanced locally by cathode protrusions and several workers have demonstrated their existence with the electron microscope.[1] A field enhancement factor can be calculated from the slope of a Fowler-Nordheim plot if it is a straight line, but deviations from linearity are common, particularly at voltages close to the breakdown value.

Exhaustive experimental and theoretical work[2] has established that surface atoms on a field emitter will migrate away from regions of high radius of curvature. The shape, consequently, changes until the electrostatic and cohesive forces balance to give an equilibrium radius of curvature, just as a suspended liquid drop would behave. The local radius of curvature at the tip establishes the field enhancement factor and, hence, the surface field which controls the current drawn from the cathode. In consequence of this, the effective emitting area of a protrusion will decrease as the field enhancement factor grows. The simple Fowler-Nordheim expression is then no longer applicable, nor will there be a fixed enhancement factor. Instead the surface field will be a function of the surface energy of the cathode material and the applied voltage.

This model of the field enhancement will be shown to be inadequate because the protrusion dimensions required to give significant field enhancement to satisfy the Fowler-Nordheim expression are inconsistent with those needed to preserve an equilibrium tip shape. It is, therefore, necessary to look for other sources of field enhancement and ionic accumulation around the tip is one which will be investigated.

A beam of electrons will emerge from the cathode creating an anode hot spot from which gas is evolved and ionized in the interelectrode space by the primary beam. Hydrogen gas has been observed[3] and its ions together with metal vapor would consequently drift to the cathode and further

enhance the local field at the emitter tip, perturbing it and, hence, the equilibrium shape. The field enhancement factor is, consequently, a variable governed by the interelectrode ionization.

7.3 Theory

The surface field strength, E_s, at the tip of a cathode protrusion is related to the macroscopic local field strength, E_o, by the field enhancement factor β:

$$E_s = \beta E_o = \frac{\beta V}{d} \tag{7-1}$$

A very good estimate of the field enhancement of a protrusion was obtained by Vibrans.[8] He considered a small sphere of radius r on the end of an infinitely thin wire in a uniform field E_o. The tip was at distance h from the cathode and a charge (q) on the sphere was calculated to give no difference of potential Φ between it and the cathode. At distance Z from the center of the sphere:

$$\Phi = E_o (Z + h - r) - \frac{E_o r^3 Z}{\left(x^2 + y^2 + z^2\right)^{3/2}} - \frac{q}{\epsilon_o \left(x^2 + y^2 + z^2\right)^{1/2}} \tag{7-2}$$

The field at the tip can then be calculated and by equating this with E_s an expression for the field enhancement factor can be obtained:

$$\frac{E_s}{E_o} \equiv \beta \equiv \frac{h}{r} + 2 \tag{7-3}$$

The field enhancement factor is thus a fixed function of the geometry.

For large values of field enhancement factor, β is given approximately by:

$$\beta = \frac{h}{r} \tag{7-4}$$

The surface field strength in a uniform field is then:

$$E_s = \frac{h}{d}\frac{V}{r} = \frac{V}{k_o r} \tag{7-5}$$

where k_o is a dimensionless parameter depending on the gap separation.

If, however, a current, I_+, of positive ions flows to the protrusion there will be a supplementary space charge field, X_s, depending upon the square root of the current density, J_+.[4] Hence,

if the ion and electron trajectories are the same and I_+ is proportional to the product of I and gas density:

$$X_s = \frac{I_+^{1/2}}{k'_i r} = \frac{I^{1/2}}{k_i r} \tag{7-6}$$

where k_i is a parameter involving gaseous current amplification and the total tip field is:

$$E_s = \frac{V}{r}\left[\frac{1}{k_o} + \frac{I^{1/2}}{k_i V}\right] = \frac{V}{k r} \tag{7-7}$$

E_s has now been represented in the same form as Equation (7-5), but the parameter k is no longer solely a function of gap separation and protrusion geometry:

$$\frac{1}{k} = \frac{1}{k_o}\left\{1 + \frac{k_o}{k_i}\frac{I^{1/2}}{V}\right\} \tag{7-8}$$

Comparing this with:

$$E_s = \frac{\beta_e V}{d} \tag{7-9}$$

where β_e is an overall effective enhancement factor, we have:

$$r = \frac{d}{k\beta_e} \tag{7-10}$$

Thus, for a particular pair of values of tip radius and gap separation, the effective field enhancement factor and k are inversely related. Hence, from Equations (7-9) and (7-5):

$$\beta_e = \beta\left\{1 + \frac{k_o}{k_i}\frac{I^{1/2}}{V}\right\} = \beta(1 + f) \tag{7-11}$$

where:

$$f = \frac{k_o}{k_i}\frac{I^{1/2}}{V}$$

Due to surface migration in an electric field, the value of r will depend upon E_s and the surface tension, γ, in the following manner:[5]

$$r E_s^2 = 12 \pi \gamma \tag{7-12}$$

Thus:

$$\frac{V^2}{d} = \frac{12 \pi \gamma k}{\beta_e} \tag{7-13}$$

or:

$$V E_s = 12 \pi \gamma k \tag{7-14}$$

Hence, the voltage required to attain a particular value of field enhancement factor varies as the square root of the gap separation. This depends upon the supposition that k is independent of d and so relies on the proviso that ionic charge field enhancement dominates the expression. In the long gap regime, it is found experimentally that the breakdown voltage varies with gap separation in this way and implies that voltage breakdown takes place at a critically low value of effective enhancement factor, β_e or k.

An order of magnitude estimate can readily be made of the ion density in a 1 cm gap at 100 kV required to produce a contribution to the enhancement equal to the geometrical component.

The criterion for significant ionic field enhancement is that the potential of the sphere in the foregoing argument should be of the same order as the induced potential difference between it and the cathode in a uniform field. The appropriate radius which the tip surface acquires by migration while developing a field strength of 10^7 volts/cm is about 10^{-5} cm and the corresponding potential will be 100 volts relative to infinity. A one-dimensional integration of Poisson's equation over a 1 cm gap containing positive charge indicates that 10^8 ions/cc will produce an ionic potential difference of 100 volts and if the interelectrode gas density is 10^{-5} torr this corresponds to a degree of ionization of 10^{-3}. Since this is the product of the ionization cross section, σ, and current density, J, then at the lowest possible value of σ (at 100 kV it is about 10^{-20} cm^2) the appropriate current density would be about 10^{-2} amp/cm^2. The latter figure requires a current from the tip of about 10^{-12} amp which is appropriately low for the assumed field intensity of 10^7 volts/cm and the mechanism can be considered numerically feasible.

An estimate can be made of the protrusion dimensions required to enhance a 10^5 volt/cm field by a factor β of 100 without ionization. From Equations (7-4) and (7-12):

$$\beta^3 = \frac{12 \pi \gamma}{E^2 h} \tag{7-15}$$

With $\gamma = 1600$ ergs/cm^2 for copper,[6] this leads to a value of h of about 10^{-5} cm which, of course, is not consistent with Equation (7-4). It must, therefore, be concluded that geometrical field enhancement alone will not account for the field intensification required by Fowler-Nordheim data.

If current is emitted mostly into a cone of semi-angle ψ about the tip axis, the emitting area is $2\pi(1 - \cos\psi)r^2$ and the total Fowler-Nordheim current is:

$$I = 2\pi(1 - \cos\psi)r^2 A E_s^2 \exp\left(-\frac{B}{E_s}\right) \tag{7-16}$$

Substitution from Equations (7-12) and (7-14):

$$I = 2\pi A(1 - \cos\psi)\left(\frac{V}{kE_s}\right)^2 E_s^2 \exp\left(-\frac{B}{E_s}\right) = \alpha V^2 \exp(-B'V) \tag{7-17}$$

where:

$$\alpha \equiv \frac{2\pi A}{k^2}(1 - \cos\psi)$$

$$B' \equiv \frac{B}{12\pi\gamma k}$$

Equation (7-17) shows that the functional form of the term $-\ln(I/V^2)$ is a measure of the value of the Fowler-Nordheim exponent. Its relation with the other parameters is evident when the total field emission current is written from Equations (7-8) and (7-17):

$$\frac{I}{V^2} = \frac{A_1}{k^2}\exp\left\{-\frac{BV}{12\pi\gamma k}\right\}$$

$$= A_1\left\{\frac{1}{k_o} + \frac{I^{1/2}}{k_i V}\right\}^2 \exp\left[-\frac{BV}{12\pi\gamma}\left\{\frac{1}{k_o} + \frac{I^{1/2}}{k_i V}\right\}\right] \tag{7-18}$$

Thus:

$$\ln\left(\frac{k^2 I}{V^2}\right) \equiv 2\ln\left(\frac{k_i f}{1 + f}\right) = \ln A_1 - \frac{BV}{12\pi\gamma k_o}(1 + f) \tag{7-19}$$

where:

$$f \equiv \frac{k_o}{k_i} \frac{I^{1/2}}{V}$$

and:

$$\frac{d\,\ell n\, f}{dV} = \frac{-\frac{B\,(1+f)}{12\,\pi\gamma\,k_o} - 2\,\frac{d\,\ell n\, k_i}{dV}}{\frac{2}{(1+f)} + \frac{V\,B\,f}{12\,\pi\gamma\,k_o}} \qquad (7\text{-}20)$$

If the Fowler-Nordheim exponent did not include f then the denominator would be absent in Equation (7-20) and the rate of rise of current would be greater. Thus, the presence of a large ionic component of field enhancement in the exponent brings about a stabilizing negative feedback effect.

The restriction is a direct consequence of surface migration and there will be an appropriate relaxation interval of some seconds before the establishment of a steady current after a voltage step is applied. For large values of f, Equation (7-20) predicts that (neglecting the k_i variation) f and hence β_e will fall inversely with voltage. Upon raising the voltage, $\ell n\,(I/V^2)$ will rise but as migration proceeds it will relax to the steady state value determined by the negative feedback.

This simple argument has neglected the possible variation of k_i with voltage, hence excluding account of possible changes in gas evolution.

It should thus be possible to measure the I-V characteristic and calculate the expression $-\ell n\,(I/V^2)$ at the same voltage, V, at any gap separation. Comparison of the results will then provide a measure of how much gas evolution is changing and contributing to the field enhancement. An especially appropriate case is at the point of breakdown when presumably enough gas is present for the system to be unstable. The parameter $-\ell n\,(I_B/V_B^2)$ expressed as a function of V_B then describes the breakdown condition in terms of the effective field enhancement factor. A linear form for this function would then imply breakdown at a critical value of field enhancement. This technique has been applied to the experimental observations about to be described.

7.4 Experimental Method and Results

A factorially designed experiment has been completed in which seven experimental variables were studied. During the experiment, procedures were developed to specify the breakdown voltage and two in particular emerged. In the first, a conventional method was used in which the voltage was raised until a limit was reached due to repetitive breakdown, earlier isolated sparks being neglected. By contrast the second procedure took isolated sparking into consideration and only one spark was permitted before switching off. Thus, conditioning was limited between tests. In each case measurements

were made consecutively at each gap separation by raising the voltage in 10 kV steps every two minutes. After a test series was over, the gap was spark conditioned at 1.0 cm separation and the procedure repeated. Prebreakdown current was measured at each voltage and gap separation.

The voltage source was a small Van de Graaff generator capable of delivering 200 μamp with 400 pF or energy storage capacitance. Each electrode was baked to 400°C for eight hours, giving an operating vacuum contamination-free at 10^{-8} torr with ion pumping. Copper and titanium electrodes were used with either spherical or Bruce profile, and coarse or fine surface finish.

The gap current, X-radiation and partial pressure of hydrogen were monitored during the tests.

Three sets of experimental results were chosen to investigate the breakdown condition according to the theory outlined. In two of the sets, a pair of Bruce profile titanium electrodes were tested initially by the repetitive sparking technique and secondly by the isolated spark technique with different electrodes similarly prepared. Thus, the Fowler-Nordheim exponent for the ultimate prebreakdown current was plotted as a function of voltage for different gap separations. With the repetitive sparking results, these curves turned out to be linear (Figure 7-1), but in the second case linearity was only approached after three previous test sequences representing about 25 prior breakdown events. The non-linear curves (numbered according to test sequence in Figures 7-2 and 7-3) are characterized by sharp peaks which diminish as conditioning proceeds.

The third set of results (Figures 7-4 and 7-5) were obtained from five successive test series on a pair of Bruce profile copper electrodes using the isolated sparking method. In one day the first three were obtained and the remaining data were gathered the next day after standing for 17 hours in 10^{-8} torr vacuum. At the fourth test immediately following the resting interval, an almost linear curve was obtained but further testing revealed the characteristic peak once more. It is noteworthy that in the test series following the initial one each day, the peaks appeared at the same voltage (200 kV).

7.5 Conclusions

Ionic field enhancement will account satisfactorily for anomalously high Fowler-Nordheim currents.

The most significant conclusion to be tak from Figures 7-1 and 7-3 together with Equation (7-18) is that voltage breakdown takes place at a critical value of k. Field enhancement is dominantly ionic and after some conditioning the tunneling probability settles to a steady constant value. Before this, however, the tunneling probability probably oscillates with applied voltage due to the resonant nature of the barrier transmission of electrons. The physical reason for this is thought to be that adsorbed gas on the cathode tip creates a double barrier such as is described by Duke and Alferieff.[7] Since ions are continually being generated in the gap, they will bombard this adsorbed layer and change its nature as time goes on. Thus conditioning is seen at least partially as cleaning up of the cathode surface by ion bombardment.

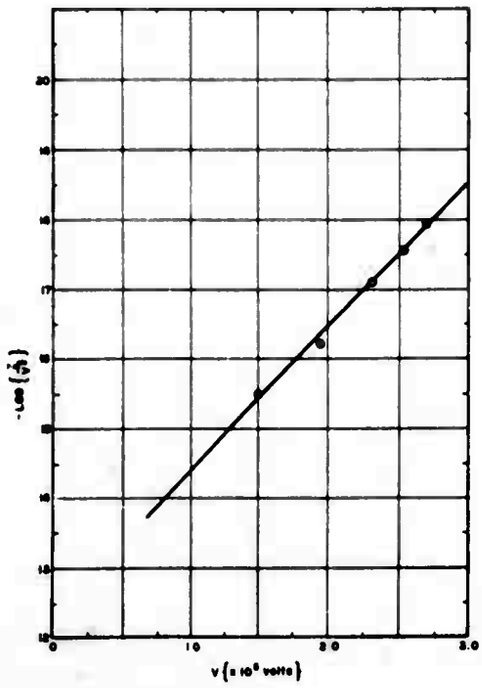

Figure 7-1. Linear Plot to Demonstrate Theory for Repetitive Sparking Conditions (Ti Fine Bruce Cathode, Ti Coarse Bruce Anode)

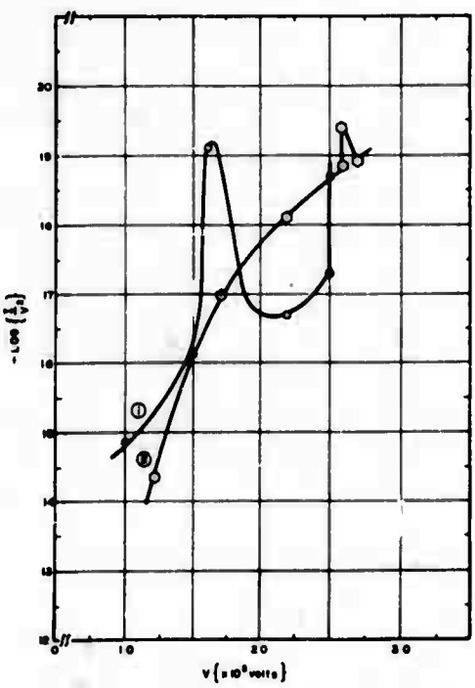

Figure 7-2. Non-Linear Plots Showing Transition to Linearity as Conditioning Proceeds (Ti Fine Bruce Cathode, Ti Coarse Bruce Anode)

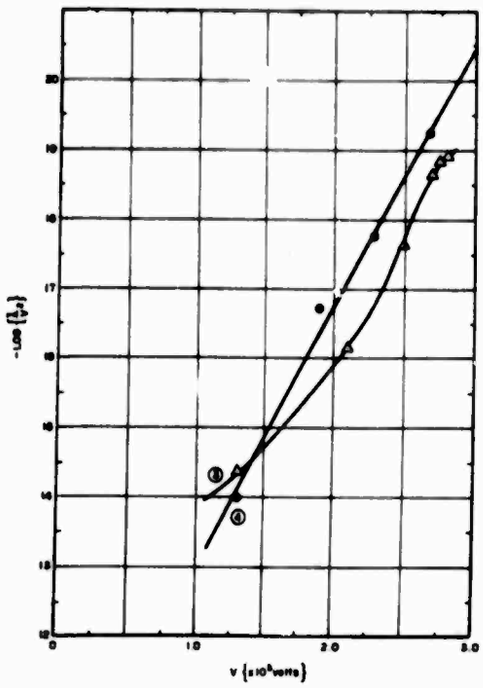

Figure 7-3. Non-Linear Plots Showing Transition to Linearity as Conditioning Proceeds (Ti Fine Bruce Cathode, Ti Coarse Bruce Anode)

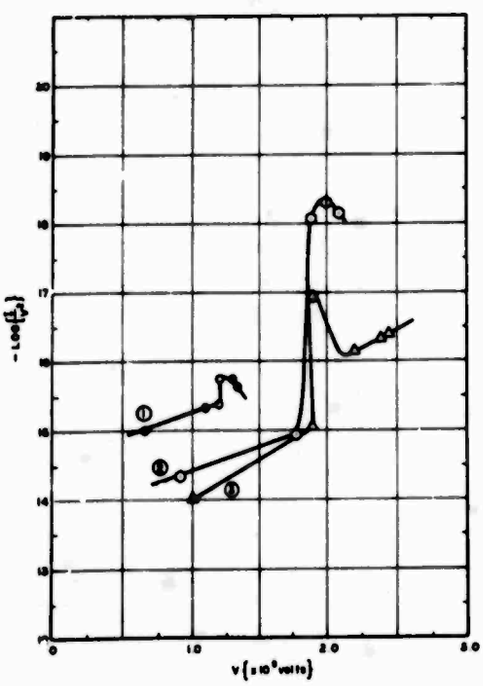

Figure 7-4. Non-Linear Plots Showing Transition to Linearity as Conditioning Proceeds (Fine Copper Electrodes)

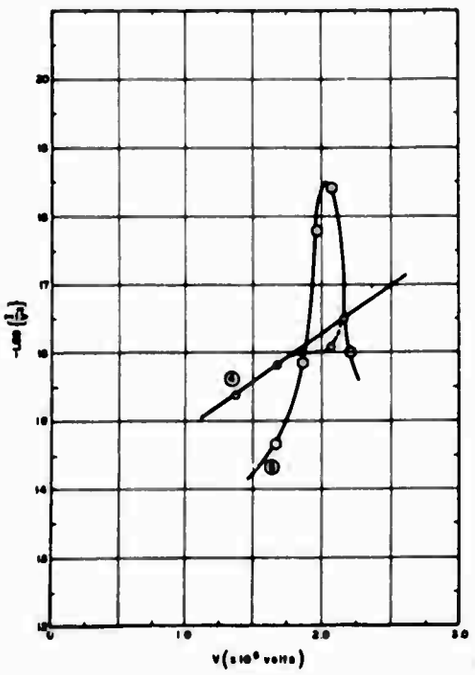

Figure 7-5. Non-Linear Plots Showing Transition to Linearity as Conditioning Proceeds (Fine Copper Electrodes)

7.6 References

(1) Little, R. P. and Smith, S. T., Proceedings of First International Symposium on Insulation of High Voltages in Vacuum (1964).

(2) Dyke, W. P. and Dolan, W. W., Advances in Electronics and Electron Physics 8, 89 (1956).

(3) Watson, A., Denholm, A. S. and Mulcahy, M. J., Proceedings of Second International Symposium on Insulation of High Voltages in Vacuum (1966).

(4) Finkelnburg, W. and Maecker, H., "Elektrische Bogen und Thermisches Plasma", Handbuch der Physik, Bd. XXII.

(5) Charbonnier, F. M., Martin, E. E., Strayer, R. W., Bennette, C. J., Proceedings of First International Symposium on Insulation of High Voltages in Vacuum (1964).

(6) Herring, C., "Structure and Properties of Solid Surfaces", University of Chicago Press (1953).

(7) Duke, C. and Alferieff, M., J. Chem. Phys. 46, 923 (1967).

(8) Vibrans, G. E., "Field Emission in Vacuum Voltage Breakdown", Technical Report No. 353, Massachusetts Institute of Technology, Lincoln Laboratory (May 1964).

SECTION 8

THE INSTABILITY MECHANISMS

8.1 Abstract

A theoretical model of the vacuum breakdown process is constructed as follows. Geometrical field enhancement by a cathode protrusion decreases due to surface migration if the applied voltage is raised. Positive ionic space charge from the accumulated impact ionization all along the resultant electron beam will supplement the enhancement and amplify the Fowler-Nordheim current by secondary emission. A voltage exists for which the overall field enhancement is unstable and depends upon the gas density. Both anode vaporization and cathode sputtering can sustain this and either one may dominate the condition determining the breakdown voltage which consequently depends upon the square root or linear power of the gap separation for uniform fields. The theory correctly accounts for the influence upon breakdown voltage of electrode material, curvature, gas sorption, gap separation and magnetic fields.

8.2 Introduction

Vacuum breakdown has been observed to occur at a voltage related to the gap separation by some simple power law.

At large gap separation, the relevant exponent has the approximate value of one-half and at low separations it is unity. Somewhere in between there is a sharp transition from one form to the other, which has often been suggested to be evidence of a change in the breakdown mechanism. Many plausible mechanisms have been suggested, but only one by Cranberg[1] has explained the half power law. It has thus been sometimes assumed that this is the only explanation and that the Cranberg mechanism should be applicable in the long gap regime. On the other hand, in the same regime, there has been growing evidence that breakdown is initiated by field emission of electrons which concentrate a critically high power into a hot spot on the anode.[2] At low gap separation, breakdown has been thought to be initiated by electrically overloading the cathode protrusion from which the prebreakdown current is emitted. The growing feeling that there are two competing processes which alternately control the breakdown has found expression in the terms "cathode dominated" and "anode dominated" to describe the appropriate regimes.

The purpose of the present work is to demonstrate that the half power law can be derived for an anode dominated mechanism and a linear law for the cathode dominant case. It has been necessary to specify the latter mechanism more precisely, as one governed by gas evolution by cathode sputtering as opposed to anode heating. This leads naturally to a changeover in the breakdown law and clarifies many apparently anomalous phenomena previously reported.

When electrodes are electrically stressed in vacuum, the tip shape of any cathode protrusion will become more blunt by surface migration at the voltage is raised.[3] Electrons emitted from it will travel in parabolic trajectories with a spread determined by the initial impulse they receive from

the high radial field component which is present around sharp tips.[4] This progressive blunting will, as the voltage is raised, dilate the beam and increase the anode power density because the field emission also increases. Eventually the anode temperature becomes high enough at some power level for vapor and gas to be evolved and ionized substantially. Positive ions attracted to the emitter will amplify the current by secondary electron emission.

Ionization in the path of the electron beam also causes a positive space charge cloud to accumulate at the emitter tip. An augmented field consequently develops there to supplement the local geometrical field enhancement. The additional enhancement from ionization will be shown to depend directly upon the overall field enhancement for any given temperature with which it also increases. An unstable situation like this would not persist were it not for the reduced availability of the other necessary ingredient for copious ionization, which is a substantial gas density evolved from the anode.

As the overall enhancement factor increases from additional ionization, it promotes a beam spread restricting the anode power density. Only enough vapor is evolved to maintain the appropriate beam spread until the number density level is too high in the gap. At a critical value of overall field enhancement factor, any further increase will raise the current density more than it will restrain gas evolution by reduction of anode power density and ionization will proceed unhindered. The cathode field intensity then rises towards infinity and the voltage drops to the level required to sustain a heavy current discharge.

Ion bombardment of the cathode also sputters neutral atoms into the gap where they can ionize and repeat the process. Regeneration can occur if there is unit probability for ionization of a sputtered atom and its consequent return to the cathode. This, in turn, depends upon current density and the magnitude of current amplification by the gas.

Two simultaneous processes thus compete to induce the ultimate current instability. The former anode dominated mechanism depends on current density and beam spreading, while in the latter cathode dominated case the factors are current density and current gain per unit of gas density.

A large current gain, by improving ionization and thus the enhancement factor, will promote beam spreading, particularly at lower gap separation where the field enhancement is dominantly ionic. On the other hand, it will promote sputtering so a low enough gap separation exists for which gas evolution from the cathode determines the breakdown. A gap separation, therefore, exists which divides the two regimes. Above it, instability occurs at a critical field enhancement factor depending on the thermal properties of the anode and breakdown voltage increases with the square root of gap separation.

In the lower part of the regime, the critical field enhancement factor varies inversely with the gap separation, consequently the breakdown voltage increases linearly with the gap separation.

8.3 Gaseous Current Amplification

A simple model of the ionization process will be considered for a uniform field region. The interelectrode space is firstly considered to be filled with rarefied gas at an arbitrary pressure, such that the electronic mean free path is much greater than the gap separation. An electron accelerated from the cathode will create other electrons directly by collisional ionization and these, in turn, will

be further energized in the field, creating more electron-ion pairs at a greater potential. The total current amplification will be calculated.

8.3.1 The Gaseous Contribution

According to the Born approximation,[5] the cross section for impact ionization depends at large energy almost exactly as the inverse of the electron energy. An approximate energy dependence can, therefore, be assumed in which the threshold value is σ_o at the ionization potential U_i, falling inversely with potential U at greater potentials. Hence:

$$\sigma(U) = \sigma_o \frac{U_i}{U} \tag{8-1}$$

The total rate of production, $\dot{n}_1$, of electron-ion pairs per second is the sum of all increments, $d\dot{n}_1(U)$, at the arbitrary potential U. Thus:

$$d\dot{n}_1(U) = \frac{I_o N \sigma_o U_i}{e} \frac{}{U} dz \tag{8-2}$$

where dz is the increment of gap length within which the potential is between U and U + dU. The ambient gas density is arbitrarily chosen to be N atoms/cc and the rate of arrival of electrons in dz due to a primary current I_o is I_o/e electrons/sec, if e is the electronic charge.

Since:

$$\frac{dU}{dz} = \frac{V}{d} \tag{8-3}$$

then:

$$\frac{d\dot{n}_1}{dU} = \frac{I_o}{e} \frac{N \sigma_o d}{V} \frac{U_i}{U} \tag{8-4}$$

Integration of this will yield the total ionization from a primary electron current falling from zero potential to potential U. The contribution from electrons generated at some other potential, ψ, must be calculated by considering how an increment of current $d\dot{n}(\psi)$ which is created at potential ψ will fall through a potential $U - \psi$ to create more secondary electrons at potential U with a cross section $\sigma(U - \psi)$. This contribution is obtained by integrating over ψ. Therefore:

$$\frac{d\dot{n}_2(U)}{dU} = \frac{N \sigma_o d}{V} U_i \int_{U_i}^{U-U_i} \frac{\left(\frac{d\dot{n}}{d\psi}\right) d\psi}{U - \psi} \tag{8-5}$$

The limits of integration arise because $(d\dot{n}/d\psi)$ is zero for $U < U_i$ and no electrons generated at less than U_i units of potential from U can contribute anything to the current generation in dU.

Since:

$$\frac{d\dot{n}}{dU} = \frac{d\dot{n}_1}{dU} + \frac{d\dot{n}_2}{dU} \tag{8-6}$$

and:

$$\frac{d\dot{n}_1}{dU} = \frac{I_o}{e} \frac{N\sigma_o U_i d}{V} \frac{1}{U} \tag{8-7}$$

then:

$$\begin{aligned} \frac{d\dot{n}_2}{dU} &= \left(\frac{N\sigma_o U_i d}{V}\right)^2 \frac{I_o}{e} \int_{U_i}^{U-U_i} \frac{d\psi}{\psi(U-\psi)} + \left(\frac{N\sigma_o U_i d}{V}\right) \int_{U_i}^{U-U_i} \frac{\left(\frac{d\dot{n}_2}{d\psi}\right) d\psi}{U-\psi} \\ &= \left(\frac{N\sigma_o U_i d}{V}\right)^2 \frac{I_o}{e} \frac{2}{U} \ln\left(\frac{U-U_i}{U_i}\right) + \left(\frac{N\sigma_o U_i d}{V}\right) \int_{U_i}^{U-U_i} \frac{\left(\frac{d\dot{n}_2}{d\psi}\right) d\psi}{U-\psi} \end{aligned} \tag{8-8}$$

This is a Volterra equation of the second kind in the function $d\dot{n}_2/dU$. Putting $d\dot{n}_2/dU \equiv y(U)$, it is of the form:

$$y(U) = \lambda_1 g_1(U) + \lambda_2 \int_{U_i}^{U-U_i} \frac{y(\psi)\, d\psi}{U-\psi} \tag{8-9}$$

A solution to this equation is obtained by the iterative process of trying:

$$y_1(\psi) = \lambda_1 g_1(\psi) \tag{8-10}$$

and studying the convergence of the solution. Only one such test is enough to establish (see Appendix A) that:

$$y(U) \doteq \left(\frac{N\sigma_o U_i d}{V}\right)^2 \frac{I_o}{e} \frac{2}{U} \ln\left(\frac{U_i}{U}\right) \tag{8-11}$$

The total rate of ionization at potential U is thus:

$$\frac{d\dot{n}}{dU} = \frac{d\dot{n}_1}{dU} + \frac{d\dot{n}_2}{dU} = \frac{I_o}{Ue}\left[\left(\frac{N\sigma_o U_i d}{V}\right)\left\{1 + \frac{2N\sigma_o U_i d}{V} \ln\left(\frac{U_i}{U}\right)\right\}\right] \tag{8-12}$$

and integration from U_i to U gives:

$$\dot{n}(U) = \frac{I_o}{e} \ln\left(\frac{U}{U_i}\right)\left\{\frac{N\sigma_o U_i d}{V}\right\}\left\{1 + \frac{N\sigma_o U_i d}{V} \ln\left(\frac{U}{U_i}\right)\right\} \tag{8-13}$$

The total secondary gaseous electron current is:

$$I_g(U) = e\dot{n}(U) \tag{8-14}$$

and may be considered as the product of a gaseous amplification factor, G(U), acting upon the primary current, I_o. Thus:

$$\frac{I_g(U)}{I_o} = G(U) = \ln\left(\frac{U}{U_i}\right)\left\{\frac{N\sigma_o U_i d}{V}\right\}\left\{1 + \frac{N\sigma_o U_i d}{V} \ln\left(\frac{U}{U_i}\right)\right\} \tag{8-15}$$

and the total current for U = V is:

$$\frac{I_g}{I_o} = G(V) = \ln\left(\frac{V}{U_i}\right)\left\{\frac{N\sigma_o U_i d}{V}\right\}\left\{1 + \frac{N\sigma_o U_i d}{V} \ln\left(\frac{V}{U_i}\right)\right\} \tag{8-16}$$

8.3.2 Secondary Emission

It should be observed that the results of the last calculation are equally valid if I_g represents either the gaseous electron or ion current. The electrons will accelerate to the anode, adding to the primary current I_o, but the ions impact on the cathode around the field emitting site and produce a secondary electron current, I_s, where:

$$I_s = \bar{F} I_g = e \int_{U_i}^{V} F(\psi) \frac{d\dot{n}}{d\psi} d\psi \tag{8-17}$$

where $\bar{F}$ is the secondary emission yield of the cathode material averaged over the electron energy range. The "primary" electron current, I_o, is thus composed of a true primary component, I_F, due to field emission, together with the component I_s. Therefore:

$$I_o = I_F + I_s = I_F + \overline{F} I_g = I_F + \overline{F} G(V) I_o \tag{8-18}$$

Therefore:

$$I_o = \frac{I_F}{1 - \overline{F} G(V)} \tag{8-19}$$

and:

$$I_g = I_F \frac{G(V)}{1 - \overline{F} G(V)} = G'(V) I_F \tag{8-20}$$

Thus, I_g can be considered as an amplified form of the true primary current I_F with the gain function improved by positive feedback due to secondary electron emission, so that the new gain, $G'(V)$, is:

$$G'(V) = \frac{G(V)}{1 - \overline{F} G(V)} \tag{8-21}$$

This function clearly becomes infinite when:

$$G(V) = \frac{1}{\overline{F}} \tag{8-22}$$

Thus, $G(V) \ll 1$ for stable gas amplification because $\overline{F} \doteq 5$[7] and so the quadratic term in Equation (8-16) can be neglected:

$$G(V) \doteq ln\left(\frac{V}{U_i}\right) \frac{N \sigma_o U_i d}{V} \tag{8-23}$$

An estimate can readily be made of the gas density required to produce regenerative instability in a 1 cm gap at 100 kV. Using the following data:

$$\sigma_o \doteq 10^{-16} \text{ cm}^2$$

$$U_i \doteq 10 \text{ kV}$$

then:

$$G(V) \doteq 10^{-19} N$$

Thus, if $\overline{F} \doteq 5$ the gas density required to make the current rise to infinity would be about 2×10^{18} atoms/cc (i. e., about 1/10 of the gas density at standard temperature and pressure.

Conversely, at moderate vacuum pressure of, say, 10^{-4} torr (which is the approximate vapor pressure of copper at its melting point) the value of G is about 10^{-7}.

8. 3. 3 Sputtering

In estimating the gas density required to produce regenerative current runaway, the influence of sputtering of neutral atoms from the cathode by energetic ions has been neglected. The sputtering yield of ions at 45 kV has been investigated[8] and the yield is known to be typically of the order of 10 for not too light elements. Thus, if Y is the factor relating gas density sputtered into the electron beam to the incident ion current, I_g, then:

$$N_s = YI_g = YGI_o \tag{8-24}$$

and if the total gas density is:

$$N = N_o + N_s \tag{8-25}$$

where N_o is the density present by anode evaporation, then:

$$N = N_o + YG\frac{I_g}{e} \tag{8-26}$$

and:

$$G(V) \doteq \ln\left(\frac{V}{U_i}\right) \frac{N\sigma_o U_i d}{V} \tag{8-27}$$

Thus:

$$N = \frac{N_o}{1 - Y\frac{I_o}{e}\left[\frac{\sigma_o U_i d}{V} \ln\left(\frac{V}{U_i}\right)\right]} \tag{8-28}$$

Again there is a possible regenerative mechanism which becomes unstable at a particular current value. The significance of this will be discussed later.

From Equations (8-21) and (8-28):

$$G' = \frac{gN_o}{1 - g\left(FN_o + Y\frac{I_o}{e}\right)} \tag{8-29}$$

where $G \equiv gN_o$ and:

$$I_o = \frac{I_F}{1 - FG}$$

and:

$$GI_o = \left(\frac{G}{1 - FG}\right) I_F = G'I_F$$

Therefore:

$$gNI_o = \frac{gN_oI_o}{1 - gY\frac{I_o}{e}} = G'I_F \tag{8-30}$$

Inverting this, we have:

$$I_o = \frac{G'I_F}{N_o g + \frac{G'Yg}{e}I_F} \tag{8-31}$$

Substituting into the expression for G':

$$G' = \frac{gN_o}{(1 - gFN_o) - \frac{\frac{G'YI_F}{eN_o}}{1 + \frac{G'YI_F}{eN_o}}} \tag{8-32}$$

This can be rewritten using the expressions:

$$\left.\begin{aligned} G_o &\equiv g N_o \\ G_o' &\equiv \frac{g N_o}{1 - F g N_o} \\ \Gamma &\equiv \frac{G' Y I_F}{e N_o} = \frac{N_s}{N_o} \end{aligned}\right\} \tag{8-33}$$

$$\frac{1}{G'} = \frac{1}{G_o'} - \frac{1}{G_o}\left(\frac{\Gamma}{1 + \Gamma}\right) \tag{8-34}$$

The factor G_o is the "open loop" gain of the system and G_o' and G' are respectively the "closed loop" gain factors accounting respectively for secondary emission feedback only and for the total feedback including sputtering.

Thus:

$$\frac{(G_o')^{-1} - (G')^{-1}}{G_o^{-1}} = \frac{\Gamma}{1 + \Gamma} \tag{8-35}$$

Since $G_o' \doteq G_o$ at low pressures, then this can be simplified to:

$$\frac{G'}{G_o} = 1 + \Gamma = \frac{N_o + N_s}{N_o} \tag{8-36}$$

Hence from the equations above:

$$\Gamma \equiv \frac{Y I_F}{e}\left(\frac{G'}{N_o}\right) = \frac{Y I_F}{e} g (1 + \Gamma)$$

Therefore:

$$\Gamma = \frac{g \frac{Y I_F}{e}}{1 - g \frac{Y I_F}{e}} \tag{8-37}$$

The ratio of the gain with sputtering to the open loop value is thus:

$$\frac{G'}{G_o} = \frac{1}{1 - g\frac{Y I_F}{e}} \tag{8-38}$$

This expression is valid for a single species of interelectrode atoms such as is the case when pure metal is used. In the more usual case, however, there is dissolved gas, in particular hydrogen which is evolved readily from the anode hot spot and a mean value of g Y is appropriate. The factor Y will be further investigated for the purpose of estimating the influence of sputtering.

At distance z from the cathode protrusion, the instantaneous gas density due to the passage of $\dot{N}_s$ atoms/sec with average velocity $\bar{v}$ is:

$$N_s = \frac{\dot{N}_s}{\alpha' z^2}\frac{1}{\bar{v}} = \frac{Y' I_g}{\alpha' z^2}\frac{1}{e\bar{v}} \tag{8-39}$$

where Y' is the sputtering yield and α' is a geometrical factor (Equation 8-47).

Ions generated from N_s at z will accelerate back to the cathode and sputter more.

The average density N_s can be obtained from the mean value of $1/z^2$ which is $1/2\, z_o^2$ where z_o is the position while $U = U_i$ and $z_o \ll d$. Thus:

$$N = N_o + \frac{Y' g I_o N}{2\alpha' z_o^2}\frac{1}{e\bar{v}} \tag{8-40}$$

Since $z_o \doteq r$, then:

$$N = N_o + \frac{Y' g J_o N}{2e\bar{v}}$$

Therefore:

$$N = \frac{N_o}{1 - \frac{Y' g J_o}{2e\bar{v}}} \tag{8-41}$$

The sputtering feedback mechanism thus depends upon the current density at the cathode.

The value of g is about 10^{-19} and the sputtering yield is of the order of 10.[8] If $\bar{v}$ corresponds to thermal velocities, then it is about 10^5 cm/sec. Hence:

$$\frac{Y' g J_o}{2 e \bar{v}} \doteq \frac{10 \cdot 10^{-19} J_o}{10^{-19} \cdot 10^{5}} = 10^{-4} J_o$$

Thus, the denominator can cause significant gas density amplification if J_o is about 10^{+4} amp/cm^2. Thus, if the emission site is about 10^{-10} cm^2, then I_o is 10^{-6} amp.

8.4 Ionic Field Enhancement

The direct multiplication of the primary field emission current is not the only effect of ionization upon the system. Ions are attracted to the cathode where they can increase the local field strength and add to the purely geometrical field enhancement at the cathode protrusion.

An ion produced at potential ψ will accelerate to a velocity, v_+, at potential U, where:

$$v_+ = \sqrt{\frac{2 e (\psi - U)}{m_+}} \tag{8-42}$$

and the instantaneous charge density there will be:

$$\rho_+ = \frac{dJ_g(\psi)}{\sqrt{\frac{2 e (\psi - U)}{m_+}}} \tag{8-43}$$

Similarly, an electron starting from potential ψ' will contribute a charge density, ρ_e, to the region with potential U, where:

$$\rho_e = - \frac{dJ_g(\psi')}{\sqrt{\frac{2 e (\psi' - U)}{m_e}}} \tag{8-44}$$

Those electrons on the other hand which begin from the cathode at zero potential contribute another component, ρ_{eo}, where:

$$\rho_{eo} = - \frac{J_o}{\sqrt{\frac{2 e U}{m_e}}} \tag{8-45}$$

The sum of all of this accumulated charge will determine the divergence of electric field strength according to Poisson's equation. The system will be considered to be one-dimensional, so

that, for the moment, no radial component of electric field is considered. Local conditions around the cathode protrusion and non-uniform fields will be discussed afterwards.

Hence:

$$\frac{d}{dz}\left\{\frac{dU}{dz}\right\} = \frac{1}{2}\frac{d}{dU}\left(\frac{dU}{dz}\right)^2 = \rho_+ - \rho_e - \rho_{eo} \qquad (8\text{-}46)$$

The electric field at any potential U due to the instantaneous distribution of space charge can be calculated by summing the terms of Equations (8-43) through (8-45) from zero to potential U and integrating Poisson's equation:

$$\frac{1}{2}\frac{d}{dU}\left(\frac{dU}{dz}\right)^2 = \frac{1}{\sqrt{\frac{2e}{m_e}}}\left[\mu\int_o^{V-U}\frac{\left(\frac{dJ_g}{d\psi''}\right)d\psi''}{\sqrt{(V-U)-\psi''}} - \int_o^{U}\frac{\left(\frac{dJ_g}{d\psi}\right)d\psi}{\sqrt{U-\psi}} - \frac{I_o}{\alpha' r^2\sqrt{U}}\right] \qquad (8\text{-}47)$$

where:

$$\mu = \sqrt{\frac{m_+}{m_e}}$$

$$\alpha' = \pi(1 - \cos\theta)$$

The potential $\psi'' = V - \psi'$ is merely ψ' expressed with reference to the anode instead of the cathode.

The term $(dJ_g/d\psi)$, however, is zero in the region for which $U < U_i$ so the lower limit can be replaced by U_i. Electrons created by ionization will not pass through this and make no contribution to the space charge there. Ions, on the other hand, will do so. The ionic integral will, therefore, be divided:

$$\int_o^{V-U} = \int_{U_i}^{V-U} + \int_o^{U_i}$$

Equation (8-47) can then be written:

$$\frac{1}{2}\frac{d}{dU}\left(\frac{dU}{dz}\right)^2 = \frac{(\mu - 1)}{\sqrt{\frac{2e}{m_e}}} S' + \int_o^{U_i} \frac{\left(\frac{dJ_g}{d\psi''}\right) d\psi''}{\sqrt{(V - U) - \psi''}} - \frac{I_o}{\alpha' r^2 \sqrt{U}} \tag{8-48}$$

where:

$$S' \equiv \int_{U_i}^{V-U} \frac{\left(\frac{dJ_g}{d\psi''}\right) d\psi''}{\sqrt{(V - U) - \psi''}} \equiv \int_{U_i}^{U} \frac{\left(\frac{dJ_g}{d\psi'}\right) d\psi'}{\sqrt{U - \psi'}} \equiv \int_{U_i}^{U} \frac{\left(\frac{dJ_g}{d\psi}\right) d\psi}{\sqrt{U - \psi}}$$

This integral can be evaluated with the substitution:

$$\psi = v + U_i$$

$$S' = \int_o^{U-U_i} \frac{\left(\frac{dJ_g}{dv}\right) dv}{\sqrt{(U - U_i) - v}} \tag{8-49}$$

The integral is now in the Abel form with properties[6] such that the differential operator, d/dv, can be removed to outside the integral provided the operation is understood to be carried out at the point $v = U - U_i$ for which $\psi = U$. Therefore:

$$S' = \frac{d}{dv} \int_o^{U-U_i} \frac{J_g(v)\, dv}{\sqrt{(U - U_i) - v}} \equiv \frac{d}{dv} \int_{U_i}^{U} \frac{J_g(\psi)\, d\psi}{\sqrt{U - \psi}} = \frac{dS}{du} \tag{8-50}$$

The other integral in Equation (8-48) can also be reduced to the Abel form by writing it as:

$$\sqrt{\frac{U_i}{V - U}} \int_o^{U_i} \frac{\left(\frac{dJ_g}{d\psi''}\right) d\psi''}{\sqrt{U_i - \psi''\left(\frac{U_i}{V - U_i}\right)}} \equiv \sqrt{\frac{U_i}{V - U}} \int_o^{U_i} \frac{\left(\frac{dJ_g}{d\xi}\right) d\xi}{\sqrt{U_i - \xi}} \tag{8-51}$$

where:

$$\xi = \psi'' \frac{U_i}{V - U}$$

Again the differential operator can be taken outside the integral which becomes:

$$\sqrt{\frac{U_i}{V-U}} \frac{d}{d\xi} \int_0^{U_i} \frac{J_g(\xi)\, d\xi}{\sqrt{U_i - \xi}} = \left(\frac{U_i}{V-U}\right)^{3/2} \frac{d}{dU} \int_0^{V-U} \frac{J_g(\psi')\, d\psi''}{\sqrt{(V-U) - \psi''}} \tag{8-52}$$

$$= \left(\frac{U_i}{V-U}\right)^{3/2} S'$$

When $U_i << V - U$, this term can thus be neglected and Equation (8-48) becomes, after integration:

$$\left(\frac{dU}{dz}\right)^2 = \frac{(\mu - 1)}{\sqrt{\frac{2e}{m_e}}} S - \frac{2I_o}{\alpha' r^2} \sqrt{U} \tag{8-53}$$

The integral S(U) must now be evaluated where:

$$J_g = \int \frac{dJ_g}{d\psi} d\psi = \int J_o \frac{N\sigma_o U_i d}{V} \frac{d\psi}{\psi} = J_o \frac{N\sigma_o U_i d}{V} \ln \psi = J_o g \ln \psi \tag{8-54}$$

Thus (see Appendix B):

$$S = g \int_{U_i}^{U} \frac{\ln \psi\, d\psi}{\sqrt{U - \psi}} \doteq G(U) \ln U_i \tag{8-55}$$

So far, the integration of Poisson's equation has been carried out assuming that the current density was determined at each cross section only by the rate of ionization. In fact, the electron beam from a protrusion has been shown by Chatterton[4] to spread parabolically (see next section). The beam radius, R_z, at distance z from the cathode is given in a form similar to Equation (8-75):

$$R_z^2 = 4\beta_e r z \sin^2 \theta \tag{8-56}$$

This can be presented in terms of the potential ψ at z in a uniform field in a gap length d by:

$$\frac{R_z^2}{R^2} = \frac{z}{d} = \frac{\psi}{V} \tag{8-57}$$

The corresponding value of J_g is thus divided by this factor within the Poisson integral:

$$J_g(\psi) \doteq J_g(o)\left(\frac{r}{R_z}\right)^2 \doteq J_g(U_i)\left(\frac{r}{R_z}\right)^2 = J_g(U_i)\left(\frac{r}{R}\right)^2 \frac{V}{\psi} \tag{8-58}$$

Thus, in the integration of the Poisson equation:

$$\left(\frac{dU}{dz}\right)^2 = \frac{(\mu - 1)}{\sqrt{\frac{2e}{m_e}}}\left(\frac{r}{R}\right)^2 \int_{U_i}^{U} \frac{V J_g \frac{d\psi}{\psi}}{\sqrt{U - \psi}} \tag{8-59}$$

$$= \frac{(\mu - 1)}{\sqrt{\frac{2e}{m_e}}} J_o \left(\frac{r}{R}\right)^2 V g \int_{U_i}^{U} \frac{\ell n\,(\psi)\,\frac{d\psi}{\psi}}{\sqrt{U - \psi}}$$

This differs from the earlier simple integration in the factor $(r/R)^2$ and the new integral:

$$S_p = \int_{U_i}^{U} \frac{\frac{V}{\psi}\,\ell n\,(\psi)\,d\psi}{\sqrt{U - \psi}} \tag{8-60}$$

Integration yields (see Appendix C):

$$S_p(V) \doteq \sqrt{V}\,\ell n\,U_i\,\ell n\left(\frac{4V}{U_i}\right) \tag{8-61}$$

From Equation (8-77):

$$\left(\frac{r}{R}\right)^2 = \frac{1}{k\beta_e^2}\,\frac{1}{4\sin^2\theta} \tag{8-62}$$

Therefore:

$$\left(\frac{dU}{dz}\right)^2 = \frac{(\mu - 1)}{\sqrt{\frac{2e}{m_e}}} \frac{1}{4k\beta_e^2 \sin^2\theta} S_p \tag{8-63}$$

Integration over the whole gap for which U = V gives for the cathode surface value X_s of (dU/dz):

$$X_s^2 \doteq \frac{I_o}{r^2} \sqrt{V} \left[\frac{(\mu - 1)}{\sqrt{\frac{2e}{m_e}}} \frac{\ln U_i}{4k\beta_e^2 \sin^2\theta} G(V) - \frac{2}{\alpha'} \right] \tag{8-64}$$

Neglecting the second term in these brackets, which is due to the primary electronic space charge, we have:

$$X_s = \frac{C_1}{r} \left\{ \frac{G(V) I_o}{k\beta_e^2} \right\}^{1/2} \tag{8-65}$$

where:

$$C_1 = \left(\frac{m_e V}{2e} \right)^{1/4} \frac{\left[(\mu - 1) \ln U_i \right]^{1/2}}{2 \sin\theta}$$

The parameter C_1 will be treated as a constant because of its very feeble variation with voltage.

The total cathode surface field, E_s, due to geometrical and ionic field enhancement, can now be written:

$$E_s = \frac{V}{k_o r} + X_s = \frac{V}{k_o r} \left[1 + C_1 k_o \left\{ \frac{G(V) I_o}{k V^2 \beta_e^2} \right\}^{1/2} \right] \tag{8-66}$$

This enhanced field can be represented in terms either of an effective field enhancement factor, β_e, or of a "local field factor", k:

$$E_s \equiv \frac{\beta_e V}{d} \equiv \frac{V}{kr} \tag{8-67}$$

Hence:

$$\frac{1}{k} = \frac{1}{k_o}(1 + f) \tag{8-68}$$

and:

$$\beta_e = \beta(1 + f) \tag{8-69}$$

where:

$$f = C_1 k_o \left\{ \frac{G(V) I_o}{k V^2 \beta_e^2} \right\}^{1/2} \tag{8-70}$$

The parameter f is an amplifying factor multiplying the geometrical field enhancement according to the interelectrode ionization level.

The equations for cathode protrusion equilibrium by surface migration may be derived now using these expressions. Thus:

$$r E_s^2 = 12 \pi \gamma \tag{8-71}$$

$$E_s = \frac{V}{k_o r}(1 + f) = \beta_e \frac{V}{d}$$

Therefore:

$$\frac{V}{k_o}(1 + f) \beta_e \frac{V}{d} = 12 \pi \gamma$$

Hence:

$$\frac{V^2}{d} = \frac{12 \pi \gamma k}{\beta_e} = \frac{12 \pi \gamma k_o}{\beta (1 + f)^2} \tag{8-72}$$

This is a relationship between the two factors k and β_e. They have occurred because the local protrusion field strength E_s can be considered either as an amplified form of the average field E with β_e as the gain factor or as an inverse function of the local radius of curvature r. The latter form has more physical significance but in the absence of a means to measure r the surface migration mechanism provides a relationship between β_e and d. Thus, any value of k is related to the corresponding β_e by the voltage and gap separation which can be measured.

8.5 The Anode Hot Spot Temperature

An expression will be derived for the anode hot spot temperature and will then be related to the effective field enhancement factor. The basic method follows the technique of Chatterton[4] beginning with the expression:

$$T_s - T_a = \frac{W}{4KR} \tag{8-73}$$

The hot spot temperature, T_s, exceeds the ambient value, T_a, according to the power dissipation, W, the hot spot radius, R, and the thermal diffusivity, K, of the anode material. At high temperatures, T_s, the ambient value may be neglected.

The radius, R, of the spot where the electron beam hits the anode is given by Chatterton as:

$$R = 2d^{1/2} (\beta\delta \sin\theta)^{1/2} \tag{8-74}$$

where:

$$\delta = r \sin\theta$$

and θ is the conical semi-angle into which most electrons are emitted from the tip. Therefore:

$$R = 2 \sin\theta (\beta r d)^{1/2} \tag{8-75}$$

and since:

$$d = k\beta r \tag{8-76}$$

then:

$$R = (2k^{1/2} \sin\theta)\beta r = C_2 \beta r = (2 \sin\theta) \frac{d}{k^{1/2}} \tag{8-77}$$

where:

$$C_2 = 2k^{1/2} \sin\theta$$

The calculation is based upon the approximation that an electron leaving the cathode protrusion receives a radially directed impulse over an approximate distance of δ which is the radius of the emitting area. It continues to drift radially while accelerating axially, resulting in a parabolic orbit. When there is additional ionic field enhancement, the factor β is amplified to β_e by space charge separation along the beam.

The solution of Poisson's equation for parabolic electron trajectories was made assuming that the ion and electron currents flowed through the same cross sections all along the beam without radial charge separation. Energetic ions, however, would be expected to overshoot the emitting tip, creating a radial charge separation. Since, however, there is also an axial charge separation, there would, therefore, exist a local solenoidal electric field $\vec{E}$ with curl $\vec{E}$ directed around the beam periphery. Thus, the value of curl curl $\vec{E}$ would be finite.

Maxwell's equations require, however, that:

$$\text{Curl Curl } \vec{E} = -\left\{\mu \frac{\partial \vec{J}}{\partial t} + \epsilon\mu \frac{\partial^2 \vec{E}}{\partial t^2}\right\}$$

Thus, although ions can overshoot the emitting tip, there will be no radial charge separation as long as the current density and electric field are assumed to be time invariant.

The calculation of W will now be made, allowing for the power dissipation from all electrons at different potentials U in the gap. In addition to the primary power dissipation, W_o, there will thus be some W_g due to gaseous multiplication of electrons. Therefore:

$$W_g = \int_o^V I_g(U)\,(V - U)\,dU = e\int_o^V \left(\frac{d\dot{n}}{dU}\right)\,(V - U)\,dU \qquad (8\text{-}78)$$

Integrals of this type are soluble with the help of a theorem given by Courant:[6]

$$\int_o^V (V - U)\,\frac{d\dot{n}}{dU}\,dU = \Gamma(2)\,D^{-2}\left(\frac{d\dot{n}}{dU}\right)_{U=V} \qquad (8\text{-}79)$$

Thus:

$$W_g = 2D^{-1}\dot{n}(U) = 2I_o\int_o^V G(\psi)\,d\psi = 2I_o g\int_o^V \ell n\,\psi\,d\psi = 2I_o g\int_{U_i}^V \ell n\,\psi\,d\psi \qquad (8\text{-}80)$$

because $G(U) = 0$ for $0 < U < U_i$:

$$W_g = 2I_o g U_i \left[\frac{U}{U_i}\left\{\ln\left(\frac{U}{U_i}\right) - 1\right\}\right]_{U_i}^{V} = 2I_o g U_i \left[\frac{V}{U_i}\left\{\ln\left(\frac{V}{U_i}\right) - 1\right\} + 1\right] \tag{8-81}$$

and, since $V >> U_i$, then:

$$W_g \doteq 2I_o V G(V) \tag{8-82}$$

Hence, the total power dissipation is:

$$W = W_o + W_g = I_o V \left\{2G(V) + 1\right\} \tag{8-83}$$

Thus, the anode temperature, T_s (now employing the total enhancement factor β_e), is:

$$T_s = \frac{I_o V \left[2G(V) + 1\right]}{4K C_2 \beta_e r} \tag{8-84}$$

The gain, $G(V)$, for stable amplification is usually very small when the secondary emission yield, $\overline{F}$, is high. Hence:

$$T_s \doteq \frac{I_o V}{4K C_2 \beta_e r} \tag{8-85}$$

or:

$$T_s = \frac{I_o V k^{1/2}}{8K \sin\theta d} \tag{8-86}$$

Apart from determining the anode hot spot temperature, beam spread affects the integration of Poisson's equation because the current density is a function of gap position and, hence, of potential. This effect was taken account of in the previous section.

8.6 The Instability Conditions

The anode hot spot temperature and the accumulated ionic field at the cathode protrusion are each functions of the current, voltage and beam spread. Since gaseous evolution and, hence, the current gain and ionization are direct functions of hot spot temperature, it is desirable that the latter should be used as a variable instead of electrical quantities. The instability of the ionic field enhancement can then be studied as a consequence of a small temperature perturbation.

Equation (8-66) can be written:

$$\frac{1}{k} = \frac{1}{k_o} + \frac{r X_s}{V} \tag{8-87}$$

Substituting for X_s and taking account of the parabolic beam spread:

$$\frac{1}{k} = \frac{1}{k_o} + \frac{1}{V} C_1 \left\{ \frac{G(V) I_o}{k \beta_e^2} \right\}^{1/2} \tag{8-88}$$

Eliminating I_o with Equation (8-85), we have:

$$\frac{1}{k} = \frac{1}{k_o} + C_1 \left[\frac{G(V)}{k \beta_e^2 V^2} 4 K C_2 \beta_e r \frac{T_s}{V} \right]^{1/2} \tag{8-89}$$

and using Equation (8-23):

$$\frac{1}{k} = \frac{1}{k_o} + C_1 \left[\ln \left(\frac{V}{U_i} \right) \frac{N \sigma_o U_i d}{V} \frac{1}{k \beta_e^2 V^2} 4 K C_2 \beta_e r \frac{T_s}{V} \right]^{1/2} \tag{8-90}$$

$$= \frac{1}{k_o} + C_1 \left[\ln \left(\frac{V}{U_i} \right) \frac{4 \sigma_o U_i K C_2}{k} \left(\frac{d}{\beta_e V^2} \right) \left(\frac{r}{V^2} \right) (N T_s) \right]^{1/2}$$

which because of the surface migration equilibrium conditions becomes:

$$\frac{1}{k} = \frac{1}{k_o} + C_1 \left[\ln \left(\frac{V}{U_i} \right) \frac{8 \sigma_o U_i K \sin \theta}{(12 \pi \gamma)^2} \frac{k^{1/2}}{k^4} (N T_s) \right]^{1/2} \tag{8-91}$$

$$= \frac{1}{k_o} + \frac{C_1}{k^2} \left[k^{1/2} \ln \left(\frac{V}{U_i} \right) \frac{8 \sigma_o U_i K \sin \theta}{(12 \pi \gamma)^2} (N T_s) \right]^{1/2}$$

The factor k relating the local cathode field intensification to the radius of curvature of the protrusion has now been reduced to terms dependent solely on the hot spot temperature, T_s, as a variable. There will be a relationship (unspecified) between N and T_s which will remain implicit for the moment. The term $\left[k^{1/2} \ln (V/U_i)\right]^{1/2}$ will be considered constant because it is a very weakly varying factor compared with k^2. Hence:

$$\frac{1}{k} = \frac{1}{k_o} + \frac{C_3 (N T_s)^{1/2}}{k^2} \tag{8-92}$$

where:

$$C_3 = \left[\frac{8 \sigma_o U_i K \sin \theta}{(12 \pi \gamma)^2} k^{1/2} \ln \left(\frac{V}{U_i} \right) \right]^{1/2} C_1$$

Differentiating this expression for (1/k) with regard to $(N T_s)^{1/2}$ as a variable reveals that the rate of change is infinite when:

$$k_c = 2 C_3 \left(N T_s \right)_c^{1/2} \tag{8-93}$$

where the subscript c refers to a critical value of the parameters.

This signifies that the rate of change of ionic field enhancement with $(N T_s)^{1/2}$ is infinite at a particular value of $(N T_s)^{1/2}$. If the gas density N is a function only of T_s, then a critical temperature exists for this runaway condition.

Solving the algebraic expression for i/k gives:

$$\frac{i}{k} = \frac{1}{2C_3 (N T_s)^{1/2}} \left[1 \pm \left\{ 1 - \frac{4C_3 (N T_s)^{i/2}}{k_o} \right\}^{1/2} \right] \tag{8-94}$$

Inspection of this shows that at the runaway condition $(N T_s)^{i/2}$ is related to k_o, thus:

$$k_o = 4C_3 \left(N T_s \right)_c^{1/2} = 2k_c \tag{8-95}$$

Hence, when $d(i/k)/d(N T_s)^{1/2}$ becomes infinite it does so at a critical value of $k_c^{-i} = 2k_o^{-1}$, and there can, therefore, be a maximum stable value of 1/k which is only two times the purely geometrical factor $1/k_o$. When 1/k rises to this value, however, this does not mean that the local cathode field strength cannot increase further. It merely means that surface migration is unable to reshape the tip to a stable radius but ionization can proceed unhindered to complete voltage breakdown.

The foregoing analysis was considered in terms of a temperature instability because the critical condition is a function of $N T_s$ and gas density is a function of T_s. This form of solution is useful when considering a gas density which varies with temperature. An analysis to include constant gas density, however, can be made directly from Equation (8-88).

The factor 1/k can be expressed as follows:

$$\frac{i}{k} = \frac{i}{k_o} + C_i \left[\frac{GI}{k \beta_e^2 V^2} \right]^{1/2} = \frac{1}{k_o} + \frac{C_1}{d} \left[\frac{GI}{k E_s^2} \right]^{1/2} \tag{8-96}$$

The modified Fowler-Nordheim expression for the current is:

$$I_F = A_1 \left(\frac{V}{k} \right)^2 \exp \left\{ - B' \left(\frac{V}{k} \right) \right\} = \frac{A_1'}{E_s^2} \exp \left\{ - \frac{B}{E_s} \right\} \doteq I \tag{8-97}$$

These two expressions are mutually dependent and serve to determine the values of I and 1/k at any gap separation. For sufficiently low values, I will increase with 1/k. Beyond a critically high value of (V/k), however, any further increase of this causes I to decrease and Equation (8-96) shows that 1/k will, therefore, stabilize. The feedback between the two terms is then negative and I is consequently almost constant. At low values of d, Equation (8-96) shows that this is very pronounced but

when d is great enough I will reach a maximum beyond which further increases will change the feedback to positive.

Equation (8-88) can also be written as:

$$\frac{1}{k} = \frac{1}{k_o} + \frac{C_1}{d}\left[\frac{GIV^2}{(12\pi\gamma)^2 k^3}\right]^{1/2} = \frac{1}{k_o} + \frac{C_1}{12\pi\gamma}\frac{V^2}{d}\frac{(GA_1)^{1/2}}{k^{5/2}}\exp\left\{-\frac{B'V}{2k}\right\} \tag{8-98}$$

$$= \frac{1}{k_o} + \frac{CV^2}{k^{5/2}}\exp\left\{-\frac{B'V}{2k}\right\}$$

where:

$$C = \frac{C_1 (GA_1)^{1/2}}{12\pi\gamma d}$$

Differentiating with respect to V for the condition for runaway, we have:

$$\frac{d}{dV}\left(\frac{1}{k}\right)\left[1 - \left(\frac{1}{k} - \frac{1}{k_o}\right)\left(\frac{5}{2}k - \frac{B'V}{2}\right)\right] = \left(2V - \frac{B'V^2}{2k}\right)\left(\frac{1}{k} - \frac{1}{k_o}\right) \tag{8-99}$$

The condition for runaway of the factor 1/k is that:

$$\left(\frac{1}{k} - \frac{1}{k_o}\right)\left(\frac{5}{2}k - \frac{B'V}{2}\right) = 1 \tag{8-100}$$

If $B'V/k \ll 5$, then $k_c/k_o = 3/5$ where k_c is the critical value of k. This is close to the simpler calculation which gave $k_c/k_o = 1/2$.

The significance of this calculation is that $1/k_c$ is not quite a constant but depends upon the Fowler-Nordheim exponent:

$$\frac{k_c}{k_o} = 1 - \frac{2}{5 - \frac{B'V_B}{k_c}} \tag{8-101}$$

Thus, k_c decreases as V_B (or V_B/k_c) increases.

Thus:

$$\left(\frac{1}{k_c} - \frac{1}{k_o}\right) = \frac{2}{k_c} \frac{1}{5 - \frac{B' V_B}{k_c}} = C_1 \left[\frac{GI}{k_c \beta_e^2 V_B^2}\right]^{1/2}$$

Therefore:

$$\frac{2}{5 - \frac{B' V_B}{k_c}} \left(\frac{\beta_e}{k_c}\right) = C_1 \left[\frac{GI}{k_c V_B^2}\right]^{1/2} = C_1 \left[\frac{G A_1}{k_c^3} \exp\left\{- \frac{B' V_B}{k_c}\right\}\right]^{1/2} \qquad (8\text{-}102)$$

But:

$$\frac{\beta_e}{k_c} = 12 \pi \gamma \left(\frac{d}{V_B^2}\right)$$

Hence:

$$\frac{V_B^2}{d} \frac{G^{1/2}}{k_c^{3/2}} \left(5 - \frac{B' V_B}{k_c}\right) \exp\left\{- \frac{B' V_B}{2 k_c}\right\} = \frac{24 \pi \gamma}{C_1 A_1^{1/2}} \qquad (8\text{-}103)$$

Reducing this explicitly into terms of V_B and k_c, we have:

$$\frac{V_B^2}{d} \frac{G^{1/2}}{k_c^{3/2}} \left\{\frac{1}{1 - \frac{k_c}{k_o}}\right\} \exp\left\{- \frac{5}{2} + \frac{1}{1 - \frac{k_c}{k_o}}\right\} = \frac{12 \pi \gamma}{C_1 A_1^{1/2}} \qquad (8\text{-}104)$$

When the Fowler-Nordheim exponent can be neglected, this reduces to:

$$\frac{V_B^2}{d} \frac{G^{1/2}}{k_c^{1/2}} \doteq \frac{24 \pi \gamma}{5 C_1 A_1^{1/2}} \qquad (8\text{-}105)$$

In this case, k_c is a constant and $V_B \propto d^{1/2}$.

When, however, V_B increases at larger gap separations, the exponent becomes significant and k_c decreases. Ultimately the expression approaches the asymptotic form:

$$\frac{V_B^2}{d} \frac{G^{1/2}}{k_c^{3/2}} \exp\left\{-\frac{5}{2}\right\} = \frac{12\pi\gamma}{C_1 A_1^{1/2}} \tag{8-106}$$

The breakdown law is then no longer a power law and the value of V_B^2/d decreases with V_B. If sputtering is accounted for, it will influence V_B through the factor G and the total closed loop gain expression (Equation (8-38)) must be substituted in the equations above.

A concurrent mechanism of gas evolution into the gap is by sputtering of neutral atoms at the cathode by positive ion bombardment. If N_o atoms are evolved into the gap thermally, they will ionize and sputter N_s more into it.

This mechanism will clearly lead to a regenerative release of cathode material and subsequent breakdown when the denominator is zero. This condition leads to an almost linear relationship between breakdown voltage and gap separation and from Equation (8-28):

$$\frac{V_B}{d} = \frac{\gamma I_o}{e} \sigma_o U_i \ln\left(\frac{V_B}{U_i}\right) \tag{8-107}$$

The breakdown law will be almost linear if I is constant. At low values of d this is so for the reasons outlined and an approximately linear law therefore applies. This law will prevail up to a transitional gap separation beyond which the square root law will cause breakdown, because ultimately such a law must give rise to the lower breakdown voltage.

8.7 The Factors Influencing Breakdown

8.7.1 Gas Density

The principal factors found to influence breakdown voltage were anode gas content, electrode shapes and electrode area. It has already been suggested that the influence of electrode area arises because of the effect of pumping conductance in concentrating gas density in the gap so it will be considered as part of the influence of gas on the system. There is still the paradox, however, that area effect works oppositely to additional gas content in the results of the full factorial experiment. This can now be readily explained with the help of Equation (8-104). Consider two systems, identical except for having two different gas densities $N_1 < N_2$ and, consequently, two gain factors $G_1 < G_2$. The expression in Equation (8-104) can be written:

$$\frac{V_B^2}{d} \frac{G^{1/2}}{\phi(k_c)} = \text{Constant} \tag{8-108}$$

where:

$$\phi(k_c) = k_c^{3/2}\left(1 - \frac{k_c}{k_o}\right) \exp\left\{\frac{5}{2} - \frac{1}{1 - \frac{k_c}{k_o}}\right\}$$

and:

$$\frac{k_c}{k_o} = 1 - \frac{2}{5 - \frac{B'V_B}{k_c}} \tag{8-109}$$

This equation is quadratic in k_c. It can be expressed thus:

$$k_c^2 - k_c\left[\frac{k_o}{5}\left(3 + \frac{B'V_B}{k_o}\right)\right] + \frac{B'V_B k_o}{5} = 0 \tag{8-110}$$

There are thus two possible solutions for k_c:

$$k_c = \frac{k_o}{10}\left(3 + \frac{B'V_B}{k_o}\right)\left[1 \pm \left\{1 - \frac{\frac{5B'V_B}{k_o}}{\left(3 + \frac{B'V_B}{k_o}\right)^2}\right\}^{1/2}\right] \tag{8-111}$$

This is a function of the exponent $x = 5B'V_B/k_o$ and differentiation of the last term shows that the discriminant will decrease with x until $x = 3$ and then increase again. Thus there are two solutions for k_c, one of which first decreases from the value $k_c = 0.6$ for $x = 0$, and the other increases from $k_c = 0$ for $x = 0$.

Thus:

$$\phi(k_c) \equiv \phi_1(V_B)$$

and it may increase or decrease according to the value of V_B. The value of G will determine the value of V_B for a solution of Equation (8-108) so changes in gas density may either increase or decrease V_B.

Hence, since electrode pumping conductance or anode gas content change gas density by different amounts, V_B may either increase or decrease.

8.7.2 Electrode Curvature

The influence of curvature of the cathode on breakdown voltage can be seen by defining the field enhancement factor for such a case:

$$E_s = H(d)\,\beta_e \frac{V}{d} = \frac{V}{kr} \tag{8-112}$$

where H(d) is a curvature factor. If a protrusion together with its associated ionic space charge has a local field, E_s, at the tip surface, then k and r are determined. The value of β_e, however, is quite arbitrary because $\beta_e H(d)$ is related to k for fixed values of V and d.

Thus, the actual value of β_e will be inversely proportional to H(d) and for a convex cathode the field enhancement factor is consequently lower than for a planar system. Accounting for this in the breakdown equations, this results in an increase in breakdown voltage. Hence anything tending to increase the macroscopic cathode field strength will increase the breakdown voltage and vice versa.

The reduced field enhancement factor at a convex cathode surface causes the beam cross section to be less than for a planar surface. Thus the space charge density is greater, consequently the regenerative feedback is reduced and the critical voltage raised (Appendix D).

There is another contribution to the breakdown voltage from electrode curvature due to its influence upon the gain factor G. The previous calculations have been made assuming ionization in a uniform field. This influences the value of G because the term E = V/d enters into it. An approximate analysis will now be made to estimate the effects of non-uniformity.

For uniform fields:

$$G = N\sigma_o U_i \int_{U_i}^{V} \frac{dU}{U\left(\frac{dU}{dz}\right)} = \frac{N\sigma_o U_i d}{V} \int_{U_i}^{V} \frac{dU}{U}$$

When dU/dz is no longer uniform but takes the form E(U), then:

$$G = N\sigma_o U_i \int_{U_i}^{V} \frac{dU}{E_z(U)\,U} \tag{8-113}$$

Integrating by parts:

$$G = N\sigma_o U_i \left[\frac{\ln U}{E_z(U)}\right]_{U_i}^{V} - N\sigma_o U_i \int_{U_i}^{V} \frac{\ln U}{E_z^2} \frac{dE_z}{dU}\,dU \tag{8-114}$$

The second integral can be shown to be small under conditions along the axis of a cylindrically symmetrical system. From Laplace's equation:

$$\frac{dE_x^2}{dU}\vec{i} + \frac{dE_y^2}{dU}\vec{j} + \frac{dE_z^2}{dU}\vec{k} = 0 \qquad (8\text{-}115)$$

Thus, along the axis of a cylindrically symmetrical system the transverse electric field gradients will be very small and so:

$$\frac{1}{E_z^2}\frac{dE_z}{dU} \doteq 0 \qquad (8\text{-}116)$$

Hence the second integral in Equation (8-114) almost vanishes and the general gain equation is:

$$G = N\sigma_o U_i \left[\frac{\ell n\, V}{E_z(V)} - \frac{\ell n\, U_i}{E_z(U_i)}\right] \qquad (8\text{-}117)$$

If the anode and cathode surface fields, E_{z_s}, are equal as in a symmetrical electrode arrangement (e.g., a sphere-sphere gap):

$$G = \frac{N\sigma_o U_i}{E_{z_s}} \ell n\left(\frac{V}{U_i}\right) \qquad (8\text{-}118)$$

Thus the gain factor G is reduced for such a field distribution and the corresponding value of k_c will also be changed.

The effect upon V_B of changing G by gas density modification has been discussed in the previous section. Curvature of the electrodes has thus a similar effect upon G and the result is either an increase or reduction of V_B according to the value of the Fowler-Nordheim exponent.

Thus electrode curvature has two effects, one of which is positive, increasing V_B for increased cathode field strength, and another effect due to lowering G, which superimposes either a positive or negative contribution.

8.8 Conclusions

The qualitative agreement between the results of factorial experimentation and the foregoing theoretical prediction confirm the validity of the basic assumption that the cause of breakdown is an instability of the ionic field enhancement by space charge. It is evident from the analysis that gas density and field emission current each contribute significantly to the breakdown mechanism.

Interference with either one of these will consequently introduce changes in the breakdown voltage. Gas density can be manipulated by changing the anode material, its gas sorption, and the electrode areas if the main supply of atoms is from an anode hot spot but this is supplemented by neutral atoms sputtered from the cathode by ions, generated within the gap. At sufficiently low gap separations, this mechanism is dominant in providing a discharge medium.

The theory can give a unifying account of vacuum breakdown phenomena in the long and short gap regimes and for long and short time duration of voltage application. In such cases, when anode material cannot enter the gap, overheating of the cathode may provide the gas required to initiate significant self-sputtering and subsequent cathode dominated voltage collapse. This would be expected for short pulses, when the ion transit time is too large, for short gaps (as described in the analysis) and perhaps for transverse magnetic fields strong enough to deflect electrons out of the gap. Weak transverse magnetic fields, however, have another influence by altering the field emission characteristics of protrusions and this will be described in the following section.

8.9 References

(1) Cranberg, L. C., J. Appl. Phys. 23, 518 (1952).

(2) Utsumi, T. and Dalman, G. C., Proceedings of Second International Symposium on Insulation of High Voltages in Vacuum, 151 (1966).

(3) Dyke, W. P. and Dolan, W. W., Advances in Electronics and Electron Physics, Vol. VIII, 89 (1956).

(4) Chatterton, P. A., Proc. Phys. Soc. 88, 231 (1966).

(5) Schiff, L. I., "Quantum Mechanics", McGraw-Hill (1955).

(6) Courant, R., "Differential and Integral Calculus", Vol. II, Interscience Publishers (1959).

(7) Hill, A. G., Buechner, W. W., Clark, J. S. and Fisk, J. B., Phys. Rev. 55, 463 (1939).

(8) Almen, O. and Bruce, G., Nucl. Inst. and Meth. 11, 257, 279 (1961).

SECTION 9
MAGNETIC INFLUENCES ON BREAKDOWN

9. 1 Abstract

Experimental evidence indicates that very weak transverse magnetic fields will either increase or reduce field emission while at the same time influencing breakdown voltage correspondingly. The reduction of field emission is accounted for in terms of the magnetic transport properties of the cathode surface and breakdown voltage variations are shown to be consistent with the unified theory of vacuum breakdown.

9. 2 Introduction

The prebreakdown current in vacuum originates as electrons tunneling from intensified field regions at the cathode. Field enhancement, though primarily geometrical in nature, is considerably augmented by positive space charge from interelectrode gas being ionized by the primary electron stream. As the voltage is raised, a critical value of enhancement factor is attained for which it is unstable and the voltage collapses. A weak transverse magnetic field can influence the current emitted by a protrusion through the Hall effect and the resulting current reduction introduces a lower value of enhancement factor with a consequently lower breakdown voltage in the anode dominated region.

Both experimental and analytical studies have been made to confirm this view of the influence of weak transverse magnetic fields on the breakdown process. Extremely little attention has previously been given to this, largely because it was thought that only magnetic fields strong enough to deflect electrons from the gap would be significant. One brief report of the effects was, however, given by Sanford[1] withwhose simple results the factorial experiments are in agreement. The theory to be presented explains the results in detail.

9. 3 Magnetic Field Influence on Field Emission

Apart from the dramatic effects of the transverse magnetic field strength on breakdown voltage, the next most important experimental observation has been that the prebreakdown current was reduced progressively as the field strength was increased. Current-voltage characteristics at various magnetic field strengths are presented in Figure 9-1. The undulations in the characteristics are thought to be due to resonant variation of the tunneling probability as proposed by Duke and Alferieff.[2]

The field strengths involved were extremely small, the greatest being 250 gauss and the significant current changes were too much to be explained by the minute changes made to the electron vacuum trajectories. It is, however, possible to explain it in the following manner by studying the surface physics of a field emitter in a transverse magnetic field.

Consider the physical situation of a strong field emission current density, J_x, flowing into vacuum across a metal surface. Ordinarily, an ohmic electric field develops inside the metal in the x

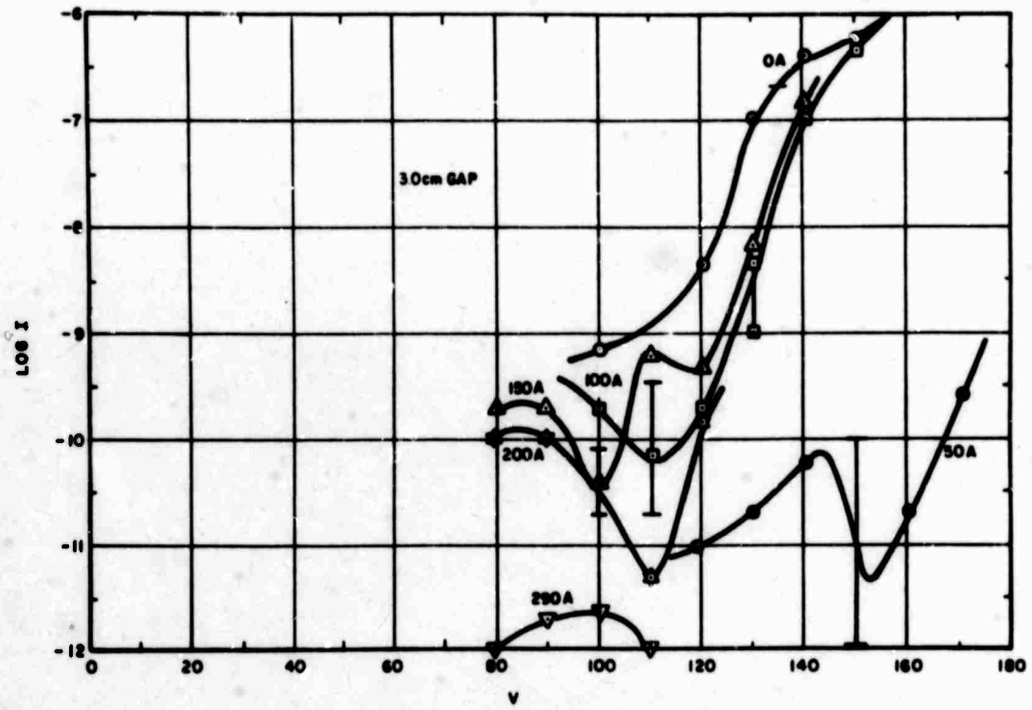

Figure 9-1. V-I Characteristics for Different Magnetic Field Strengths

direction when a transverse H_z field is applied and a field, E_y, develops but is shorted out if there is an internal conduction path. A system of such shorting loops is shown for an emitting tip in Figure 9-2 and an enlarged portion of the surface is shown in Figure 9-3. The reaction of this against the H_z field is such as to reduce the J_x current. Thus, J_x and J_y are complimentary to one another and are related by a tensor conductivity. The appropriate electron transport data, of course, pertain to the surface states of the metal.

In the present case, however, no applied electric field drives the drift current. Instead, a small fraction of the electron energy distribution escapes by tunneling through the barrier. This fraction is determined by the tunneling probability which is strongly dependent on the angle of incidence to the barrier. For normal incidence, the tunneling probability, D, is of the form:[3]

$$D = D_o \exp\left\{-\frac{B}{E_s}\right\} \tag{9-1}$$

The fraction leaving the surface normally will perturb the energy distribution by ∂f_o:

$$\partial f_o = D f_o = v_x \frac{\partial f_o}{\partial v_x} \tag{9-2}$$

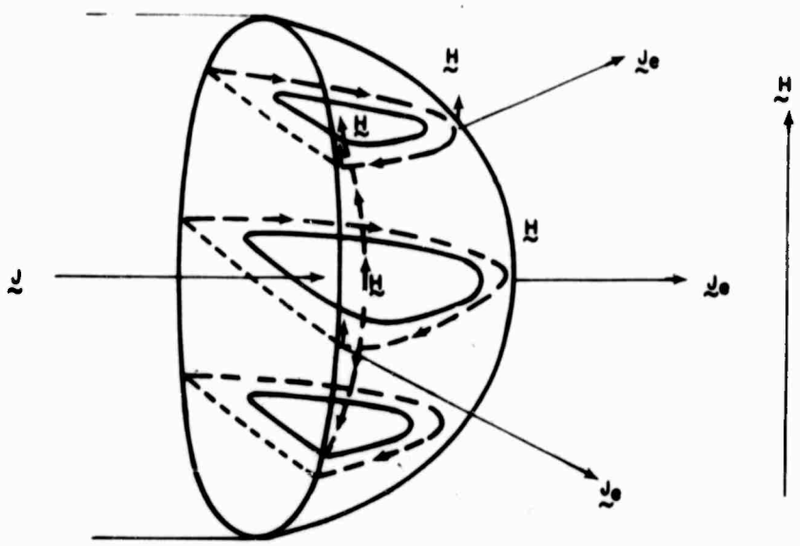

Figure 9-2. Hall Effect in Field Emission

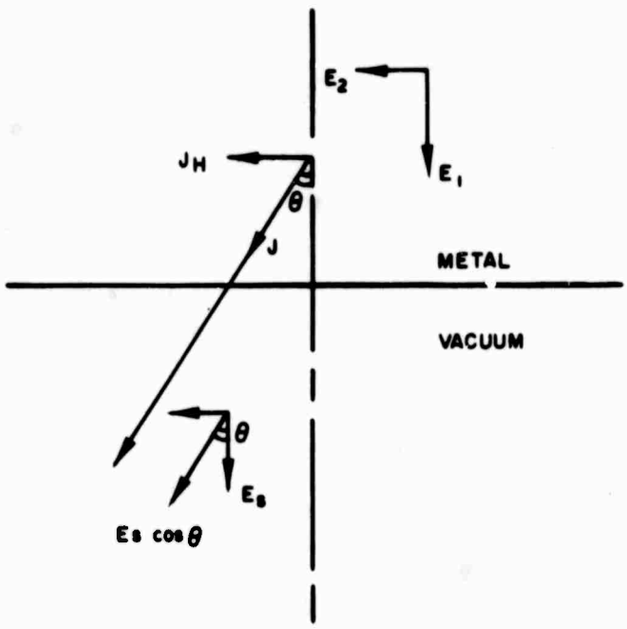

Figure 9-3. Diagram to Illustrate Passage of Electron Current from Metal into Vacuum

All tunneling at angles ± θ to the normal must occur with equal probability to ensure that there is no transverse component of current drift at the surface because there should be continuity of the magnetic field vector parallel to the surface. With the introduction of a transverse magnetic field, however, the conductivity becomes a tensor quantity and electron transport normal to the surface is associated with a transverse electric field. If this field is short circuited, there will be a transverse

current drift parallel to the surface. The resultant current drift will be at an angle θ to the normal and continuity of the magnetic field vector at the surface demands that the tunneling current shall be parallel to this. Thus, the electronic energy distribution perturbation, ∂f_o, is described in the following analysis which closely follows that of Seitz:[4]

$$\partial f_o = D(\theta) f_o = v_x \frac{\partial f_o}{\partial v_x} + v_z \frac{\partial f_o}{\partial v_z} \tag{9-3}$$

The tunneling current is thus:

$$\int_o^\infty v_\theta D(\theta) f_o \, dv = \int_o^\infty v_x^2 \frac{\partial f_o}{\partial v_x} dv + \int_o^\infty v_z^2 \frac{\partial f_o}{\partial v_z} dv \tag{9-4}$$

The distribution function, f_o, is a function of v^2 which is made up from each component with equal probability:

$$v_x^2 = v_y^2 = v_z^2 = \frac{v^2}{3} \tag{9-5}$$

By rotating the axes, the current equation can be written:

$$\int_o^\infty v_\theta D(\theta) f_o \, dv = \int_o^\infty v_\theta^2 \frac{\partial f_o}{\partial v_\theta} dv = \int_o^\infty \frac{v^2}{3} \frac{\partial f_o}{\partial v_\theta} dv$$

$$= \cos\theta \int_o^\infty \frac{v^2}{3} \frac{\partial f_o}{\partial v_x} dv \tag{9-6}$$

The current equation corresponding to Equation (9-2) is:

$$\int_o^\infty v_x D f_o \, dv = \int_o^\infty v_x^2 \frac{\partial f_o}{\partial v_x} dv = \int_o^\infty \frac{v^2}{3} \frac{\partial f_o}{\partial v_x} dv \tag{9-7}$$

Comparison of this with Equation (9-6) shows that the current represented by the right hand side of Equation (9-7) is changed by the magnetic field so that:

$$\int_o^\infty \frac{v^2}{3} \frac{\partial f_o}{\partial v_x} dv = \frac{1}{\cos\theta} \int_o^\infty \frac{1}{\cos\theta} D(\theta) f_o \, dv = \frac{D(\theta)}{\cos^2\theta} \int_o^\infty v_x f_o \, dv \tag{9-8}$$

The probability, $D(\theta)$, is taken as independent of electron velocity because tunneling occurs mostly from the narrow band of energies at the top of the Fermi-Dirac distribution. This assumption would be somewhat modified for temperature assisted emission when the electron gas is no longer degenerate.

The tunneling probability for an electron crossing the barrier at angle θ to the normal is reduced to:

$$D(\theta) = D_o \exp \left\{ - \frac{B}{E_s \cos \theta} \right\} \tag{9-9}$$

The reason for this is that the normal component of the electron velocity and, hence, of its wavelength, is changed by the factor $\cos \theta$.

The Fowler-Nordheim expression is then of the form:

$$J_F = \frac{A}{(E_s \cos \theta)^2} \exp \left\{ - \frac{B}{E_s \cos \theta} \right\} \tag{9-10}$$

The value of $\cos \theta$ can be derived in terms of the electron gyration angle, $s = \omega\tau$, from consideration of the Boltzmann transport equation solutions:[4]

$$\left.\begin{aligned} \omega &= \frac{eH}{mc} \\ \tau &= \frac{\ell}{v} \end{aligned}\right\} \tag{9-11}$$

where:

ℓ = electronic mean free path

and:

$$J_x = \frac{2\pi\ell}{3} \left(\frac{e}{m}\right)^2 \int_o^\infty \epsilon \frac{\partial f_o}{\partial \epsilon} \frac{1}{1 + s^2} \left[E_x - s E_y \right] \tag{9-12}$$

$$J_y = \frac{2\pi\ell}{3} \left(\frac{e}{m}\right)^2 \int_o^\infty \epsilon \frac{\partial f}{\partial \epsilon} \frac{1}{1 + s^2} \left[s E_x + E_y \right] \tag{9-13}$$

When E_y is shorted out, then:

$$\tan \theta = \frac{J_y}{J_x} = s \tag{9-14}$$

Hence the Fowler-Nordheim expression is:

$$I_F = \frac{A}{E_s^2} (1 + s^2) \exp \left\{ - \frac{B}{E_s} \sqrt{1 + s^2} \right\} \tag{9-15}$$

The total current expression, accounting for surface migration and changing emission area is of the form:

$$I_F = A' V^2 (1 + s^2) \exp \left\{ - B' V \sqrt{1 + s^2} \right\} \tag{9-16}$$

Hence:

$$- \frac{1}{V} \ln \left(\frac{I_F}{V^2} \right) = - \frac{\ln A'}{V} + B' \sqrt{1 + s^2} - \ln (1 + s^2) \tag{9-17}$$

A plot of the left hand side of this has been made with experimental data as a function of magnetic field strength and is compared in Figure 9-4 with the above function of s:

$$\phi(s) = B' \sqrt{1 + s^2} - \ln (1 + s^2) \tag{9-18}$$

The curves have been fitted with $B' = \sqrt{2}$ and have a common minimum at $s = 1$ for a magnetic field strength of 50 gauss. Hence:

$$\frac{eH}{mc} = \omega = 7.05 \times 10^{14} \text{ radians/sec}$$

The collision interval, τ, for Cu at 0°C is 27×10^{-15} sec[5] and at high temperature, say 900°C, it would be about half of this figure, since τ is proportional to $1/\sqrt{T}$. Therefore:

$$s = \omega\tau = 7 \times 10^{14} \times 13 \times 10^{-15} \sim 10 \text{ radians}$$

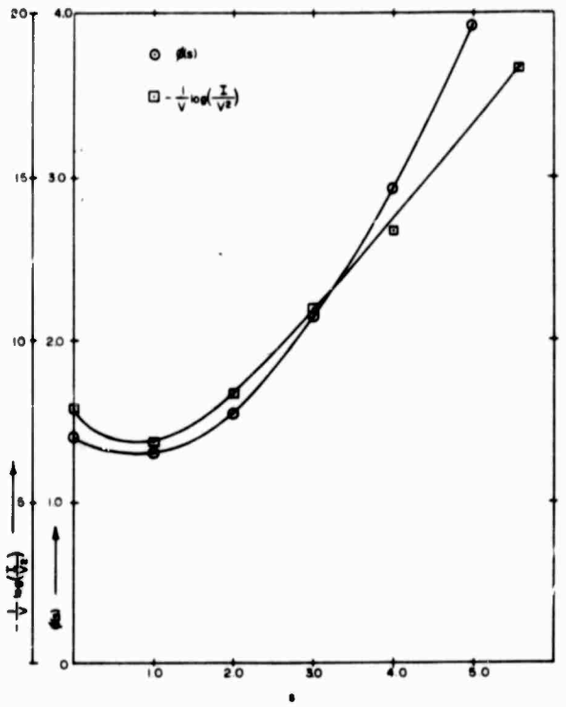

Figure 9-4. Comparison Between Theory and Experiment

Thus, the experimentally determined value of s is an order of magnitude too low. It should be noted, however, that the bulk properties of Cu were used for the estimate and the carrier mobility is an order of magnitude lower[6, 7] in the surface layers.

9.4 Influence of Magnetic Fields on the Breakdown Strength

The electric field enhancement required for Fowler-Nordheim emission is created largely by electron impact ionization and subsequent positive space charge accumulation at cathode protrusions. When the interelectrode gas density is provided by anode material evaporated from the hot spots terminating each electron beam, then the above mechanism goes unstable at a characteristic voltage and breakdown occurs. Alternatively, the gas density can come from sputtering of cathode material by ions generated by electron impact in the primary beam.

In either case, the ionic contribution to field enhancement depends upon the electron beam current. Anode dominated breakdown takes place at a critically high value of the overall field enhancement factor at the cathode and so depends upon the electron beam current producing it. Hence, any changes in current which are magnetically induced by the mechanism described above will raise or lower the ionic field enhancement. Accordingly, the voltage must be lowered or raised to achieve this critically high level of field enhancement factor and the breakdown voltage as a function of magnetic field strength has a similar form to the corresponding ultimate prebreakdown current.

A similar argument can also be made for the cathode dominated case although the critical condition is different.

In each of five consecutive test cycles, the expression $-V^{-1} \log (I/V^2)$ varies with the magnetic field strength as shown in Figures 9-5 through 9-9. At the highest field strengths, the Fowler-Nordheim exponent increased significantly and dominated the current equation. For very weak fields, however, the magnetic influence on the pre-exponential factor dominated the expression and had an opposite effect. Thus, as the magnetic field strength is increased from zero for conditioned electrodes, the current first of all increases a little and then decreases (Figure 9-9). The breakdown voltage for the reasons given above will thus undergo a similar variation (Figure 9-10). The curves $\phi(V)$ represent the variation of $-V^{-1} \log (I/V^2)$ with voltage and arise from the first term in Equation (9-17).

The close relationship between these two curves is evident from a study of Equation (8-102) which can be written in the form:

$$\frac{24\pi\gamma}{5 - \frac{B' V_B}{k_c}} = C_1 \left(\frac{V_B^2}{d} \right) \left[\frac{GI}{k_c V_B^2} \right]^{1/2} \tag{9-19}$$

Thus, neglecting the factor $B' V_B / k_c$ on the left hand side and considering k_c almost constant as the magnetic field H varies at constant gap separation, we have:

$$\frac{d}{dH} \left[\log \frac{V_B^2}{d} \right] = - \frac{d}{dH} \left[\ln \left(\frac{I}{V_B^2} \right) \right] \tag{9-20}$$

This is the analytical confirmation of the reason for similarity of the two curves in Figure 9-10.

It also follows from Equation (9-19) that for a fixed magnetic field strength and a variable gap separation, the value of V_B^2/d will undergo the same changes as does $\ln (I/V_B^2)$. These changes take the same form as those for magnetic field variation and this is shown in Figure 9-11 which is V_B^2/d plotted as a function of $d^{1/2}$ from Figure 5-18.

9.5 Discussion

The theoretical model seems justified that the prebreakdown tunneling current into vacuum is adjusted by weak transverse magnetic fields to match corresponding changes within the metal due to the Hall effect. In Figure 9-4 the discrepancy between the theoretical and experimental curves is accounted for by the missing term $-\ln A'/V$ from Equation (9-17). In Figures 9-5, this term is superimposed upon the corresponding variation with magnetic field strength for five successive tests.

The identification of the theoretical predictions with experimental results (made on the fifth of these tests), however, requires an electron collision interval which is about ten times lower than that of bulk copper. This is readily accounted for by recalling that the pertinent transport

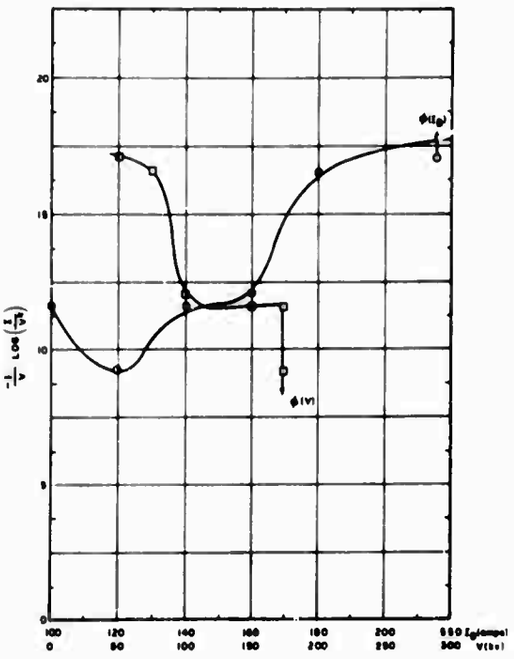

Figure 9-5. $1/V \log I/V^2$ as a Function of V and Magnetizing Current (3 cm Gap, Test No. 1) (290 amp ≡ 250 Gauss)

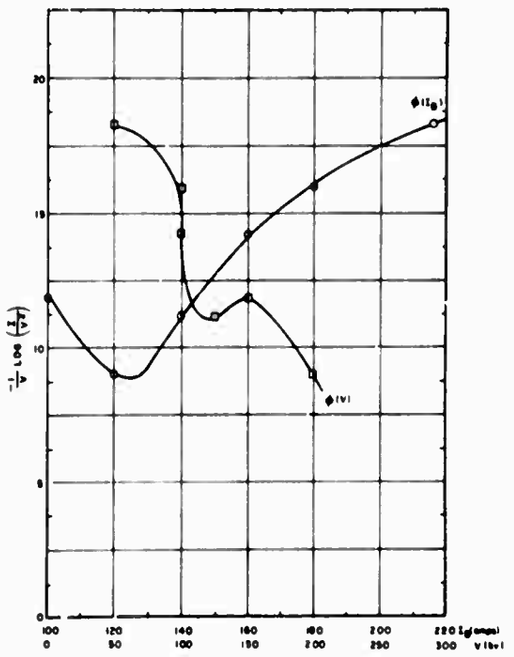

Figure 9-6. $1/V \log I/V^2$ as a Function of V and Magnetizing Current (2 cm Gap, Test No. 2) (290 amp ≡ 250 Gauss)

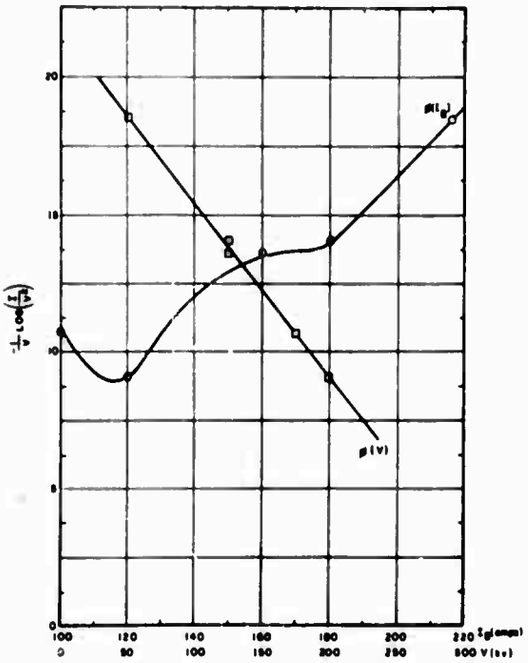

Figure 9-7. $1/V \log I/V^2$ as a Function of V and Magnetizing Current (2 cm Gap, Test No. 3) (290 amp ≡ 250 Gauss)

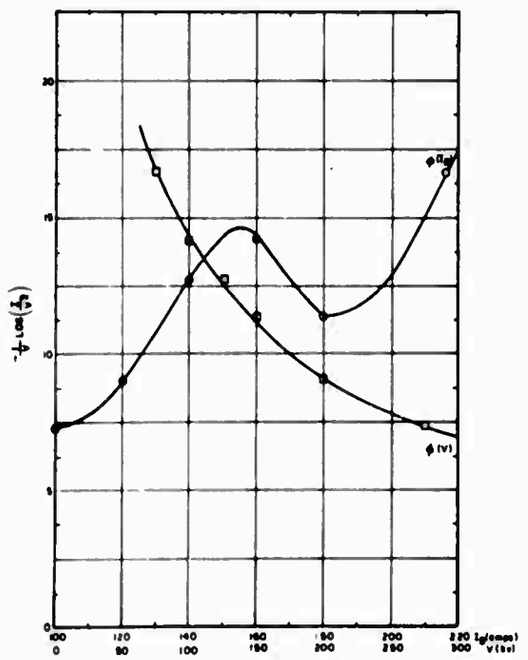

Figure 9-8. $1/V \log I/V^2$ as a Function of V and Magnetizing Current (3 cm Gap, Test No. 4) (290 amp ≡ 250 Gauss)

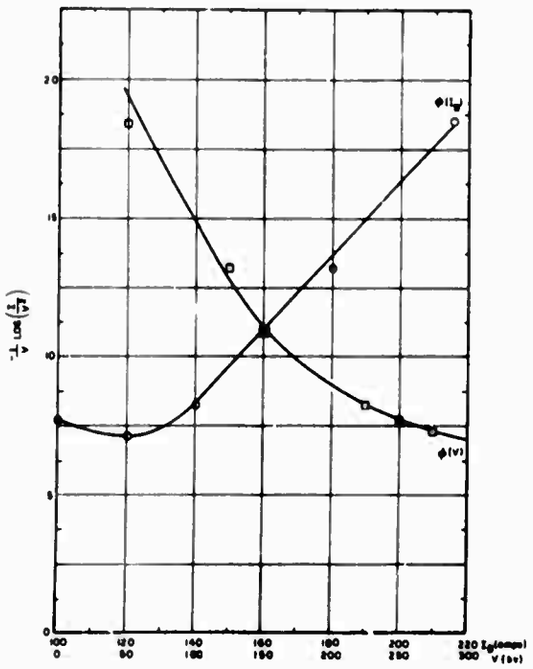

Figure 9-9. $1/V \log I/V^2$ as a Function of V and Magnetizing Current (3 cm Gap, Test No. 5) (290 amp ≡ 250 Gauss)

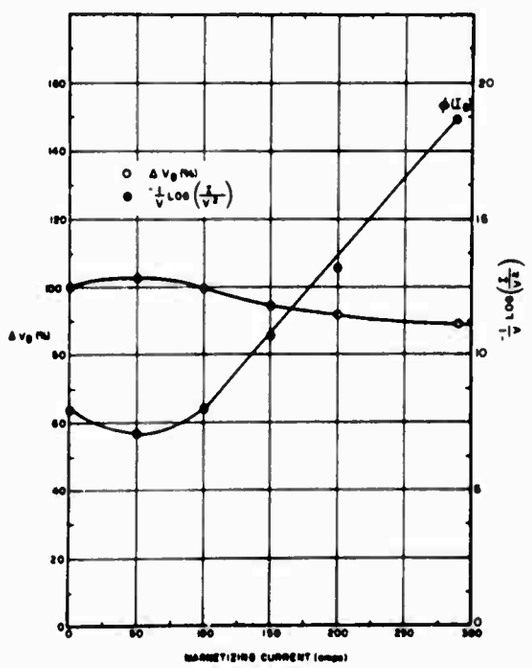

Figure 9-10. Comparison of Variations of Breakdown Voltage and Fowler-Nordheim Exponent with Magnetic Field Strength (290 amp ≡ 250 Gauss)

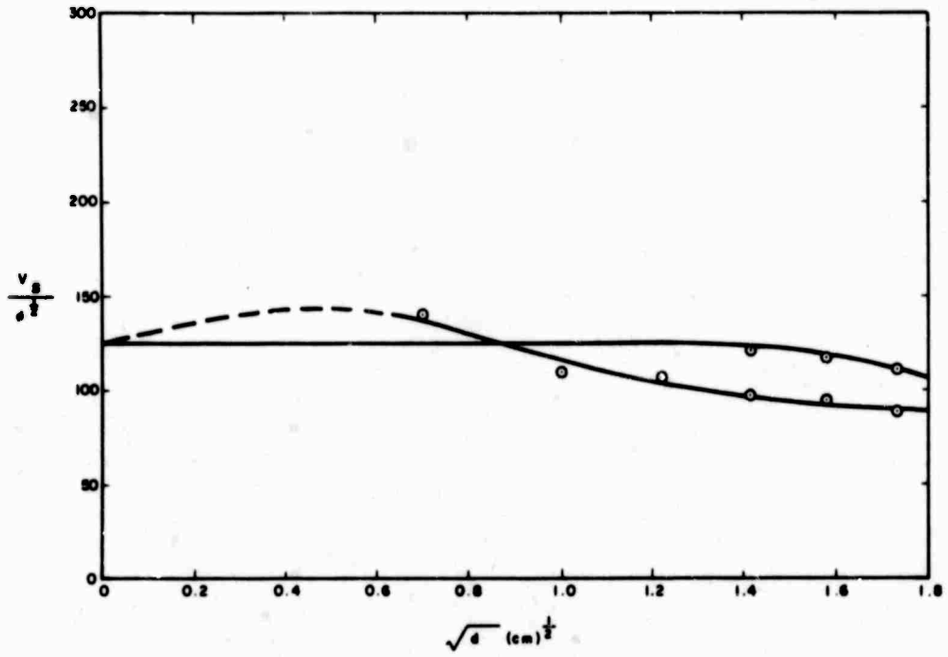

Figure 9-11. Functional Variation of V_B^2/d at Constant Magnetic Field

parameters to be used are those of the surface. When the thickness of a thin film conductor is much smaller than the mean free path of electrons, the transport properties are considerably modified. The Hall coefficient was found by Sondheimer to be much greater than the bulk solid value when the film thickness was small enough.

It has been pointed out by Schrieffer[7] that chemisorbed impurities on a surface will induce a space charge layer with consequently different charge density. This type of layer could be the origin of the thin film transport anomalies required to explain magnetic effects on field emission.

It is much more likely, of course, that the metallic surface under most experimental conditions is covered with a layer of oxide. The field emission and electron transport parameters are thus those of a semiconductor or dielectric. In the case of copper, the oxide layer is semiconducting and the electron relaxation time would be about one order of magnitude less than that of a metal.

If there is an oxide layer on the cathode, then the electron density there will be a function of the applied electric field. It is a well known fact that semiconductors and metals have surface states with such a field effect and that after the removal of the applied field a memory of its influence remains for some time afterwards. This could account for the fact that immediately after magnetic field tests were carried out neither the breakdown voltage nor the associated prebreakdown current returned to their previous values.

9.6 References

(1) Sanford, J. R., Proceedings of First International Symposium on Insulation of High Voltages in Vacuum, 431 (1964).

(2) Duke, C. and Alferieff, M., J. Chem. Phys. 46, 923 (1967).

(3) Gomer, R., "Field Emission and Field Ionization", Chapt. 1, Harvard University Press (1961).

(4) Seitz, F., "The Modern Theory of Solids", Chapt. 4, Sec. 31, McGraw-Hill (1940).

(5) Olsen, J. L., "Electron Transport in Metals", Chapt. 1, Interscience Tracts on Physics and Astronomy (1962).

(6) Sondheimer, E. H., Phys. Rev. 80, 401 (1950).

(7) Schrieffer, J. R., "Effective Carrier Mobility in Surface-Space Charge Layers". Phys. Rev. 97, 641 (1955).

BLANK PAGE

SECTION 10
SUMMARY OF CONCLUSIONS

The purpose of this extended investigation into vacuum breakdown has been primarily to discover those factors most important in determining breakdown voltage and secondly to formulate a credible mechanism to describe insulation failure.

Preliminary experiments revealed some prebreakdown runaway phenomena potentially useful in defining a non-destructive criterion for spark initiation, but they were insufficiently reliable. X-ray monitoring provided evidence that, no matter how polished the electrodes were initially, a steady field emission current eventually appeared under electrical stress and hydrogen seemed to be evolved into the gap.

An exploratory factorial experiment demonstrated the significance of electrode shapes and bakeout, underlining again the role played by outgassing. The high level of statistical scatter, however, was evidence that at least one factor was not under control and, since bakeout was so significant, it was natural to suspect the missing factor to be the gas concentration in the electrodes.

Following this, a carefully controlled factorial experiment was performed to demonstrate the influence of this last factor and to look for its predicted interaction with area effect. The introduction of extremely low statistical scatter into the results proved the effectiveness of the factorial method in showing up this missing factor. Moreover, the appearance of the predicted interaction between anode gas content and electrode area was added confirmation. In addition to this, weak magnetic field influences appeared with equal statistical reliability in this experiment. An extremely reliable measurement of the functional relationship between breakdown voltage and gap separation verified its close relationship to a square root law.

Current measurements in the exploratory experiment led to a theoretical attempt to relate them to the field emission current from the tip of a cathode protrusion which assumes an equilibrium shape by surface migration. There was good agreement between experiment and the theory of the breakdown which was based on the supposition that the protrusion tip assumed a value which changed with voltage and ultimately becomes critical.

The reason why the protrusion tip becomes critical was then investigated analytically assuming a model in which residual gas ionization contributed to the field enhancement. Electrons leave the tip in a parabolic beam within which heavy ions are generated by impact. The space charge field depends upon charge density and, hence, increases with the current density which decreases as the beam spreads. Thus, most of the supplementary field enhancement arises from charge lying close to the protrusion. As the voltage is raised, there is an increase in current and ionization which, of course, improves the ionic field contribution. This disturbs the tip equilibrium such as to reduce the radius and, because of increased current density, the space charge field increases further. Hence, this constitutes a positive feedback which can lead to regenerative instability at a critical level of field enhancement.

This model has been successful in relating all of the experimentally observed factors with one another. Moreover, the theory is flexible enough to account for a cathode dominated mechanism for which breakdown occurs by regenerative sputtering of cathode material by ion bombardment. This model leads naturally to a linear variation between breakdown voltage and gap separation. The regimes of applicability of this latter mechanism are for short gaps, short time duration, and possibly for magnetic fields strong enough to deflect the electron beam out of the gap. Thus, the combined theory represents a unified approach to many vacuum breakdown phenomena. It has, moreover, wide applicability as a guide to understanding the diverse range of phenomena plaguing high voltage electron tube operation.

For the first time, a theory based upon field emission current as the breakdown precursor has succeeded in explaining not only the square root law but also the transition to a linear law. The cathode and anode dominated regimes of operation are thus quite naturally defined. Breakdown, however, always proceeds from the cathode although at large gap separations the anode conditions are dominant in controlling it because they are most important in governing the gas or vapor concentration which is ionized by electron impact. For many years, it has been appreciated that this ionization should play a part in assisting field emission but no attempt was made until now to incorporate it as a term in the field intensification factor. This naturally explains many perplexing data which show that this factor is not a constant but seems to vary with gap separation and with the experimental history of an electrode system. It is only a simple step further to show that such a model field intensification mechanism is unstable for a critical field intensification factor. The instability is thus identified with the breakdown condition. There is no need to look for anode heating mechanisms sufficient to cause boiling and vapor pressures in the Paschen minimum regime because electron multiplication does not occur by multiple gas collisions. Instead, it proceeds by interaction of the rarefied ionized gas with the cathode. Drawing an analogy with the electron multiplication mechanisms influencing high pressure gas breakdown, it is seen that ionic field intensification with subsequent field emission plays a role similar to a special secondary surface emission coefficient. The anomalies of vacuum breakdown are due to the details of this mechanism. Vacuum breakdown is thus a solid state problem on the cathode surface. The conditioning process is readily understood as a gradual change in the surface state induced by constant steady ion bombardment under electrical stress, whether or not sparks take place. Conditioning thus proceeds at a rate depending on the ion bombardment current and, hence, on the anode material and its gas content.

APPENDIX A

SOLUTION OF THE VOLTERRA EQUATION

The trial solution of Equation (8-10) introduces a second term into Equation (8-9):

$$\int_{U_i}^{U-U_i} \frac{\ell n\left\{\frac{U-\psi}{U_i} - 1\right\}}{(U-\psi)^2}\, d\psi \equiv \frac{1}{U_i^2} \int_{U_i}^{U-U_i} \frac{\ell n\left\{\frac{U-\psi}{U_i} - 1\right\}}{\left(\frac{U-\psi}{U_i}\right)^2}\, dx$$

Put:

$$\frac{U-\psi}{U_i} = x$$

$$d\psi = -U_i\, dx$$

Thus the integral becomes:

$$-\frac{1}{U_i} \int \frac{\ell n\,(x-1)}{x^2}\, dx$$

The limits change to:

$$\psi = U_i$$

then:

$$x = \frac{U-U_i}{U_i} = \frac{U}{U_i} - 1$$

and:

$$\psi = U - U_i$$

then:

$$x = \frac{U - (U - U_i)}{U_i} = 1$$

The integral is thus:

$$\int_1^{\frac{U}{U_i}-1} \frac{\ell n\,(x - 1)}{x^2}\,dx = \left[- \ell n\, x - \left(\frac{1}{x} - 1\right) \ell n\,(x - 1)\right]_1^{\frac{U}{U_i}-1}$$

$$= \left[- \ell n \left(\frac{U}{U_i} - 1\right) - \left(\frac{1}{\frac{U}{U_i} - 1} - 1\right) \ell n \left(\frac{U}{U_i}\right)\right]$$

$$= \left[- \ell n \left(\frac{U}{U_i} - 1\right) - \left(\frac{U_i - (U - U_i)}{U - U_i}\right) \ell n \left(\frac{U}{U_i}\right)\right]$$

$$= - \ell n \left(\frac{U}{U_i} - 1\right) + \left(1 - \frac{U_i}{U - U_i}\right) \ell n \left(\frac{U}{U_i}\right)$$

When $U >> U_i$, then the integral becomes:

$$\ell n\ \frac{U}{U_i}\ \left[\left(1 - \frac{U_i}{U}\right) - 1\right] = - \left(\frac{U_i}{U}\right) \ell n \left(\frac{U}{U_i}\right) = \left(\frac{U_i}{U}\right) \ell n \left(\frac{U_i}{U}\right)$$

Thus:

$$\frac{d\dot{n}_2}{dU} = \left(\frac{N \sigma_o U_i d}{V}\right)^2 \frac{I_o}{e} \frac{2}{U} \ell n \left(\frac{U - U_i}{U_i}\right) + \left(\frac{N \sigma_o U_i d}{V}\right)^3 \frac{2 I_o}{e} \left[\left(\frac{U_i}{U}\right) \ell n \left(\frac{U_i}{U}\right)\right]$$

$$\doteq \left(\frac{N \sigma_o U_i d}{V}\right)^2 \frac{2 I_o}{e} \left[\left(\frac{U_i}{U}\right) \ell n \left(\frac{U_i}{U}\right)\right] \left[\frac{1}{U_i} + \left(\frac{N \sigma_o U_i d}{V}\right)\right]$$

Now $U_i \approx 10$ V, so the second term can be neglected. Thus, one iteration is quite accurate:

$$\frac{d\dot{n}_2}{dU} \doteq \left(\frac{N\sigma_o U_i d}{V}\right)^2 \frac{I_o}{e} \frac{2}{U} \ell n \left(\frac{U_i}{U}\right)$$

APPENDIX B

THE INTEGRALS OF POISSON'S EQUATION FOR PARALLEL CYLINDRICAL BEAMS

THE INTEGRALS OF POISSON'S EQUATION FOR PARALLEL CYLINDRICAL BEAMS

$$S_1 \equiv \int_{U_i}^{U} \frac{\ell n\, \psi\, d\psi}{\sqrt{U - \psi}}$$

The substitution, $U - \psi \equiv y^2$, converts this to:

$$2 \int_0^{\sqrt{U-U_i}} \ell n\,(U - y^2)\, dy = \frac{1}{\sqrt{U}} \left[\int_0^{\sqrt{U-U_i}} \frac{dy}{\sqrt{U} - y} + \int_0^{\sqrt{U-U_i}} \frac{dy}{\sqrt{U} + y} \right]$$

$$= \frac{1}{\sqrt{U}} \left[\left(\sqrt{U} + y\right) \left\{ \ell n \left(\sqrt{U} + y\right) - 1 \right\} \right.$$

$$\left. - \left(\sqrt{U} - y\right) \left\{ \ell n \left(\sqrt{U} - y\right) - 1 \right\} \right]_0^{\sqrt{U-U_i}}$$

$$= \frac{1}{\sqrt{U}} \left[\sqrt{U}\, \ell n \left\{ \frac{\sqrt{U} + y}{\sqrt{U} - y} \right\} + y\, \ell n\,(U - y^2) - 2y \right]_0^{\sqrt{U-U_i}}$$

$$= \frac{1}{\sqrt{U}} \left[\sqrt{U}\, \ell n \left\{ \frac{\sqrt{U} + \sqrt{U - U_i}}{\sqrt{U} - \sqrt{U - U_i}} \right\} + \sqrt{U - U_i}\, \ell n\, U_i \right.$$

$$\left. - 2\sqrt{U - U_i} \right]$$

When $U >> U_i$, this is approximately:

$$S_1 = \ell n \frac{4U}{U_i} + \ell n U_i - 2 = \ell n U - (2 + \ell n 4)$$

$$\boxed{S_1 \doteq \ell n U}$$

Thus:

$$S(U) = g S_1 \equiv \frac{N \sigma_o U_i \ell n U_i d}{V} \ell n \frac{U}{U_i} = G(U) \ell n U_i$$

APPENDIX C

THE INTEGRALS OF POISSON'S EQUATION FOR PARABOLIC BEAMS

THE INTEGRALS OF POISSON'S EQUATION FOR PARABOLIC BEAMS

$$S_{pl} = \int_{U_i}^{U} \frac{\frac{V}{\psi} \ln \psi \, d\psi}{\sqrt{U - \psi}}$$

With the same substitution as in Appendix B, we have:

$$S_{pl} = 2 \int_{o}^{\sqrt{U-U_i}} \frac{\ln (U - y^2) dy}{U - y^2} = \frac{1}{\sqrt{U}} \left[\int_{o}^{\sqrt{U-U_i}} \frac{\ln\left(\sqrt{U} - y\right) dy}{\sqrt{U} - y} \right.$$

$$+ \int_{o}^{\sqrt{U-U_i}} \frac{\ln\left(\sqrt{U} - y\right) dy}{\sqrt{U} - y} + \int_{o}^{\sqrt{U-U_i}} \frac{\ln\left(\sqrt{U} + y\right) dy}{\sqrt{U} - y}$$

$$\left. + \int_{o}^{\sqrt{U-U_i}} \frac{\ln\left(\sqrt{U} - y\right) dy}{\sqrt{U} - y} \right]$$

The second and third integrals are equal and opposite as is readily seen by changing the sign of the variable. Hence:

$$S_{pl} = \frac{1}{\sqrt{U}} \left[\left\{ \ln\left(\sqrt{U} + y\right) \right\}^2 - \left\{ \ln\left(\sqrt{U} - y\right) \right\}^2 \right]_{o}^{\sqrt{U-U_i}}$$

$$= \frac{1}{\sqrt{U}} \left[\ln (U - y^2) \ln \left\{ \frac{\sqrt{U} + y}{\sqrt{U} - y} \right\} \right]_{o}^{\sqrt{U-U_i}}$$

$$= \frac{1}{\sqrt{U}} \left[\ln U_i \ln \left\{ \frac{\sqrt{U} + \sqrt{U - U_i}}{\sqrt{U} - \sqrt{U - U_i}} \right\} \right]$$

and when $U >> U_i$:

$$S_{pl} \doteq \frac{1}{\sqrt{U}} \ln U_i \ln\left(\frac{4U}{U_i}\right)$$

and:

$$\boxed{S_p(V) = \sqrt{V} \ln U_i \ln\left(\frac{4U}{U_i}\right)}$$

APPENDIX D

THE INFLUENCE OF CURVATURE

THE INFLUENCE OF CURVATURE

To understand the influence of electrode curvature on breakdown voltage, it is instructive to study the physics of the overall geometric and ionic field enhancement as expressed in Equation (8-88):

$$\frac{1}{k} = \frac{1}{k_o} + C_1 \left[\frac{G I_o}{k \beta_e^2 V^2} \right]^{1/2}$$

Due to surface migration causing area changes of the field emission site, the field emission current $I_F \doteq I_o$ is given by:

$$I_F = A_1 \left(\frac{V}{k} \right)^2 \exp \left\{ - \frac{B' V}{k} \right\}$$

This, therefore, is a major source of positive feedback in determining the variation of $1/k$ with voltage. Due, however, to the field enhancement, the emitted electron beam spreads out parabolically and the influence of this is to reduce the density of ionization and hence the value of the cathode field. Thus the beam spread reduces the magnitude of the positive feedback.

As the voltage is raised more ionization takes place and the protrusion field E_s increases. Surface migration then causes the radius, r, to decrease and so improve the field enhancement, but the additional beam spread inhibits this. Ultimately, the voltage rises until total instability takes place at some critical value of the factor k.

When convex electrodes are employed, the non-uniform macroscopic field is stronger than for uniform field electrodes at the same gap separation. Consequently, a protrusion under the same field enhancement conditions just described will emit a more dilated beam because electrons are then more strongly accelerated axially. The effective value of β_e is thus smaller and the ionic space charge field is less inhibited by beam spreading, causing E_s to be greater and the tip radius, r, will be less.

The actual value of $1/k$ at which it increases at an infinite rate with voltage is obtained by differentiating Equation (8-88) with respect to voltage. In a non-uniform field this has a lower value so k_c is higher than for planar electrodes.

Comparing the two systems, it is seen that since the effective value of β_e is smaller for the non-uniform than for the uniform field situation for the same protrusion, then the critical value will be reached for a smaller value of β_e. This signifies that the breakdown voltage is greater because:

$$\frac{V_B^2}{d} = \frac{12 \pi \gamma k_c}{\beta_e}$$

Comparing this argument with the analysis leading to Equation (8-100), we see that the value of $(1/k - 1/k_o)$ has decreased, giving a greater V_B, but the exponent in this expression will cause the increase to be a little less than is predicted from the simple argument. If β_e is reduced approximately by the factor H, then the expression of Equation (8-101) becomes:

$$\frac{k_c}{k_o} = H - \frac{2}{5 - \frac{B' V_B}{k_c}}$$

DECLARATION OF OATH

As a declaration of oath, I state that the work presented in this thesis is all my own and that all other sources of assistance are quoted in the reference and acknowledgments sections.

Alan Watson

Burlington, Massachusetts
October 1968

ALAN WATSON
M. Sc. Tech.
Diploma of Southampton University
B. Sc.

46 Faulkner Hill Road
Acton, Massachusetts, U. S. A.

RESUME

I was born on 11 May 1932 in Ashington, Northumberland, England.

Following primary education, I entered the King Edward VI Grammar School, Morpeth, Northumberland; a school founded perhaps before 1301 to provide a basically classical and liberal education for boys. I left school in 1951 after the customary Oxford Higher School Certificate examination. In 1951 I entered the Victoria University of Manchester with the James Gaskill Entrance Scholarship (Open). I was in the Honours School of Physics under Professor P. M. S. Blackett and graduated B. Sc. in 1954.

In August 1954, I began employment with Vickers-Armstrongs (Aircraft) Limited where I trained as a graduate apprentice in aircraft control and electronics engineering. During one year of leave between 1955 and 1956, I attended Southampton University, graduating with a Diploma from the Department of Electronics under Professor E. E. Zepler. Before returning to Vickers-Armstrongs, I studied aircraft autopilot control engineering techniques at Smiths Aircraft Instruments Limited until 1957 and spent the remaining period at Vickers-Armstrongs as an aircraft control engineer. In 1958, I changed employment to begin research work into spectroscopic properties of the plasma of vacuum arcs leading to the writing of a thesis in 1963 for the M. Sc. Tech. degree of the Victoria University of Manchester in the Faculty of Technology under Professor Colin Adamson. In addition I carried out experimental work on heavy current arcs, plasma torches and magnetohydrodynamic power generation.

In January 1964, I emigrated to the U. S. A. to take up employment with the Curtiss-Wright Corporation in the field of plasma propulsion.

I began working for Ion Physics Corporation in August 1964, being primarily engaged to carry out a five year research contract into Vacuum Breakdown for the U. S. Army, Fort Monmouth, New Jersey from December 1964 through the present time. Prior to this I carried out experimental and theoretical investigations into nanosecond pulsed flashover in vacuum leading to a new theory of the phenomenon. In collaboration with Julian Dow, I developed a theory of high energy electron injection into dielectrics. I am also concerned with studies into fast transient spark damage. In my principal field of vacuum breakdown, I have presented numerous papers at scientific meetings since 1965 and the present thesis represents an analysis of the work up to mid-1968. Professor Heinz Fischer has taken an interest in my work since September 1966 and has advised me since September 1967 in the presentation of the work as a Doctoral dissertation.

I have been married since 1955 and have three children aged 11, 8 and 2 years. I have had interests in gliding, photography and music, but more practical family interests have necessarily displaced them.

I am a member of the Institution of Electrical Engineers (London), a Chartered Engineer (United Kingdom), and a Graduate of the Institute of Physics and the Physical Society.

LIST OF PUBLICATIONS AND PATENTS

- "An Investigation of the Parameters of the Plasma of a Vacuum Arc", M. Sc. Thesis, University of Manchester (1963).
- "Pulsed Flashover of Dielectrics in Vacuum", with J. Shannon, Proceedings of Second International Symposium on Insulation of High Voltages in Vacuum (1966).
- "Prebreakdown Phenomena in Vacuum Gaps", with A. S. Denholm and M. J. Mulcahy, Proceedings of Second International Symposium on Insulation of High Voltages in Vacuum (1966).
- "Designed Experiments on High Voltage Vacuum Breakdown", with M. J. Mulcahy, A. S. Denholm, G. Taylor and M. Chrepta, Proceedings of Second International Symposium on Insulation of High Voltages in Vacuum (1966).
- "Microdischarge Phenomena in Vacuum Gaps", with A. S. Denholm and M. J. Mulcahy, Bul. APS 11, 504 (June 1966).
- "Vacuum Breakdown as a Function of Gap Separation", with M. J. Mulcahy, Bul. APS 12, 226 (1967).
- "Pulsed Flashover in Vacuum", J. Appl. Phys. 38, 2019 (1967).
- "Field Enhancement in Vacuum Breakdown", Presented at Twentieth Gaseous Electronics Conference, San Francisco, California (1967).
- "Electrode Size and Pretreatment Effects on Vacuum Breakdown in a Transverse Magnetic Field", Presented at Twentieth Gaseous Electronics Conference, San Francisco, California (1967).
- "A Unified Theory of Vacuum Breakdown", Proceedings of Third International Symposium on Discharges and Insulation in Vacuum (September 1968).
- "Factorially Designed Vacuum Breakdown Experiments. I. Influence of Electrode Size, Shape and Gas Content", with W. Bell and M. J. Mulcahy, Proceedings of Third International Symposium on Discharges and Insulation in Vacuum (September 1968).
- "Factorially Designed Vacuum Breakdown Experiments. II. Influence of a Weak Transverse Magnetic Field", with W. Bell and M. J. Mulcahy, Proceedings of Third International Symposium on Discharges and Insulation in Vacuum (September 1968).
- "Ionic Field Enhancement Instability as the Cause of Vacuum Breakdown", Presented at Twenty-First Gaseous Electronics Conference, Boulder, Colorado (October 1968).
- "Processes Accompanying Megavolt Electron Irradiation of Dielectrics", with Julian Dow, To be Published, J. Appl. Phys. (December 1968).
- "Electrode Damage from Transient Heavy Current Sparks, Internal Report, Ion Physics Corporation (1968).
- British Patent No. 885461, Issued 1961 (Vacuum dc Interruptor Switch).
- U. S. Patent Pending, "High Voltage Pulse Rectifier and Triggered Switch".